Titre: Title:	Dynamic Modelling and Optimisation of Microbial Fuel Cells and Microbial Electrolysis Cells
Auteur: Author:	Roberto Pires Pinto
Date:	2011
Type:	Mémoire ou thèse / Dissertation or Thesis
Référence: Citation:	Pinto, R. P. (2011). Dynamic Modelling and Optimisation of Microbial Fuel Cells and Microbial Electrolysis Cells [Ph.D. thesis, École Polytechnique de Montréal]. PolyPublie. https://publications.polymtl.ca/613/

UNIVERSITÉ DE MONTRÉAL

DYNAMIC MODELLING AND OPTIMISATION OF MICROBIAL FUEL CELLS AND MICROBIAL ELECTROLYSIS CELLS

ROBERTO PIRES PINTO
DÉPARTEMENT DE GÉNIE CHIMIQUE
ÉCOLE POLYTECHNIQUE DE MONTRÉAL

THÈSE PRÉSENTÉE EN VUE DE L'OBTENTION
DU DIPLÔME DE PHILOSOPHIAE DOCTOR
(GÉNIE CHIMIQUE)
JUILLET 2011

UNIVERSITÉ DE MONTRÉAL

ÉCOLE POLYTECHNIQUE DE MONTRÉAL

Cette thèse intitulée:

DYNAMIC MODELLING AND OPTIMISATION OF MICROBIAL FUEL CELLS AND MICROBIAL ELECTROLYSIS CELLS

présenté par : PINTO Roberto Pires
en vue de l'obtention du diplôme de: Philosophiae Doctor
a été dûment accepté par le jury d'examen constitué de:

M. PERRIER Michel, Ph.D., président
M. SRINIVASAN Bala, Ph.D., membre et directeur de recherche
M. TARTAKOVSKY Boris, Ph.D., membre et codirecteur de recherche
M. CHARTRAND Patrice, Ph.D., membre
M. BUDMAN Hector, Ph.D., membre

DEDICATION

This thesis is dedicated to

Paulo Henrique da Silva Pires & Madeleine Elise Bird

ACKNOWLEDGEMENTS

This work would never have been completed without the support of several people to which I will always be deeply grateful for all the help they gave me during the last four and a half years.

Professor Bala Srinivasan, thank you for all the talent, patience, availability, and wisdom you provided. I will always be impressed by your outstanding qualities. Srini, thank you for teaching me so much. Boris Tartakovsly, my co-research director, thank you for all your patience, persistence, organization and rigour. Thank you for guiding me throughout this project. Finally, thank you Professor Michel Perrier for all the guidance you provided, as well as your pertinent and important comments on this work. I would also like to thank Professors Hector Budman and Patrice Chartrand for their valuable comments on this thesis.

Most of all I would like to thank Srini, Boris and Michel for their friendship throughout these years; for always treating me as an equal and a friend. I am finishing my PhD with three excellent friends, which I will keep for the rest of my life.

I would also like to thank so many important friends that were beside me during these years: Jean-Martin and Lyne thank you so much for your amazing friendship. All dear friends from Poly: Ricardo, Agnès, Bahador, Dimitris, Enrique, Max, Bertrand, Félix, Guillaume, Masood, Massi, Prof. Jean Paris, and Prof. Olivier Henry; all close friends from BRI: Adrian, Guido, Laura, Mathieu, Punita, and Michelle.

I would like to thank Liliane, Elena, Elise, Kimbal and my family for all the love, care, and unconditional support you gave me during this long great journey that has been my PhD.

Papai, Mamãe, Renata e Paulo Henrique muito obrigado pelo amor, carinho e apoio sempre incondicional, mesmo sem nem sempre entender o porque de mais um diploma. Arthur, tias Xu, Tina, Verinha, e Nilda, tios Toninho, Normando, Kiko, Thielo, Nilson, Paulinho, Paulo Rogério, Rômulo, e tantos outros (família grande não é facil!), muito obrigado pelo amor e amizade.

Pablo, Kleber e Ivo obrigado por sempre manterem uma amizade tão carinhosa mesmo com toda a distante.

Finally, to the love of my life, Madeleine, I would never ever have done this work without you. Thank you so much for all your support, patience and love. I love you so much.

RÉSUMÉ

La demande mondiale croissante d'énergie, les réserves limitées de combustibles fossiles et leurs impacts environnementaux sont toutes des motivations pour trouver de nouvelles technologies énergétiques. Pour remplacer les combustibles fossiles, il faudra diversifier les sources d'énergies, et ce, par l'innovation technologique. Ces technologies peuvent utiliser des ressources renouvelables ou non renouvelables, la première option étant beaucoup plus intéressante pour l'indépendance énergétique. Parmi les technologies renouvelables, il y a l'énergie solaire, les turbines éoliennes, l'hydroélectricité, les centrales marémotrices et l'utilisation de la biomasse.

Dans un autre ordre d'idées, le traitement des déchets organiques et les résidus de la biomasse produite par l'activité humaine est un autre défi environnemental. Plus précisément, ce problème devient important avec des eaux usées, pour la conservation des ressources en eau douce. Le traitement des eaux usées exige des infrastructures importantes et utilise une grande quantité d'énergie. Cependant, les eaux usées peuvent être une source supplémentaire d'énergie. Bien qu'il y ait de la matière organique dans les eaux usées, celle-ci ne peut être récupérée par des procédés traditionnels car les concentrations sont faibles et leur composition est complexe. La plupart des technologies utilisent de l'énergie pour enlever cette matière organique de l'eau, tandis que d'autres, comme la digestion anaérobique, sont capables de produire de l'énergie renouvelable à partir de la matière organique disponible. Ces dernières sont les plus attrayantes, mais nécessitent souvent une étape de post-traitement aérobique (polissage) pour satisfaire les normes environnementales. Depuis peu, les cellules électrochimiques microbiennes sont une nouvelle option pour la production d'énergie à partir des eaux usées.

Les cellules électrochimiques microbiennes sont des bioréacteurs qui ont une conception similaire à une pile à combustible : une anode et une cathode reliées par un circuit électrique. Ces réacteurs contiennent des microorganismes anaérobiques dans la chambre anodique, qui sont capables d'oxyder la matière organique et qui transfèrent des électrons à une électrode pendant l'opération. Ce système est appelé pile à combustible microbienne (MFC). Si les électrons et les protons résultant de l'oxydation de la matière organique réagissent spontanément avec l'oxygène dans la cathode du réacteur, il y aura production de courant électrique. Une autre possibilité est

de forcer la réaction entre ces protons et des électrons dans une cathode anaérobique avec une tension électrique, ce qui conduit à la formation d'hydrogène. Les cellules électrochimiques microbiennes utilisées pour la production d'hydrogène sont appelées piles d'électrolyse microbiennes (MEC). Dans cette thèse, l'acronyme MxC sera utilisé pour se référer aux MFCs et MECs. Les MxCs sont capables de fonctionner avec une efficacité de Coulomb (la fraction d'électrons récupérés par rapport à la récupération maximale possible) supérieure à 90% et peut fonctionner à de faibles charges organiques, où la digestion anaérobique échoue en raison d'un faible taux de réaction. Ce qui éliminerait par le fait même l'étape de polissage.

Même si les MxCs sont une technologie attrayante pour le traitement des eaux usées, beaucoup d'améliorations doivent être faites pour que cette technologie soit commercialement viable. L'une des principales limitations pour l'application industrielle des MxCs est leur faible densité de puissance et leur tension électrique basse. Par conséquent, des recherches intensives se concentrent sur l'amélioration des MxCs par le développement de nouveaux matériaux pour l'anode et la cathode, une meilleure conception du réacteur, et l'optimisation des conditions de fonctionnement. Un autre aspect important qui doit être pris en compte dans le fonctionnement des MxCs est la présence de différents types de microorganismes. Tout comme dans un réacteur à digestion anaérobique, une MxC utilisée pour le traitement des eaux usées contient toujours des populations microbiennes complexes à cause de la nature même de l'eau usée. Normalement, l'anode d'une MxC contient des microorganismes fermentatifs, méthanogènes, facultatifs et électrogènes. L'existence de plusieurs populations microbiennes affecte la performance de la cellule microbienne, car tous les microorganismes ont un impact sur la production d'électricité. En particulier, la compétition pour le même substrat (acétate) entre méthanogènes et électrogène affecte directement la génération de courant électrique. Les conditions d'opération peuvent également affecter l'équilibre entre les microorganismes méthanogènes et électrogènes.

Une solution pour améliorer la performance des MxCs est d'identifier les principales étapes limitantes du système et de les améliorer. Cela peut être fait à l'aide d'un modèle mathématique qui permet de décrire la dynamique de la consommation de substrat, la croissance des microorganismes et la génération de produits (de l'électricité pour les MFCs et de l'hydrogène pour les MECs). Ce modèle peut être utilisé pour l'optimisation des processus, une meilleure

compréhension des opérations et il pourrait aider à identifier les principales étapes limitantes d'une MxC.

Malgré leur importance, il existe très peu de modèles pour les MFCs dans la littérature, tandis qu'aucun modèle pour les MEC est actuellement disponible. Le processus de transfert d'électrons (Andrew Kato Marcus, Torres, & Rittmann, 2007) et la production d'électricité (Y. Zeng, Choo, Kim, et Wu, 2010; X. C. Zhang & Halme, 1995) ont été modélisés mais n'ont pas pris compte de la compétition microbienne pour une source commune de carbone. Picioreanu et al. (2007; 2008) ont mis au point un modèle détaillé en 3 dimensions pour le biofilm anodique. L'objectif principal de ce modèle était d'analyser la formation du biofilm et la distribution des espèces au sein de celui-ci. Ce fut le premier modèle à prendre en compte les différentes populations microbiennes en compétition pour l'espace dans le biofilm et la consommation de substrat.

Bien que les modèles de Zhang et Halme (1995), Marcus et al. (2007), et Zeng et al. (2010) simplifient beaucoup la dynamique du biofilm dans les MFCs, le modèle de Picioreanu et al. (2007; 2008) a fourni une description très détaillée des populations électricigènes et non-électricigènes dans le biofilm en utilisant des équations aux dérivées partielles, qui résulte en un calcul computationnel très long. Cette thèse argumente qu'un modèle plus simple constitué d'équations différentielles ordinaires peut décrire adéquatement les populations microbiennes dans les MFCs et les MECs à diverses conditions d'opération, sa génération de produits, et la consommation de substrat, tout en étant adapté à l'optimisation des processus et le contrôle de procédé.

Cette thèse présente le développement de modèles pour les MFCs et MECs, capables de décrire la dynamique de la consommation de substrat, la croissance des microorganismes, et la génération de l'électricité (MFC) ou de H_2 (MEC). En utilisant les équations différentielles ordinaires pour décrire la croissance de la biomasse et la consommation du substrat dans l'anode, des solutions numériques rapides ont été trouvées pour les deux modèles. Premièrement, un modèle pour les MFCs qui considère la compétition pour l'acétate entre les microorganismes électricigènes et méthanogènes acétoclastiques a été développé. Le modèle pour les MECs a été fondé avec les concepts présentés dans le modèle pour les MFCs. En incluant les

microorganismes fermentatifs et hydrogenotrophique méthanogènes, le modèle de MEC a été en mesure de prédire la production d'hydrogène à partir de la dégradation des eaux usées. Les paramètres identifiables des deux modèles ont été estimés avec des résultats expérimentaux obtenus par des MFCs et MECs opérés en continu. De plus, en utilisant des données expérimentales indépendantes, les deux modèles ont été validés et ont réussi à décrire les résultats expérimentaux pour diverses conditions d'opération.

Cette thèse présente également des analyses pour les deux modèles en ce qui a trait à l'optimisation des processus. Premièrement, des analyses ont démontré l'influence des conditions d'opération sur la production d'électricité et de H_2 pour les deux modèles. Fait intéressant: le choix de résistance externe et de la tension appliquée (variables manipulées pour les MFCs et les MECs, respectivement) ont affecté significativement la composition microbienne du biofilm. Cet aspect a été analysé en détail pour le modèle des MFCs par une analyse de la composition du biofilm en régime permanent. Il a été montré que, selon le choix de la résistance externe, le biofilm d'une MFC peut présenter trois compositions différentes: (i) la coexistence de deux populations microbiennes ou; l'exclusion de l'une de ces populations microbiennes avec seulement (ii) les électricigènes ou seulement (iii) les méthanogènes présents. Suite à ce résultat, une comparaison entre la consommation de substrat dans les trois scénarios a été réalisée, la conclusion étant que la coexistence conduit toujours à une consommation minimale du substrat. La capacité de traitement des MFCs a ensuite été optimisée en plaçant deux réacteurs en série, qui a démontré une efficacité par rapport à un branchement en parallèle. La capacité de traitement optimale de cette unité a été démontrée dépendante de la concentration de l'influent et du choix de concentration de l'effluent. Enfin, des expériences utilisant une MFC alimentée en acétate ont été présentées pour confirmer qualitativement les effets de la résistance externe sur la composition du biofilm.

La dernière partie de cette thèse présente un modèle unifié pour la MFC et la MEC, qui prend en compte la présence de microorganismes électricigènes et méthanogènes acétoclastiques dans le compartiment anodique, les différences entre les réactions de la cathode entre la MFC et la MEC étant représentées par le bilan électrochimique. Le modèle est d'abord analysé en termes de la composition du biofilm, qui est montrée dépendante du courant électrique du réacteur. Une fois

de plus le biofilm a présenté une coexistence de microorganismes pour une petite gamme de courants d'opération. Enfin, une étude d'optimisation a été réalisée afin de maximiser l'électricité (MFC) ou la production de H_2 (MEC), tout en respectant les exigences de traitement des eaux usées. Des expressions pour les productivités ont été déterminées pour les deux réacteurs. Également, des expressions analytiques pour les courants optimaux ont été développées, qui se sont montrés être les mêmes pour la MFC et la MEC. En plus, les optimums se sont montrés être dépendants de la résistance interne du réacteur. Enfin, une fonction alternative pour la productivité a été définie et analysé pour les MECs. Cette deuxième productivité est fonction de l'efficacité de la production de H_2 et sa solution analytique optimale s'est montrée indépendante de la résistance interne du réacteur.

ABSTRACT

Low reserves of fossil fuels and the environmental impact of their use to produce energy are leading to a search for novel renewable energy technologies. Electricity production in Microbial fuel cells (MFCs) and hydrogen production in Microbial electrolysis cells (MECs) from a variety of highly diluted organic matter, including wastewater, are among such technologies. Biocatalytic activity of MFCs and MECs depends on anaerobic bacteria, which populate the anode compartment. These anaerobic electricigenic (exoelectricigenic) microorganisms, oxidise organic matter and transfer electrons to an electron acceptor (electrode). When wastewater is fed to the anode compartment, MFCs and MECs consume the organic matter thus performing the wastewater treatment while recovering energy. Therefore this process provides a possibility of energy-producing wastewater treatment plants. This novel technology can be operated at temperatures below 20 °C and at low substrate concentration levels, conditions in which the conventional anaerobic digestion fails due to low reactions rates and washout of methanogenic microorganisms.

The major bottleneck of the MFC/MEC technology is its relatively low current density, which restricts most of its commercial application. Furthermore, due to the nature of the process, MFC and MEC research demands a diverse range of coordinated expertise including those of microbiologists, environmental biotechnologists, and engineers, in order to achieve further improvements in performance. One possibility to better understand and enhance this technology is to build a dynamic mathematical model that can describe the fundamental phenomena taking place in the system, indicating its main rate limiting steps. After a critical analysis of the MFC models in the literature, none were found that would include several microbial populations competing for the same substrate, while providing fast numerical solution. The only models that were available were either oversimplified or too complex to be rapidly solved.

The first contribution of this thesis is the development of MFC and MEC models capable of describing the dynamics of substrate consumption, microorganism's growth, and electricity (MFCs) or H_2 (MECs) generation. By using ordinary differential equations to describe biomass growth and substrate consumption in the anodic compartments, a fast numerical solution was found for both models. First a MFC model describing the acetate competition between

electricigenic and acetoclastic methanogenic microorganisms was developed. The MEC model foundation was based on the concepts presented in the MFC model. By including fermentative and hydrogenotrophic methanogenic microorganisms, the MEC model was able to predict hydrogen production from wastewater degradation. Model parameters were estimated for both models with experimental results obtained in continuous flow, gas diffusion cathode MFCs and MECs. Only model parameters with small confidence intervals were selected to be estimated. Moreover, using independent experimental data sets, both models were validated and were successful in describing experimental results at diverse operating conditions.

A further contribution of this thesis is the analysis of both models for process optimisation. Preliminary analysis demonstrated the influence of operating conditions on product generation for both models. Interestingly, the external resistance and the applied voltage (manipulated variables for MFCs and MECs respectively) were shown to significantly influence the biofilm microbial composition. This aspect was further analysed for the MFC model with a steady state analysis of the biofilm composition. It was shown that depending on the selection of the external resistance, the MFC biofilm could present three scenarios: (i) the coexistence of both microbial populations; or the exclusion of one of the microbial population with (ii) only electricigens, or (iii) only methanogens present. Following these results, a comparison between the substrate consumption of the three scenarios was performed, showing that coexistence always leads to lower substrate consumption. The treatment capacity of MFCs was then optimised by reactor staging. The optimum treatment capacity of a unit with two staged reactors was shown to depend on the influent concentration and effluent requirement. Finally, experiments using acetate-fed MFCs were presented to qualitatively confirm the effects of external resistance on the biofilm composition.

The last contribution of this thesis is the presentation of a unified MFC/MEC model, which includes electricigenic and methanogenic microorganisms in the anode compartment, while the electrochemical balance accounts for the cathode differences between the MFC and MEC. The model is first analysed in terms of biofilm composition, which is shown to depend on the reactor's operating current. Once more, biofilm coexistence was present only for a defined interval of operating current. An optimisation study was performed to maximise electricity

(MFC) or H_2 production (MEC), while respecting a treatment requirement. By defining power productivity functions for both reactors, analytical optimum current expressions were found and were shown to be the same for MFCs and MECs. Furthermore, these expressions were dependent on the reactor's internal resistance. Finally, an alternative MEC productivity function was defined and analysed. This productivity was a function of the H_2 production efficiency and its unique analytical optimum solution was shown to be independent of the reactor's internal resistance.

TABLE OF CONTENTS

LIST OF TABLES

LIST OF FIGURES

LIST OF ABBREVIATIONS AND ACRONYMS

2D	Two dimension
3D	Three dimension
AD	Anaerobic Digestion
ADM1	The IWA Anaerobic Digestion Model No 1
ADP	Adenosine Diphosphate
ATP	Adenosine-5'-triphosphate
CEP	Competitive exclusion principle
COD	Carbon oxygen demand
CSTR	Continuous Stirred Tank Reactor
FBBRs	Fluidised Bed Biofilm Reactors
FIM	Fisher Information Matrix
HRT	Hydraulic retention time
IWA	International Water Association
MEC	Microbial electrolysis cell
MFC	Microbial fuel cell
MPPT	Maximum Power Point Tracking
MSE	Mean squared error
MU	Multiunit
MxC	Microbial fuel cell and Microbial electrolysis cell
NAD	Nicotinamide Adenine Dinucleotide
NADP	Nicotinamide Adenine Dinucleotide Phosphate
ODEs	Ordinary differential equations
P/O	Perturbation and Observation
PDEs	Partial differential equations
PFR	Plug Flow Reactor
PI	Proportional integral controller
PT	Polarization test
R^2	Adjusted coefficient of determination
sCOD	Soluble carbon oxygen demand

sWW	Synthetic wastewater
tCOD	Total carbon oxygen demand
UASB	Upflow Anaerobic Sludge Bed
VFA	Volatile Fatty Acids
VS	Voltage scans
WW	Wastewater

NOMENCLATURE

A acetate concentration in the MxC's anodic compartment [mg-A L^{-1}]

A_0 acetate concentration in the MxC's influent [mg-A L^{-1}]

A_{ref} desired effluent concentration [mg L^{-1}]

$A_{sur,A}$ anode surface area [m^2]

c_a process variable of the a-th measurement

C_{bulk} the reactant or product concentration on the fuel cell compartment [mg L^{-1}]

$C_{surface}$ the reactant or product concentration on the electrode surface or the reactant or product reference concentration on the electrode surface [mg L^{-1}]

$\overline{D}$ diffusion coefficient [m^2 s^{-1}]

D dilution rate ($D=F_{in}\ V^{-1}$) [d^{-1}]

E_{act} activation energy [J]

E_{CEF} counter-electromotive force for the MEC [V]

E_{MAX} highest observed E_{OCP} value [V]

E_{MIN} lowest observed E_{OCP} value [V]

E_{OCP} MFC open circuit potential [V]

E_{output} fuel cell output voltage [V]

E_{thermo} is the thermodynamic fuel cell maximum voltage [V]

F Faraday constant [A d mole^{-1}]

F_0 incoming flow initial condition [L d^{-1}]

F_{in} incoming flow [L d^{-1}]

F_P flow rate of a two MFCs' parallel configuration [L d^{-1}]

F_S flow rate of a two MFCs' series configuration [L d^{-1}]

$I_L^{Reference}$ fuel cell limiting reference current [A]

I^*_{MxC} average current produced by the MxC during Δt [A]

i_0 exchange current density in reference conditions [A $m^{2\,-1}$]

I_{cell} fuel cell current [A]

I_{MEC} MEC current [A]

I_{MFC} MFC current [A]

J objective or cost function to be optimised

K half-saturation (Monod) constant [mg-S L^{-1} or mg-A L^{-1} or mg-M L^{-1} or mg-H_2 L^{-1}]

k iteration number

K_d decay rate [d^{-1}]

K_i half-saturation inhibition parameter [L^2 mg-S^{-2}]

K_i integral error [L^2 mg^{-1} d^{-2}]

K_p the controller gain [L^2 mg^{-1} d^{-1}]

K_R constant, which determines the curve steepness [L mg-x^{-1}];

K_x steepness factor [L mg-x^{-1}]

m number of electrons transferred per mol of mediator or per mol of hydrogen [mol-e^- mol_{med}^{-1} or mol-e^- mol_{H2}^{-1}]

$\dot{m}$ mass flow rate [kg s^{-1}]

MM molar mass [kg mol^{-1}]

M_{ox} oxidised mediator fraction per each electricigenic microorganism [mg-M mg-x^{-1}]

M_{red} reduced mediator fraction per each electricigenic microorganism [mg-M mg-x^{-1}]

M_{Total} total mediator weight percentage in each electricigenic microorganism [mg-M mg-x^{-1}]

n_i number of measurements of the i-th state variable

P anode compartment pressure [atm]

$P_{applied}$ power used by the applied voltage in the MEC [W]

p_l is the l-th model parameter

$Q_{CH4,A}$ methane production in the anode compartment [mL-CH_4 d^{-1}]

$Q_{CH4,C}$ methane production in the MEC cathode compartment [mL-CH_4 d^{-1}]

q_e substrate consumption rate by electricigenic microorganisms [mg-A mg-x^{-1} d^{-1}]

q_f substrate consumption rate by fermentative microorganisms [mg-S mg-x^{-1} d^{-1}]

Q_{H2} hydrogen production in the MEC cathode compartment [mL-H_2 d^{-1}]

q_m substrate consumption rate by methanogenic microorganisms [mg-A mg-x^{-1} d^{-1}]

q_{max} maximum substrate consumption rate [mg-S mg-x^{-1} $d^{-1\,1}$ or mg-A mg-x^{-1} d^{-1}]

R ideal gas constant [mL-H_2 atm K^{-1} mol-H_2^{-1} or J K^{-1} mol^{-1}]

R_{ext} MFC external resistance [Ω]

R_{int} MxC internal resistance [Ω];

R_{MAX} highest observed internal resistance [Ω]

R_{MIN} lowest observed internal resistance [Ω]

S organic substrate concentration in the MxC's anodic compartment [mg-S L^{-1}]

S_0 organic substrate concentration in the MxC's influent [mg-S L^{-1}]

SF_{al} sensitive function of the a-th measurement with respect to the l-th model parameter

t time [d]

T MxC anode compartment temperature [K]

u system output

V MxC anodic compartment volume [L];

w_i weight constant of the i-th state variable

x_e concentration of electricigenic microorganisms in the MFC biofilm or in the MEC biofilm Layer 2 [mg-x L^{-1}]

x_f concentration of fermentative microorganisms in the MEC biofilm Layer 1 [mg-x L^{-1}]

x_h concentration of hydrogenotrophic methanogenic microorganisms in the MEC biofilm Layer 3 [mg-x L^{-1}];

x_m concentration of acetoclastic methanogenic microorganisms in the MFC biofilm [mg-x L^{-1}]

$x_{m,1}$ concentration of acetoclastic methanogenic microorganisms in the MEC biofilm Layer 1 [mg-x L^{-1}]

$x_{m,2}$ concentration of acetoclastic methanogenic microorganisms in the MEC biofilm Layer 2 [mg-x L^{-1}];

X_{MAX} maximal attainable biomass concentration in a respectively biofilm layer [mg-x L^{-1}]

y system input

$\bar{y}_{j,i}^{\exp}$ normalised experimental values of the i-th state variable at j-th sampling time

$\bar{y}_{j,i}^{sim}$ normalised simulated values of the i-th state variable at j-th sampling time

Y_{CH4} yield of methane from acetate [mL-CH_4 mg-A^{-1}].

Y_{COD} acetate yield from organic substrate [mg-S mg-A^{-1}]

Y_h yield rate for hydrogen consuming methanogenic microorganisms [mL-H_2 mg-x^{-1}]

Y_{H2} dimensionless cathode efficiency

$Y_{H2/CH4}$ yield of methane from hydrogen [mL-CH_4 mL-H_2^{-1}]

Y_M mediator yield [mg-M mg-S^{-1}]

α dimensionless biofilm retention constant

β dimensionless reduction or oxidation transfer coefficient

δ distance between bulk and electrode surface [m]

ΔG^0 fuel cell's Gibbs free energy at a constant temperature [J]

ΔH_{H2} H_2 enthalpy of combustion [J mg-H_2^{-1}]

ΔS is the amount of substrate consumed during Δt [mol-S]

ζ perturbation factor in the sensitive function

μ microorganism growth rate [d^{-1}]

μ_e electricigenic microorganisms growth rate [d^{-1}]

μ_f fermentative microorganisms growth rate [d^{-1}]

μ_h hydrogenotrophic methanogenic microorganisms growth rate [d^{-1}]

μ_m methanogenic microorganisms growth rate [d^{-1}]

μ_{max} maximum growth rate [d^{-1}]

ρ_{H2} H_2 density [mg-H_2 mL-H_2^{-1}]

Γ pre-exponential coefficient function fuel cell temperature and reactant and product partial pressures [A $m^{2\,-1}$]

γ mediator molar mass [mg-M mol-M^{-1}]

ε constant [mg-M mg-x^{-1}]

η_{act} activation over-potential [V]

η_{conc} concentration over-potential [V]

η_{ohm} ohmic over-potential [V]

Δt time interval used to calculate average operating conditions [s], (typically 1 day)

[S] generic substrate concentration [mg L^{-1}]

Δ MU offset parameter

ΔE amplitude of change in $E_{applied}$ [V]

ΔR amplitude of change in R_{ext} [Ω]

INTRODUCTION

Motivation

Increasing energy demands from a growing world population, and the depleting reserves of fossil fuels and their environmental impacts, are leading to a search for novel energy technologies. Most likely, a diverse portfolio of energy producing technologies will be needed to replace fossil fuels (Bruce E. Logan, 2008). These technologies may rely on renewable or non-renewable resources, the former being much more interesting because they do not depend on limited reserves. A portfolio of renewable energy technologies may include a variety of systems based on sunlight, wind, rain, tides, geothermal heat, and biomass.

Another challenge is the treatment of organic waste and biomass residue produced by society. Specifically, this problem becomes imperative with wastewater (WW) as fresh water reserves are small. WW treatment often demands high infrastructure and usually uses a great amount of energy. Nevertheless, WW may be an additional significant source of renewable energy. Organic components is WW cannot be recovered by traditional chemical processes, however, because organic matter in waste presents a complex composition and is often highly diluted. Among the available technologies to treat WW, some consume energy, while others, such as anaerobic digestion (AD), are able to produce renewable energy from available organic matter (Eddy, 2003). The latter are most promising, but often require a step of aerobic post-treatment (polishing) to satisfy wastewater treatment norms. One novel promising option of producing energy from low-strength wastewaters are Microbial electrochemical cells.

Microbial electrochemical cells are bioreactors that have a design similar to a fuel cell, with an anode and a cathode connected through an electrical circuit (B.E. Logan et al., 2006). These reactors present an anaerobic anode chamber containing electricigenic microorganisms (also often referred to as exoelectricigenic[1]), which oxidise organic matter and transfer electrons to an electrode as a part of its metabolism. These systems are called Microbial fuel cells (MFCs) if the

[1] Strictly speaking, all microorganisms transfer electrons during metabolism inside the cell, making them all electricigens. However, exoelectricigens transfer electrons outside the cell. For the sake of simplicity exoelectricigens will be referred to as electricigens in this thesis.

electrons and protons resulting from oxidation of organic matter react spontaneously with O_2 in the reactor's cathode, therefore producing current (Bond, Holmes, Tender, & Lovley, 2002; H. J. Kim et al., 2002; Bruce E. Logan & Regan, 2006b; Potter, 1915). A further possibility is to force the reaction between these protons and electrons in an anaerobic cathode by an applied voltage, which leads to hydrogen formation (René Alexander Rozendal, 2007; R. A. Rozendal, Hamelers, Euverink, Metz, & Buisman, 2006). Microbial electrochemical cells used for H_2 production are called Microbial electrolysis cells (MECs). In this thesis the MxC acronym will be used when referring to both MFCs and MECs. MxCs were shown to be able to operate with Coulombic efficiencies (the fraction of electrons recovered as current versus the maximum possible recovery) higher than 90% (Rabaey, Clauwaert, Aelterman, & Verstraete, 2005) and can be operated at low organic loads, where the conventional AD fails due to low reaction rates and washout of methanogenic microorganisms (Pham et al., 2006).

Although MxCs are a promising technology for WW treatment, improvement is required to reach feasible commercial application. One of the major bottlenecks of MxC application is their low power density and the restricted output voltage of 0.2-0.3 V (Pant, Van Bogaert, Diels, & Vanbroekhoven, 2010). Therefore, intense research is now focusing on the enhancement of MxCs through the development of new anode and cathode materials (Kang et al., 2003; Rismani-Yazdi, Carver, Christy, & Tuovinen, 2008; ter Heijne, Hamelers, Saakes, & Buisman, 2008), better reactor design (B. E. Logan, 2010; Bruce E. Logan & Regan, 2006b; Shimoyama et al., 2008), improvement of the electron transfer process (Reguera et al., 2005; C. I. Torres et al., 2010), and optimisation of operational conditions (Jadhav & Ghangrekar, 2009). Furthermore, stacks of MxCs can be used to increase the operating voltage (Aelterman, Rabaey, Pham, Boon, & Verstraete, 2006; Ieropoulos, Greenman, & Melhuish, 2008) although challenges such as voltage reversal have been encountered (Oh & Logan, 2007), leading to significant efficiency losses.

Another important aspect that affects the performance of the reactors, and needs to be taken into account for the enhancement of MxCs, is the presence of different types of microorganisms. Similar to AD, MxCs used for WW treatment always contain complex microbial communities, because the influent contains diverse microbial species. Frequently an MxCs' anode compartment contains fermentative, methanogenic, facultative, and electricigenic microorganisms (Arcand,

Chavarie, & Guiot, 1994; B. E. Logan & Regan, 2006a; Moletta, Verrier, & Albagnac, 1986; Quarmby & Forster, 1995). The existence of mixed microbial populations might affect the performance of the MxC, because not all microorganisms take part in electricity generation (Harmand, Rapaport, Dochain, & Lobry, 2008; Sheintuch, Tartakovsky, Narkis, & Rebhun, 1995; Wanner & Gujer, 1985). In particular, the competition for the same substrate (acetate) between acetoclastic methanogenic and electricigenic microorganisms has a direct impact on the MxC current generation. Furthermore, the operational conditions of MxCs may also affect the equilibrium between methanogenic and electricigenic microbial populations (Aelterman, Versichele, Marzorati, Boon, & Verstraete, 2008).

One solution for enhancing MxC performance is to identify the system's main bottlenecks and improve them. This can be done with the aid of a mathematical model that describes the dynamics of substrate consumption, multi-population microorganism growth and product generation (electricity for MFCs and H_2 for MECs). This model can be used for process and design optimisation, it may allow a deeper understanding of the operation, and it may help to identify the main bottlenecks of MxCs.

Despite their importance, few MFC models are presented in the literature, while no MEC models are currently available. The processes of electron transfer (Andrew Kato Marcus, Torres, & Rittmann, 2007) and power generation (Y. Zeng, Choo, Kim, & Wu, 2010; X. C. Zhang & Halme, 1995) have been modelled before, but do not take into account the microbial competition for a common source of carbon. Picioreanu et al. (Cristian Picioreanu, Head, Katuri, van Loosdrecht, & Scott, 2007; C. Picioreanu, Katuri, Head, Van Loosdrecht, & Scott, 2008) developed a detailed 3-dimensional model of anodic compartment biofilm. The principal aim of this model was to analyse biofilm formation and species distribution within the biofilm. This was the first model to take into account different microbial populations competing for biofilm space and substrate.

While Zhang and Halme (1995), Marcus et al. (2007), and Zeng et al. (2010) oversimplified MFC biofilm microbial dynamics, Picioreanu et al.'s (2007; 2008) model provided detailed descriptions of the electricigenic and non-electricigenic populations in the biofilm by using

partial differential equations, which led to long computational times. This thesis argues that a simpler model consisting of ordinary differential equations can adequately describe growth of microbial populations in MFCs and MECs at various operational conditions, and its product generation and substrate consumption, while being suitable for process optimisation and control.

Problematic

Overall, MxCs used for wastewater treatment represent a novel and promising renewable energy technology that can recover current or H_2 while treatment is being performed. However, MxCs present many technological challenges that need to be overcome before commercial application. These technical problems can be solved using a systems engineering approach that uses process modelling for MxC design, optimisation, and control. However, the MxC models available in the literature are either oversimplified or too complex.

Objective

The main objective of this PhD thesis is to optimise MxC reactor performance and operation through model analysis, using a fast convergence model that describes the dynamics of the mixed microbial populations in MFCs and MECs. Such models will be developed in the thesis.

Specific Objectives

The specific objectives of this thesis are to:

1. Develop a MFC dynamic model that describes the competition for acetate between methanogenic and electricigenic microorganisms.
2. Analyse the MFC model in terms of operating conditions and steady state biofilm composition, and optimise the MFC's treatment capacity (flow rate for a given effluent concentration) by the best choice of operating conditions and by reactor staging.
3. Carry out experiments aimed to qualitatively demonstrate some of the model analysis results.
4. Develop a MEC dynamic model that describes wastewater degradation, with fermentative, methanogenic and electricigenic microorganisms.
5. Analyse the MEC model in terms of operating conditions and steady state biofilm composition, and optimise the MxC's productivity by the best choice of operating conditions.

Thesis Structure

This PhD thesis is separated into six chapters. Chapter 1 contains a literature review of MxC models and some important references in AD and fuel cells modelling. Furthermore, techniques of model-based enhancement, optimisation, and process control are reviewed. Chapter 2 presents the materials and methods for all MFC and MEC experiments, and the methodology of model development, parameter estimation, and validation used in this thesis. In chapter 3, the MFC model is developed, with some of its identifiable parameters being estimated with experimental data. Independent MFC data is used for the model validation, proving the predictability of the model outside the parameters estimation region. Finally, the effects of operating conditions on the MFC power production are analysed. Chapter 4 contains the MFC model analysis, starting with the effects of external load on the steady state biofilm composition and on the substrate consumption rate. Subsequently, an optimisation of the treatment capacity of MFCs by reactor staging is presented. Last, chapter 4 includes the MFC experimental results used to qualitatively demonstrate the biofilm model analysis results. Chapter 5 presents the development of the MEC model; its identifiable parameters being estimated using different MEC data sets. Moreover, the model is validated with an independent MEC data set and the operational conditions' effect on hydrogen production and COD removal are presented. Chapter 6 presents a unified version of the MFC and MEC models. The effects of biofilm composition for this unified model are analysed in terms of reactor current. Finally, MFC and MEC productivities are defined and an optimum operation point is analytically expressed for both reactors.

CHAPTER 1: LITERATURE REVIEW

The literature review will cover two main aspects: modelling and process enhancement. Due to the lack of MxC models that include key process phenomena with a simple computational solution, the first section will include modelling concepts that might contribute to the development of a fast convergence multi-population MxC model. The second section will cover techniques used for process control, enhancement, and model based optimisation

1.1. Modelling

This section will review techniques to model anaerobic digesters and fuel cells, as some of the steps to model these processes are similar to some of those for MxC operations. Following, a critical evaluation of available MxC models in the literature is presented.

1.1.1. Anaerobic Digestion Models

The anodic chamber of MxCs operate under anaerobic conditions with microorganisms attached to the anode (Andrew Kato Marcus et al., 2007) thus forming a biofilm, as in a number of anaerobic reactors. The reactions in the biofilm of MxCs are one of the main limiting factors to enhancing MxC operation (B. H. Kim, Chang, & Gadd, 2007) and will be evaluated here.

Anaerobic digestion is a process where organic matter is degraded into a mixture of methane, carbon dioxide, and biomass (Bonnet, Dochain, & Steyer, 1997). This degradation is performed in several steps by different microorganisms, which oxidise the dissolved organic matter in WW streams (Eddy, 2003). Overall, WW degradation can be separated into three biological steps: (i) fermentation, (ii) anaerobic oxidation, and (iii) methanogenesis (D.J. Batstone et al., 2002b). The nature of the process requires the presence of complex microbial communities to support large variations on the inlet composition (WW composition and flow often vary periodically). Furthermore, because the WW influent always contains diverse microbial species, any kind of pure culture microorganism treatment is unfeasible.

Among the diverse process designs and configurations for anaerobic treatment processes (e.g. anaerobic suspended growth, upflow and down-flow anaerobic attached growth, anaerobic lagoons, upflow anaerobic sludge blanket), some previously developed AD models can give

important information about kinetics of reaction, transport, and space limitations for the MxC anode. This review will be limited to those AD models that apply, for example, models with diverse microbial populations and biofilm.

1.1.1.1. Reaction Kinetics

Substrate kinetics consumption and microorganisms growth rate in AD are often modelled by the Monod kinetics equation, also called Michaelis-Menten (Eddy, 2003). The Monod equation is one of the most widespread analytical specific reaction rate expressions used either for microorganism growth or substrate consumption. It expresses the dependence of the reaction rate in the following form: At high substrate concentration the process is at its maximum rate, while at low substrate concentrations the process becomes rate limited. The Monod equation can be represented as (Monod, 1942):

$$\mu = \mu_{\max} \frac{[S]}{K_{[S]} + [S]} \tag{1-1}$$

Generally, the substrate consumption and growth rate in the anode compartment of the MxC can be represented by Monod-type kinetics, as in AD. However, depending on the system (multiple substrates or multiple bacteria communities) modifications in the Monod kinetics may be needed. A system with multiple substrates was described by Bae & Rittmann (1996b) where a multiplicative (double-Monod) model was successfully used to describe a dual-limitation system, where together electron-donors and electron-acceptors limited the overall cell growth. The double-Monod kinetics for two substrates (S_1 and S_2) can be represented as:

$$\mu = \mu_{\max} \frac{[S_1]}{K_{[S_1]} + [S_1]} \frac{[S_2]}{K_{[S_2]} + [S_2]} \tag{1-2}$$

The double-Monod model was later successfully tested experimentally for intracellular cofactors, such as NAD, NADH, ATP and ADP (Bae & Rittmann, 1996a).

It is also common in AD modelling to describe the kinetics of substrate consumption using the "Haldane law" model (Andrews, 1968). This model illustrates a growth rate with possible substrate inhibitory effects at high concentrations, often called overloading (Andrews, 1968):

$$\mu = \mu_{\max} \frac{[S]}{K_{[S]} + [S] + \frac{[S]^2}{K_i}} \quad (1\text{-}3)$$

This equation is reduced to Monod when K_i goes to infinity (inhibition is neglected). In this thesis, Haldane kinetics was not considered for MxCs for two reasons: (i) previous experiments have shown that electricigenic microorganisms exhibit Monod-like kinetics (Cheng, Goen, & Cord-Ruwisch, 2008; Andrew Kato Marcus et al., 2007; Cesar I. Torres, Marcus, Parameswaran, & Rittmann, 2008a) and; (ii) because the substrate concentrations of wastewater treatment are usually low, and at these concentrations inhibition does not affect the growth kinetics (Andrews, 1968).

1.1.1.2. Anaerobic Digestion Modelling

Several AD models have been developed over the years (e.g. (Bernard, Hadj-Sadok, Dochain, Genovesi, & Steyer, 2001; Bonnet et al., 1997; Buffiere, Steyer, Fonade, & Moletta, 1995; Moletta et al., 1986)), but their use was limited due to their specific applications. The development of a generalised anaerobic digestion model, called the IWA Anaerobic Digestion Model No 1 (ADM1) (D. J. Batstone et al., 2002a) attempted to solve this difficulty. The complexity of the reactions that occur in wastewater degradation is reflected by the large number of model equations in the ADM1 (32 dynamic concentration state variables) and the large number of parameters required for a detailed description of the anaerobic digestion process. This general model includes multiple steps describing biochemical and physicochemical processes using Monod-type kinetics for diverse substrate consumption by various microbial populations. Death of biomass was represented by first order kinetics. The ADM1 included the disintegration of homogeneous particulates to carbohydrates, proteins, and lipids, which were later hydrolysed into sugars, amino acids, and long chain fatty acids. It also considered acidogenesis from sugars and amino acids to VFAs, and hydrogen and acetogenesis of long chain fatty acids and VFAs to acetate. Finally acetoclastic and hydrogenotrophic methanogenesis steps were modelled to describe the acetate and hydrogen consumption. This model can be described by the following figure:

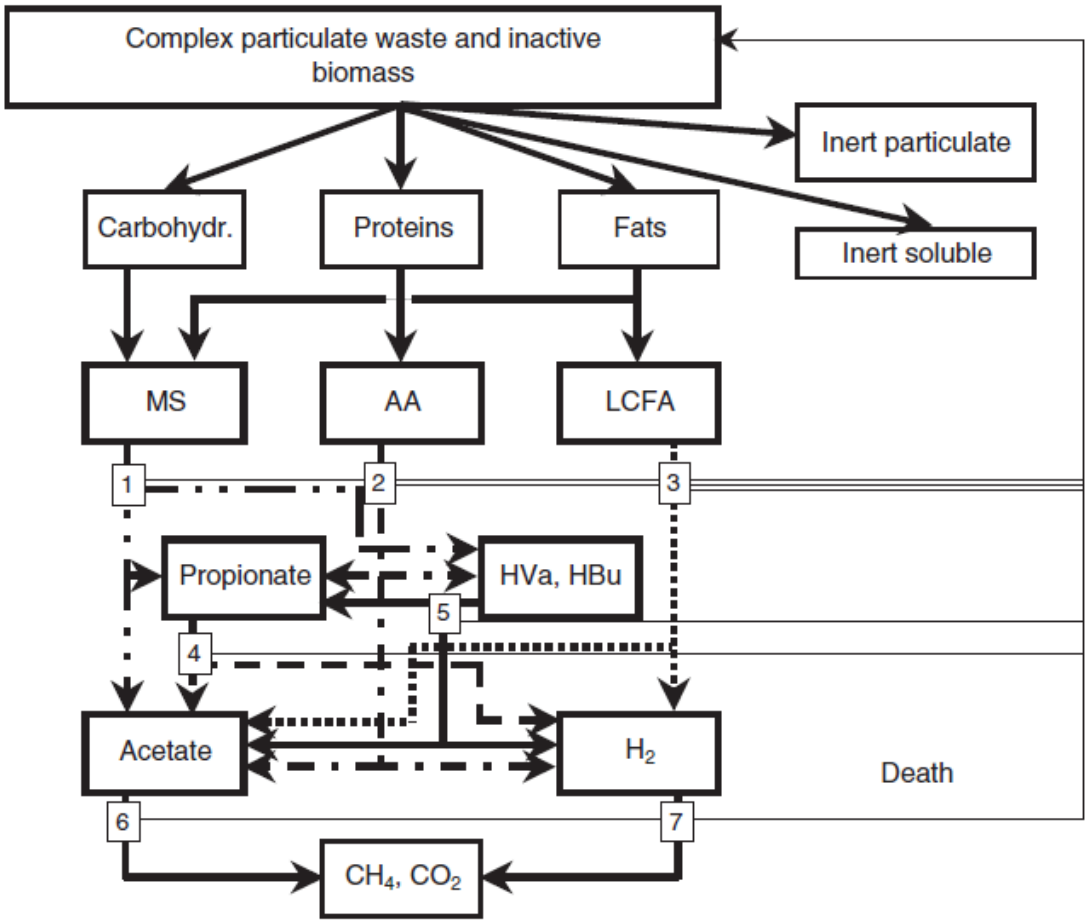

Figure 1.1. Simplified description of the ADM1 model process, which included (1) acidogenesis from sugars, (2) acidogenesis from amino acids, (3) acetogenesis from long chain fatty acids, (4) acetogenesis from propionate, (5) acetogenesis from butyrate and valerate, (6) aceticlastic methanogenesis, and (7) hydrogenotrophic methanogenesis. Picture reproduced from Batstone et al. (2002a).

The detailed description of the wastewater degradation presented in the ADM1 model presents limitations, mainly due to the large computational effort and non-identifiability of model parameters, e.g. a parameter estimation algorithm cannot fit such a high quantity of parameters within reasonable confidence levels (Ljung, 1999). Therefore, for large models like the ADM1, the task of model identification and validation is rarely performed, particularly for a diverse range of operating conditions.

To reduce model complexity, one approach is to lump several process steps into one, which reduces the number of state variables. Since the model complexity is directly associated with the number of microbial populations considered in its material balances (Bernard et al., 2001), a

minimal number of microorganisms that can adequately describe the AD process has to be selected for model simplicity. As a result, several reactions can be simply described in a single step, such as when a group of microorganisms convert complex organic matter into acetate. The AD process has been relatively successfully modelled considering the lumping of several kinetics steps into one (Bernard et al., 2001; Buffiere et al., 1995; Moletta et al., 1986; Rauch, Vanhooren, & Vanrolleghem, 1999). This technique was shown to be able to describe the main rate-limiting steps in AD, while maintaining a simple model structure. Furthermore, these simplified models often feature low computational effort and straightforward model identification and validation, key features for control purposes (Bastin & Dochain, 1990).

1.1.1.3. Biofilm Modelling

One important aspect that also has to be taken into account in MxC modelling is the multi-species biofilm (also called mixed populations biofilm). Wanner and Gujer (Wanner & Gujer, 1985, 1986) defined a multi-species biofilm as a "thin layer of fixed biomass composed of several microbial species which are subject to interactions, such as symbiosis or competition for space and, in some cases for common substrates". They linked the biofilm growth and composition with three main processes: (i) space limitation; (ii) substrate conversion, and; (iii) substrate diffusion (Wanner & Gujer, 1986). The ADM1 model did not take into account the growth of microorganisms in a biofilm, assuming ideal mixing, because not all AD reactors present a biofilm.

In terms of modelling mixed population biofilm formation, the nature of the process can lead to extremely complex model structures: Picioreanu et al. (Cristian Picioreanu, Kreft, & Van Loosdrecht, 2004) is an example where the mixed composition of the biofilm was modelled in 2-dimensions (2D) or in 3-dimensions (3D). The model was able to predict substrate consumption, concentration gradients, and the biofilm composition per biofilm position. The diffusion of several substrates and the growth of microorganisms were modelled using partial differential equations (PDEs). Once again, this complex modelling approach leads to large computational effort and numerous non-identifiable model parameters.

An alternative approach to complex biofilm models is to assume that some of the biofilm's main processes are non-limiting, and to use continuous mathematical functions to avoid the use of PDEs. A number of particular AD models consider the biofilm formation and the space limitation problem. One case includes the fluidised bed biofilm reactors (FBBRs) modelling, in which the biomass is attached and grows in a fixed bed (biofilm around the bed particles) while substrate flows through this bed (Lin, 2008). Buffiere et al. (1995) developed a steady state model for the FBBRs using a constant mass transfer resistance between the bulk and bed particles. They considered that each particle had a maximum diameter, set by system boundary conditions. However, no dynamic model was proposed based on the same concept. One technique to dynamically model the biofilm space limitation was later developed in Mu et al. (Mu, Zeng, Wu, Lou, & Tartakovsky, 2008). They adapted the biotransformation kinetics of the ADM1 for an upflow anaerobic sludge bed (UASB) reactor, and modelled the formation of methanogenic biofilm granules. They used a hyperbolic tangent function to describe biomass distribution within two zones (liquid and sludge), which defined the maximum attainable biomass concentration at each reactor position. This model was later validated with laboratory scale UASB reactor data (Tartakovsky et al., 2008b). A similar technique will be used in section 3, for the development of the MFC model biofilm growth.

A simplified description of substrate and product distribution within a biofilm (diffusion) can also avoid the use of PDEs, as shown by Rauch et al. (1999), with the assumption of a simplified layered biofilm structure. They assumed that substrate diffusion and biochemical conversion were decoupled, which allowed a simple relationship between substrate penetration depth and different homogeneous biofilm layers. Therefore, the system would present different biofilm layers occupied by different microorganisms, each layer relating to a specific substrate. Rauch et al.'s (1999) model was able to predict the overall dynamics of experimental data from the literature. This technique will be used in section 5, for the development of the MEC model. An illustration of this technique can be seen in the following figure:

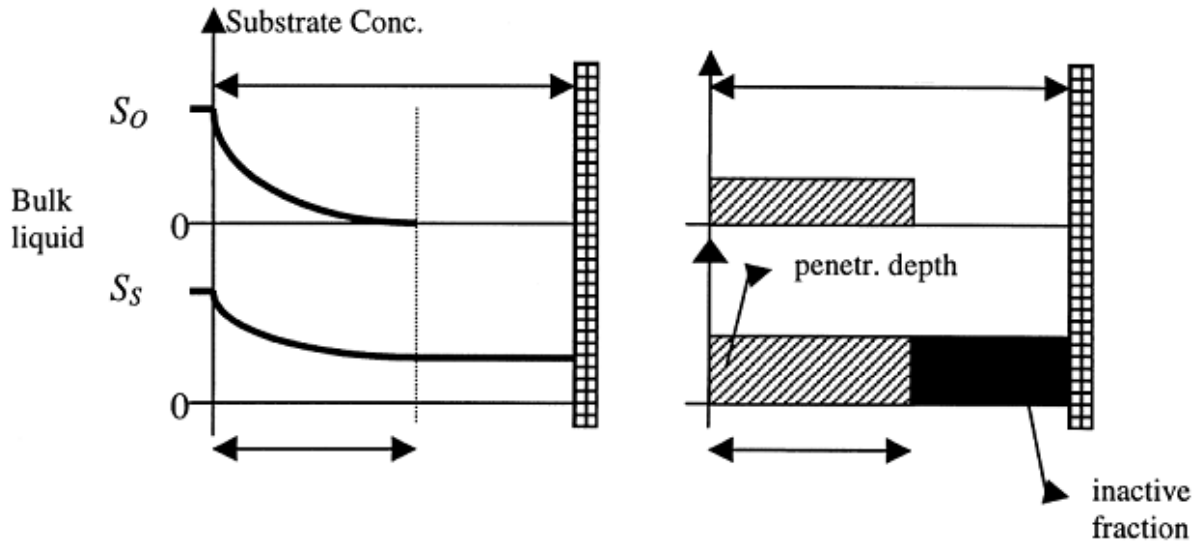

Figure 1.2. Diffusion limited reaction in a system with two substrates (S_S organic matter and S_O oxygen, the limiting substrate) and one microorganism. Picture reproduced from Rauch et al. (1999).

1.1.2. Modelling Fuel Cells

There are many similarities between fuel cells and MxCs (which are also fuel cells) specifically in their charge transport and electrochemical processes. Fuel cells are among the most promising non-petroleum dependent energy technologies and a large and diverse body of literature covers the subject (Biyikoglu, 2005; Yao et al., 2004; Yingru, Congjie, & Jincan, 2008). Because bacteria consume a substrate in a MxC, the thermodynamics and reaction kinetics should be considered differently than those of a regular fuel cell. On the other hand, mass and charge transport in fuel cells are similar to those of the MxC. This section will review the techniques used to model the electrons and mass transfer processes in fuel cells that are applicable to MxC models.

1.1.2.1. Maximal Ideal Voltage and Substrate Conversion

For the charge transport process, or electrochemical reactions, O'Hayre et al. (O'Hayre, Cha, Colella, & Prinz, 2006) proposed that the fuel cell's voltage output could be computed by the voltage predicted thermodynamically less some irreversible polarizations[2] in the fuel cell. Generally, the thermodynamic cell voltage prediction can be computed for whole or partial

[2] Note that the term polarization is here equivalent to the term losses.

limitations of the current by the rate at which the electroreactants are transported to the electrode surface. This can be described by the Nernst equation as follows ("Fuel Cell Handbook," 2005):

$$E_{thermo} = -\frac{\Delta G^0}{nF} + \frac{RT}{nF}\ln\left(\frac{\prod reactant\ fugacity}{\prod product\ fugacity}\right) \quad (1\text{-}4)$$

Since fuel cells operate at low pressures, the fugacity can often be approximated by the partial pressure of the components (Yao et al., 2004). Note that once the temperature and pressure of the system are constant, the fuel cell will present a constant thermodynamic maximum voltage. By neglecting irreversible processes occurring at open-circuit (fuel cell not connected to an external load), such as electrolyte crossover (Noren & Hoffman, 2005), the maximum thermodynamic voltage can be assumed to be experimentally equal to the open circuit potential ($E_{thermo} = E_{OCP}$).

Furthermore, the electricity produced in a fuel cell can be correlated with the consumption of a substrate in an electrode chamber during electrolysis through Faraday's law of electrolysis:

$$\dot{m}_{substrate} = MM_{substrate}\frac{I_{cell}}{mF} \quad (1\text{-}5)$$

1.1.2.2. Irreversible Voltage Losses

Once the fuel cell starts to deliver current to an external load, the output voltage drops from its maximum (E_{thermo}) due to irreversible losses, which are often separated in three major groups (Yao et al., 2004):

1. Activation losses (due to activation energies and electrochemical reactions)
2. Ohmic losses (due to resistance to the flow of ions in the electrolyte and electrode)
3. Concentration losses (due to mass transfer limitations)

Therefore, an electrochemical balance that can be used to compute the output voltage of a fuel cell can be written as (O'Hayre et al., 2006):

$$E_{output} = E_{thermo} - \eta_{act} - \eta_{ohmic} - \eta_{conc} \quad (1\text{-}6)$$

Each of these polarizations has a different magnitude for different current density degrees. At low current densities, activation losses (η_{act}) are dominant due to reaction energy barriers at the electrode-electrolyte interface, which need to be overcome to start the reaction. At high current densities, reactant and product diffusion limitations lead to high concentration losses (η_{conc}) (Noren & Hoffman, 2005). Finally, ohmic losses (η_{ohm}) increase linearly with current due to electron and ion conduction at the electrodes, electrolytes, contact resistance across each material's interface, and interconnections to electrodes. Note that the output voltage of a fuel cell is directly proportional to the cell current, following Ohm's law:

$$E_{output} = R_{ext} I_{cell} \tag{1-7}$$

The electrochemical balance can be better exemplified in a polarization curve, e.g. a plot of fuel cell voltage against current density. Fig. 1.3 represents a polarization curve for a fuel cell, with the regions of main losses clearly shown:

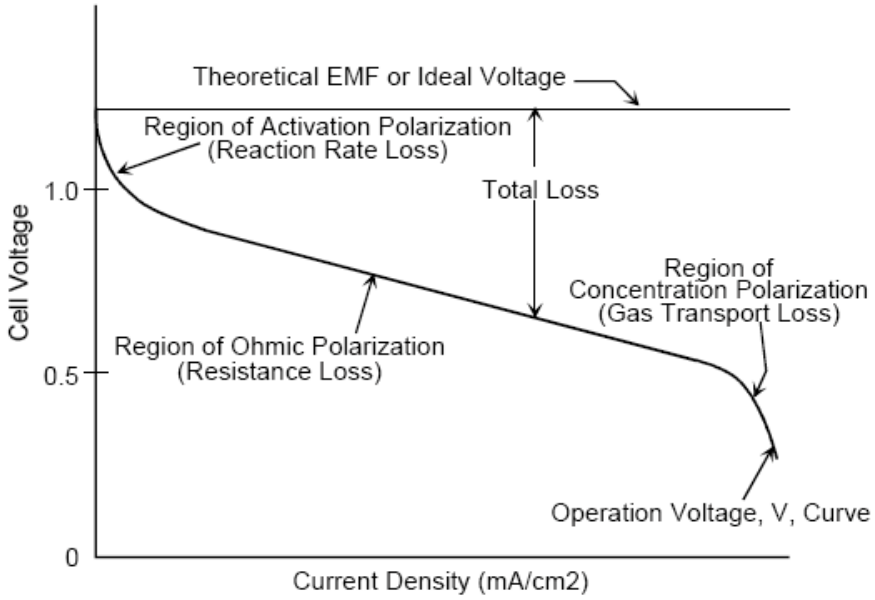

Figure 1.3. Theoretical voltage and actual polarization curves (voltage vs. current) for fuel cells. The three losses and their main causes are indicated in the curve. Picture reproduced from Fuel Cell Handbook ("Fuel Cell Handbook," 2005)

Furthermore, since activation and concentration losses are directly related to the reactions happening at the anode and cathode, these can be divided between anode ($\eta_{act,A}$, $\eta_{conc,A}$) and cathode ($\eta_{act,C}$, $\eta_{conc,C}$). The next sections will discuss each of these losses.

1.1.2.3. Activation Losses

The activation losses at each electrode of a fuel cell are governed by the Butler-Volmer equation (Noren & Hoffman, 2005):

$$I_{cell} = i_0 A_{sur}\left[\exp\left(\frac{\beta_1 mF\eta_{act}}{RT}\right) - \exp\left(\frac{-\beta_2 mF\eta_{act}}{RT}\right)\right] \quad (1\text{-}8)$$

The reduction (β_1) and oxidation (β_2) transfer coefficients are determined by the electron transfer processes at the electrode-electrolyte interface. These coefficients are directly related to electrode reaction mechanisms and are difficult to identify (Noren & Hoffman, 2005). The exchange current density in reference conditions (i_0) is a strong function of electrode materials, design, reactant and product concentrations, and temperature. It can be calculated using an Arrhenius-type relation:

$$i_0 = \Gamma\left(\frac{C_{Surface}^{reactant}}{C_{Surface}^{ref.-r.}}\right)\left(\frac{C_{Surface}^{ref.-p.}}{C_{Surface}^{product}}\right)\left[\exp\left(\frac{-E_{act}}{RT}\right)\right] \quad (1\text{-}9)$$

Three main explicit approximations of the Butler-Volmer equation are constantly used in the literature ("Fuel Cell Handbook," 2005). For large values of activation losses, at a range of $i/i_0 > 4$, this equation can be reduced to the Tafel equation:

$$\eta_{act} \cong \frac{RT}{\beta_1 mF}\ln\left(\frac{I_{cell}}{i_0 A_{sur}}\right) \quad (1\text{-}10)$$

For small values of η_{act} ($i/i_0 < 1$) it can be reduced to a linear relationship between current and activation losses, this reduction is often called “linear current-potential equation” as shown in O’Hayre et al. (2006):

$$\eta_{act} \cong \frac{RT}{mF}\left(\frac{I_{cell}}{i_0 A_{sur}}\right) \quad (1\text{-}11)$$

Finally, the Butler-Volmer equation can be further simplified once each reaction is assumed to occur in a one-step, single electron transfer. Under this assumption, the transfer coefficients are a

function of a symmetric factor (β_1 = 1-β and β_2 = β), often assumed to be 0.5 for fuel cells (O'Hayre et al., 2006). Therefore, for a symmetric reaction (β = 0.5) the Butler-Volmer equation can be represented as:

$$\eta_{act} = \frac{RT}{\beta mF}\sinh^{-1}\left(\frac{I_{cell}}{2i_0 A_{sur}}\right) \quad (1\text{-}12)$$

Note that, Noren & Hoffman (2005) have clearly demonstrated that Butler-Volmer approximations leading to Tafel and linear current-potential equations should be avoided in modelling and model analysis because they significantly diverge from the Butler-Volmer equation outside their range of applicability.

1.1.2.4. Ohmic Losses

Resistance to the flow of electrons and ions during the fuel cell operation generates ohmic losses. These losses increase as the current flow augments and this linear relationship obeys Ohm's law, therefore ohmic losses can be described by ("Fuel Cell Handbook," 2005):

$$\eta_{ohm} = R_{\text{int}} I_{cell} \quad (1\text{-}13)$$

The fuel cell internal resistance (R_{int}) represents the sum of the resistances offered at different sections of the reactor and can often be divided in electrode-electrolyte, ionic, and contact resistances. These components are extremely dependent on the reactor design and operational conditions, and are a key factor in fuel cell operation. As in any electric power source, the maximum power is drawn when the external resistance (R_{ext}) equals the power source's internal resistance (L. Woodward, Perrier, Srinivasan, Pinto, & Tartakovsky, 2010). Due to the R_{int} effect in the power production of MxCs, a number of studies to investigate the causes of MxCs' R_{int} have been presented. Liang et al. (Liang, Huang, Fan, Cao, & Wang, 2007) separated a MFC's internal resistance in cathodic, anodic and ohmic resistances. By using two different methods (current interrupt and steady discharge) each resistance term was computed for two air-cathode MFCs, one with the anode placed adjacent to the cathode, the other with an anode at a 4 cm distant from the air-cathode. These resistance terms were also calculated for a typical two-chamber MFC. They found extremely different values for the resistances for each MFC,

demonstrating the impact of reactor design and anode-cathode distance on these losses. Afterwards, Fan et al. (Fan, Sharbrough, & Liu, 2008) considered the internal resistance of MFCs to be part of anodic, cathodic, membrane (if present in the MFC), and electrolyte resistance. The contact resistance was neglected due to an assumption that it would be less the 1% of the reactor R_{int} in a "well designed MFC". A comparison between each internal resistance component for single and double chamber MFCs was made, showing the importance of each resistance factor. Furthermore, they showed that by decreasing the conductivity of the anode solution (from 200 to 50 mM), the electrolyte resistance contribution in the total internal resistance increases from 47% to 78%.

1.1.2.5. Concentration Losses

The reactants and products concentration of the fuel cell at the compartment bulk phase are often different than their concentration at the electrode surface. Due to consumption and formation reactions, reactants are sparse at the electrode surface, while products are abundant. This concentration gradient leads to a mass transport phenomenon that is controlled by diffusion. Since the current produced by the fuel cell is linked to the electrode reactions, the diffusion of reactants and products affects the fuel cell performance. This influence is called concentration losses (Cannarozzo, Grosso, Agnew, Del Borghi, & Costamagna, 2007).

The concentration losses contribute significantly to a decrease in cell potential, particularly at high current densities and low bulk reactant concentrations (Noren & Hoffman, 2005). These losses can be determined by the potential difference (ΔE) between the voltage at open circuit (bulk concentration, $E_{i=0}$) and the cell voltage at high current rates ($E_{i\text{-}high}$) ("Fuel Cell Handbook," 2005). So, the Nernst equation can be applied between the reactants concentrations in the bulk liquid and on the electrode surface, as:

$$\Delta E = \eta_{conc} = \frac{RT}{mF} \ln\left(\frac{C_{Bulk}}{C_{Surface}}\right) \tag{1-14}$$

Furthermore, the bulk (C_{bulk}) and the electrode surface ($C_{surface}$) concentrations can be related to the fuel cell current by Fick's law of diffusion:

$$I_{cell} = \frac{mF\overline{D}\left(C_{Bulk} - C_{Surface}\right)}{\delta} \tag{1-15}$$

In addition, one can define $I_L^{Reference}$ as the limiting reference current, e.g. the maximum possible current density, at which the maximum rate of reactants can be supplied to the electrode. By this definition, the $C_{surface}$ is zero at $I_L^{Reference}$. Now by applying Fick's law at the limiting reference current and by using Eq. (1-15) one can find ("Fuel Cell Handbook," 2005):

$$\frac{C_{Bulk}}{C_{Surface}} = \frac{I_L^{Reference}}{I_L^{Reference} - I_{cell}} \tag{1-16}$$

Therefore, the concentration losses can be written as a function of fuel cell current and its limiting reference current:

$$\eta_{conc} = \frac{RT}{mF}\ln\left(\frac{I_L^{Reference}}{I_L^{Reference} - I_{cell}}\right) \tag{1-17}$$

1.1.3. Modelling MFCs

Few MFC models have been reported in the literature. This section will evaluate each of these models. Furthermore, an MEC model capable of simulating hydrogen production from complex organic matter has not yet been reported.

1.1.3.1. Mono-Population Bulk MFC Model

The earliest published MFC model was presented by Zhang and Halme (X. C. Zhang & Halme, 1995) and considered the use of external mediators to transfer electrons. This study used a batch MFC with 2-hydroxy-1,4 naphthoquinon (HNQ) as an exogenous mediator for the electron transport. The purpose of this model was to establish a relationship between power output and the external mediator concentration. This dynamic model combined biochemical reactions and an electrical circuit balance. Zhang and Halme (1995) modelled the biological processes in the MFC by Monod-type equations and the reaction between metabolites and mediator (redox) as first order reactions. All transport processes were assumed to be faster than the biochemical and redox

reactions and thus were not considered. For the electrochemical balance, they considered the Nernst equation for the maximal ideal voltage, and activation losses were assumed to be a first order linear function of current. Furthermore, ohmic losses were calculated with Ohm's law, while concentration losses were neglected. Finally, the MFC current output was linked to chemical reactions through Faraday's law of electrolysis.

Although this work presented a simplified fast convergence model, it has many limitations. For example, it does not consider multi-population microbial consortium in the MFC, it considers first order reactions between metabolites and mediators, and assumes suspended cells instead of biofilm. In addition, the electrochemical balance neglects concentration losses even though experimental results of MFCs clearly present this behaviour (see for example (Martin, Savadogo, Guiot, & Tartakovsky, 2010; Tartakovsky, Manuel, Neburchilov, Wang, & Guiot, 2008a)).

The use of external mediators is another main limitation of this model: at the time of publication, MFCs were believed to only be able to operate with the addition of toxic external mediators. However, a breakthrough discover by Kim et al. (H. J. Kim et al., 2002), showed that some microorganisms were able to transfer electrons to an electrode naturally, therefore the addition of external mediators was proven to be unnecessary. As a result, exogenous mediators are no longer added to MxCs because of their toxicity and cost (Bond et al., 2002).

The natural process of electron transfer by microorganisms is an important subject to be investigated and optimised in MxC operation, since these processes can directly affect the operation performance of the MxC. Intense research is ongoing in this area (e.g. (B. E. Logan & Regan, 2006a; Reguera et al., 2005; C. I. Torres et al., 2010)) and up to now, three forms of naturally occurring electron transfer mechanisms have been reported: direct contact, nano-wires, and endogenous mobile electron shuttles. Due to the direct impact on current production, the electron transfer mechanisms have to be included in any MxC model that simulates current production.

Another mono-population bulk MFC model was presented by Zeng et al. (2010). They developed a fast convergence MFC model for control proposes. Time varying overpotentials at the anode

and cathode were incorporated into the reaction rate equations to simulate the electrochemical balance. Two cases were studied: First an acetate fed MFC and second a MFC fed with sWW (solution of glucose and glutamic acid). Sensitivity analysis of the model parameters was used to indicate identifiable model parameters for both cases. Six and five model parameters were respectively estimated for the acetate and WW fed cases, by minimizing the absolute differences between measured and simulated voltages. Steady state analysis was used to compare experimental and predicted results, with a good agreement for the acetate case, while the WW case presented relatively large deviations. Furthermore, a dynamic simulation of the acetate-fed model was performed to study the effects of step changes on the feed concentration variations and on a periodic switching feed flowrate operation.

The modelling method shown by Zeng et al. (2010) represents an interesting alternative to describe MFCs with a simple set of ODEs identifiable model. However, important aspects of the system were not taken into account as the model did not consider the formation of biofilm in the anode (suspended biomass) and it assumed that all microorganisms present in the anode were accounted by one parameter (biomass), even for the WW case. Moreover, this modelling method did not consider any diffusion limitations, or the competition between microorganisms for substrate or space.

1.1.3.2. Anodic MFC Biofilm Models

More than ten years after the first MFC model publication, Marcus et al. (2007) developed a model for the MFC biofilm describing the anode potential losses of electricigenic bacteria that transfer electrons through a solid conductive matrix. This model had a detailed description of bio-electrochemical reactions in the anode of the MFC and was used to study the limitations of the biofilm by electricigenic bacteria concentration and local potentials. The biofilm and the solid conductive matrix built by microorganisms were labelled “biofilm anode” and this model attempted to correlate the MFC electrical load with the matrix conductivity. The steps that were assumed to occur in the anode biofilm were modelled as: (i) the acceptance of electrons by the biofilm matrix from biofilm bacteria, and; (ii) the conduction of electrons to the anode. The authors derived a Nernst-Monod expression, which described the relationship between the rate of substrate utilization and two variables: substrate concentration and electrical potential. The

Nernst-Monod equation was then linked with the matrix conductivity using a steady-state substrate and electron balance, Ohm's law, and a dynamic biomass balance. Their biofilm was composed of two types of biomass, inert and active, both competing for space on the surface of the anode. Marcus et al.'s (2007) contribution lies in correlating the conductivity effects of the biofilm with the power generation of the MFC. This model did not consider reaction rates, diffusion limitations, activation losses, ohmic losses, concentration losses, or the existence of several microbial populations in the anodic compartment competing for the same substrate.

Further research has been done following Marcus et al.'s (2007) model. Torres et al. (Cesar I. Torres, Marcus, & Rittmann, 2008b) developed an experimental setup to successfully demonstrate that this model was able to represent anode potential losses. Two main steps were hypothesised to limit the current generation: proton (H^+) and substrate transport through the biofilm matrix. However in subsequent work, Torres et al. (2008a) found experimentally that only H^+ transport appears to limit the current generation. Furthermore, they hypothesised that other processes not accounted for in Marcus et al.'s (2007) model might restrict current production in MFCs. Therefore some other processes of the MFC operation must be considered and modelled in attempting to optimise the power density of an MFC.

Following these results, a new model was developed by Marcus et al. (Andrew K. Marcus, Torres, & Rittmann, 2011) to describe the limitations of alkalinity (pH) in the MxC current density. A balance of the H^+ was linked to the production of acid or base, a methodology based in relating slow microbial reactions to fast aqueous acid/base reactions. Finally, a review of the kinetics of the electrons transfer process was presented by Torres et al. (2010). They analysed extracellular electron transfer mechanisms (direct electron transfer, electron shuttles, and solid conductive mechanisms) and correlated activation, ohmic, and concentration losses with these processes. These modelling efforts attempted to analyse the diverse electron transfer mechanisms and their limiting steps; it did not consider the microorganism's competition for substrate.

A MxC anode model was developed by Hamelers et al. (Hamelers, ter Heijne, Stein, Rozendal, & Buisman, 2011) to describe the kinetics of electricigenic microorganisms. This model was compared with the model in Marcus et al. (2007) and presented significantly better results. They

assumed that the electrode's potential dependency on the electrochemical reaction was described by a Butler-Volmer model. Furthermore, the redox component acting as electron acceptor and donor were assumed to be the same, i.e. the effects of any intermediate process did not affect the rate of reaction. Finally, a constant total amount of mediator was assumed per cell, varying between oxidised and reduced form. This methodology can be better described by the following figure:

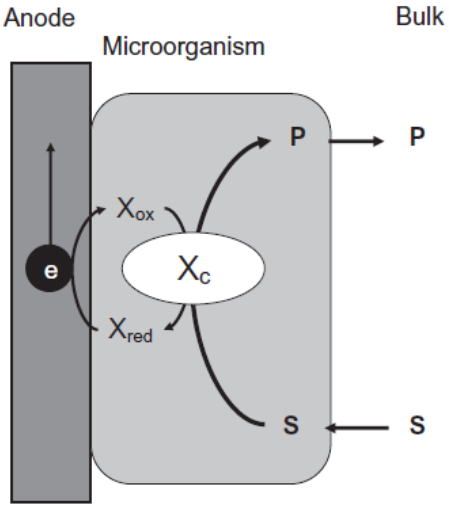

Figure 1.4. Reproduction of the MxC anode model developed by Hamelers et al. (2011). Picture reproduced from the article (Hamelers et al., 2011).

A very similar technique to describe the electron transfer mechanism will be used in sections 3 and 5 for the model development in this thesis. However, the electron transfer mechanism presented in this thesis was developed independently (at the same time) from the one presented by Hamelers et al. (2011).

1.1.3.3. Three Dimensions MFC Model

Another MFC model was presented by Picioreanu et al. (2007), with the development of a 3D model of an anode biofilm of a MFC. This model was based on the biofilm model developed for AD in Picioreanu et al. (2004) and its principal goal was to analyse the thickness and distribution of the biofilm as a function of local potential. This model presented a detailed description of several processes occurring in the MFC anode by dividing each process into the following sub-models (Figure 1.5): electrochemical reactions, biochemical reactions of methanogenic and electricigenic communities, biofilm formation, mass transport, reactions in biofilm, and reactions in bulk liquid.

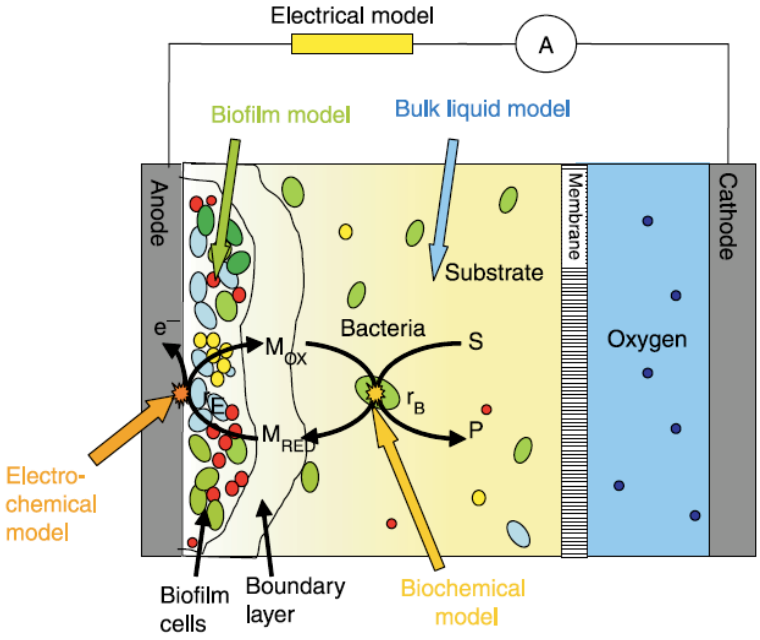

Figure 1.5. Reproduction of the model developed by Picioreanu et al. (2007). Picture reproduced from the article (C. Picioreanu et al., 2008) .

In Picioreanu et al. (2007), the electrochemical balance was represented by activation losses (Butler-Volmer equation), concentration losses, and ohmic losses. Biochemical reactions occurring both in the biofilm and suspended cells were based on the ADM1 model. The bulk liquid model used mass balances to determine solute and suspended biomass concentrations through time. Finally, the biofilm was modelled in two different parts: solute and biomass. The first part used a system of PDEs that related diffusion and reaction rates to locate solute distributions in the biofilm. The second part treated the spatial distribution of microorganisms in the biofilm using growth, division, and an empirical shoving algorithm of biomass particles.

The model proposed by Picioreanu et al. (2007) was the first to consider two populations competing for the same substrate (methanogens and electricigens competing for acetate), however it required complex numerical procedures: the 3D model version took around 14 hours to converge while the 1D took about 6 minutes (Cristian Picioreanu et al., 2007). These complex numerical procedures required for model solution make the model unsuitable for process control purposes and parameters estimation. In addition, because parameters were not estimated, electricigenic and methanogenic maximum specific rate constants were assumed to be the same,

which directly affects the growth competition results (Harmand et al., 2008). Furthermore, this model had no description of the cathode compartment and it considered exogenous mediators instead of the three known processes of natural electron transfer.

A next step taken by the same research group was to expand the MFC model to WW degradation. This was presented in Picioreanu et al. (2008), where the MFC model was integrated with the ADM1, for the conversion of glucose into propionate, acetate, hydrogen, methane, and electricity. Six different microbial populations were simulated, while the redox mediators were assumed to be soluble in the bulk phase. The electrochemical balance, diffusion coefficients, and electricigenic parameters were based on the previous MFC model (Cristian Picioreanu et al., 2007), while kinetic and stoichiometric parameters for acidogenesis, acetogenisis, and methanogenesis were taken from the ADM1. Model predictions presented similar characteristics to batch experimental MFC polarization curves, even with the complex model structure, large computational effort, and numerous unknown parameters of the model. Once more, electricigenic and methanogenic maximum specific rate constants were equal.

An extension of this MFC model was used to evaluate the reactor performance for a range of pH and electrode geometry in Picioreanu et al. (Cristian Picioreanu, van Loosdrecht, Curtis, & Scott, 2010b). This model used Nerst-Planck fluxes of ions with an ionic charge balance to account for pH variation, while mass transport by convection and liquid flow over biofilm and electrodes were modelled to account for different geometries. Three cases were simulated: single electricigenic microorganisms (either planar or porous electrode), and multi-species WW degradation with a planar electrode. The model follows most of the previously presented assumptions (Cristian Picioreanu et al., 2007) with some exceptions: the mediator diffusion was not considered, and electricigenic and methanogenic microorganisms were represented by the same microbial population. The external electron shuttle mediator was assumed to be thionine and two domains were simulated: bulk liquid and biofilm. In this work, model predictions were not compared with any experimental results and were only discussed qualitatively. Once more, the complex PDEs model presented several unknown parameters and large computational effort. The authors recognised the complexity of the model and point out that “a main obstacle” for it would be a model identification step, especially for the multi-species case.

An attempt to model MxCs in a simpler manner was presented in Picioreanu et al. (Cristian Picioreanu, Katuri, Van Loosdrecht, Head, & Scott, 2010a). They proposed a suspended biomass, no biofilm, and single population model with external mediators to transfer electrons. The inclusion of known electron transfer mechanisms, such as direct contact or nano-wires in the model, was intended to be presented in future studies. Two reactions were assumed to take place in different spatial compartments: (i) the oxidation of organic substrate in bulk liquid by a mediator, and (ii) the mediator oxidation at the anode surface releasing electrons. The cathode reactions were not included in the model. The concentration of substrate and mediator was assumed to vary between bulk and anode surface through diffusion in a mass transfer boundary layer, which lead to a system of PDEs. Finally, the electrochemical balance considered activation and ohmic losses, while the diffusion layer allowed the calculation of the elements at the electrode surface, i.e. no need for concentration losses. Coulombic efficiency and substrate yields were fitted from current-time and charge-time plots from an MFC experiment with thionine as the external mediators.

Although this paper presented an excellent alternative for a simpler MxC model structure, many assumptions may limit its application. The assumptions of external mediators and single suspended microorganisms are considerable drawbacks. As discussed in sections 1.1.1 and 1.1.3.1, WW treatment always contains multiple microbial populations in a biofilm and no modern MFC experiments use external mediators. Furthermore, these simplifications and assumptions did not avoid a system with PDE, which leads to long computational times, and only two model parameters were fit to experimental data (no objective function was minimised), with all substrate consumption and growth rates being assumed from other papers.

1.1.3.4. MFC Model Comparisons

A comparison of all available MFC models reviewed in this section shows that either the models do not include important process aspects of MxC operation or are too complex to be easily solved. This aspect can be clearly seen in table 1-1, which summarises the characteristics of the different models. Note that most of the model extensions, presented in subsequent papers from

the same research groups, were not included in the table, except for the simpler version of Picioreanu et al.'s (2010a) model.

Table 1-1: Comparison of characteristics included in all available MFC models.

Model	Type of MFC model	Multi-population	Biofilm	Ease of convergence
Zhang and Halme (1995)	Anode and Cathode	No	No	✔
Zeng et al. (2010)	Anode and Cathode	No	No	✔
Marcus et al. (2007)	Only Anode	No*	✔	✔
Hamelers et al. (2011)	Only Anode	No	✔	✔
Picioreanu et al. (2007)	Anode and Cathode	✔	✔	No
Picioreanu et al. (2010a)	Anode and Cathode	No	No	No

*This model assumed inert and active biomass competing only for space on the anode surface

This table indicates if these models included: anode and/or cathode description, multi-populations competing for space and substrate, an assumed biofilm or suspended biomass, and whether the models would demand large computational effort to be solved (ease of convergence). The necessity of a fast convergence multi-population MxC model becomes clear after this comparison. Therefore, one of the objectives of this thesis is to develop a fast convergence, multi-population, biofilm model of the anode and the cathode of MFCs and MECs.

1.2. MFC Process Improvement

After a model is developed and validated, it can be applied. One possibility is to use the model to understand process configuration and improve its design. A large number of model-based applications exist for process design and optimisation. Although no articles have presented model-based optimisation strategies for MxCs, this section will present a number of these strategies that could possibly be applied to improve MxC design and operation.

Another possible alternative to improve the performance of MxCs is to operate the reactor at optimum operating conditions. This can be done by first determining the optimum operating

conditions and then by maintaining the process on these conditions. Strategies to determine optimum operating conditions for MxCs will be also evaluated in this section.

1.2.1. Reactor Design

Most studies of MxCs are at the experimental level and use batch-fed reactors. However, the continuous feed is usually a more attractive option because it provides a constant rate of microbial metabolism with substrate concentration and other conditions also remaining constant. Continuous processes provide constant environmental conditions for growth and supply uniform-quality products. In a continuous process, the rate of bacterial growth and metabolism increases in direct proportion to the rate at which fresh nutrients are added to the system until it reaches a maximum limit, following Monod dynamics (Shuler & Kargi, 1992).

Due to diverse design possibilities (Bruce E. Logan & Regan, 2006b) and a low number of experimental results, an optimal MxC design and its configurations are still unknown. Hence, *a priori* knowledge of the process can replace trial-and-error techniques, reduce development time and cost, and improve process performance (Galvanauskas, Simutis, Volk, & Lubbert, 1998). Galvanauskas et al. (1998) developed a conceptual framework to enhance process design for models that describe a system only under specific situations, but with high accuracy. Within their framework, the model must describe specific process characteristics that significantly affect process performance. This technique was successfully used for model-based enhancement in diverse bioprocesses (Georgieva, Hristozov, Pencheva, Tzonkov, & Hitzmann, 2003; Levisauskas et al., 2003; Levisauskas, Galvanauskas, Simutis, & Lubbert, 1999) and could be implemented to enhance a continuous feed MxC design.

1.2.2. Stack Operation

MxCs used for energy production are often linked together (stacked) because a single MxC typically produces a working voltage of only 0.2-0.3V (Oh & Logan, 2007). The same situation occurs in hydrogen and solid oxide fuel cells; single cells are assembled in a series or in parallel for better performance. Because MxC stacks are a relatively new technology, there remain many unanswered questions about its optimal design. To answer such questions, a model can be used to understand the process and optimise the design of the stack.

Wilkinson (2000) developed a 6-cell stack to digest food residues, where the cells were positioned in series. Aelterman et al. (2006) reported that a continuous feed 6-cells stack in series or in parallel increased the voltage to 2.2V (255 mA). However, the stack design presented the problem of voltage reversal, further examined by Oh & Logan (2007) with a 2-cells stack. They found that bacteria were not the cause of the voltage reversal, as the same phenomenon happened in a sterile MFC stack. Liu et al. (Z. Liu, Liu, Zhang, & Su, 2008) reported a novel configuration for stacks where the voltage output was doubled. The performance increase was attributed to better cation transfer and due to smaller stack internal resistance.

1.2.3. Staging

It is well known that when the substrate consumption is described by Monod kinetics, the reaction proceeds more rapidly in a PFR than in a CSTR (Eddy, 2003; Shuler & Kargi, 1992). This means that more substrate can be consumed in the PFR rather than using a CSTR with the same volume. In the case of MxCs, where the continuous mode is more advantageous to use (see section 1.2.1), it is recommended to use reactors in series to approach the results of plug-flow operation (Shuler & Kargi, 1992), with the first stages converting the substrate at high rates, and the final stages polishing the effluent to a specific requirement demand, a technique often called staging (Van Lier, Van Der Zee, Tan, Rebac, & Kleerebezem, 2001). Staging is often applied in WW treatment and a model of the process and information about reaction kinetics are required to apply staging techniques. As shown in Scuras et al. (Scuras, Jobbagy, & Leslie Grady C.P, 2001), the benefits of staging are only attractive for systems that are kinetically limited and/or for systems in which the effluent composition must be maintained at a low requirement.

Staging optimisation was effectively applied to activated sludge reactors by Scuras et al. (2001). The operation of three tanks in a series was compared with one tank, proving to have better results. Following these results, a procedure to determine the optimum number of CSTR reactors in a series was presented.

Van Lier et al. (2001) used the same staging optimisation concept for anaerobic wastewater treatment. Staging reactors proved to be advantageous under non-optimal temperature conditions as well as during the treatment of chemical wastewater. Later on, Gray et al. (Gray, Hake, &

Ghosh, 2006) used an AD model to predict the influence of staging, mean cell residence time, and thermophilic temperature. They compared a one-stage to a two-stage process, the latter showing the best results. Staging for MxCs will be further analysed in section 4.4.

1.2.4. Cogeneration

A model that describes the dynamics of multi-populations in an MxC can also be used to plan systems that integrate wastewater treatment, electricity (MFC), hydrogen (MEC) and/or methane (methanogens in the anode chamber of the MxC) production. Cogeneration is already widely exploited in fuel cell systems (O'Hayre et al., 2006) and in AD reactors. Cogeneration for MxCs will be analysed in detail in sections 4.4 and 6.3.

The heat from fuel cells that operates at high temperatures is used either to produce hot water or low-pressure steam in cogeneration systems ("Fuel Cell Handbook," 2005). For AD systems, the electricity can be generated from the high calorific content of municipal solid waste. Some gaseous products from an AD consist of up to 65% methane and can be combusted in a cogeneration unit, producing green energy (Siddharth, 2006).

Another important aspect that should be studied in an MxC cogeneration unit is the balance of microbial populations in the biofilm. This characteristic has been studied in depth for AD models that present multi-species biofilm, and these systems often present a phenomenon called “competitive exclusion” (Hardin, 1960). This principle states that the competition for the same substrate in the same ecological niche by two species will lead to the extinction of one of the two species. Harmand et al. (2008), simulated this phenomenon for several microbial populations competing for the same substrate in bioreactors. They showed mathematically that the “Competitive Exclusion Principle” (CEP) will occur in a bioreactor depending on the kinetics of the microorganisms, i.e. similar kinetics (e.g. Monod) for growth rate are required to cause this type of exclusion. Following this principle, Zeng et al. (R. J. Zeng, Yuan, & Keller, 2003) used available AD models to study the balance of multi-population microorganisms under various operational conditions in enhanced biological phosphorus removal systems. They developed operating strategies that allowed the growth of desired microorganisms. Furthermore, Whang et al. (Whang, Filipe, & Park, 2007) used experimental and model results to analyse the competition

between polyphosphate-accumulating and non-polyphosphate microorganism populations for organic substrate in enhanced biological phosphorus removal systems. It was shown that depending on the reactor's operating temperature and on the microorganisms' maximum specific substrate uptake rate, different populations may dominate the reactor.

Diverse experimental results from MxCs reveal the effects of operating conditions on the multi-species biofilm composition. In particular, operating conditions affect the balance between methanogenic and electricigenic microorganisms in the biofilm (Ishii, Hotta, & Watanabe, 2008). Since these microbial populations compete for acetate, this competition has a direct impact on the MxC current production and on long-term optimal performance. The influence of organic load, pH, and temperature on the biofilm concentration of a multi-species MFC was analysed by Martin et al. (2010). In this study, the ratio of methane to electricity production was shown to strongly depend on operating conditions. They derived expressions to describe the power and methane dependence on substrate concentration; power was better described by a Haldane-like expression, while methane was described by a Monod-like dependence.

Furthermore, there is a significant body of evidence correlating the R_{ext} at which the MFC operates with the microbial communities of the biofilm. Aelterman et al. (2008) observed the impact of R_{ext} on electricity and methane production in a MFC inoculated with a mixed anaerobic culture and concluded that low methane production and stable power output are only obtained if R_{ext} is set close to the MFC internal resistance. Furthermore, Chae et al. (2010) compared methanogenic activity and methane production in MFCs subjected to several external perturbations (pH, temperature, oxygen exposure, addition of a methanogenesis inhibitor, and R_{ext} variation). They concluded that electricity production was increased and methane production was decreased only when a methanogenesis inhibitor (BES, 2-bromoethanesulfonate) was added to the anodic chamber or by setting a R_{ext} close to the R_{int} values. The results presented in Lyon et al. (Lyon, Buret, Vogel, & Monier, 2010) corroborated with the experimental evidence above. In this study the microbial composition of diverse biofilm samples from MFCs inoculated with the same sludge and operated at different R_{ext} values were analysed. By using Ribosomal Intergenic Spacer Analysis, they demonstrated, based on the profiles observed, that the microbial community structure in the biofilm of a MFC operated at R_{ext} appreciably above R_{int} (1 kΩ and 10

kΩ) was significantly different from that observed in the MFC operated at low R_{ext} (10 Ω, 100 Ω, and 470 Ω). The results presented above (Aelterman et al., 2008; Chae et al., 2010; Lyon et al., 2010) qualitatively show that a selection of a low R_{ext} promotes growth and metabolic activity of the electricigenic microorganisms because electron transport to the cathode is facilitated. However a R_{ext} lower than the MFC's R_{int} value leads to a low power output, i.e. an optimal R_{ext} value should always be maintained. Note that, all of the experiments mentioned above were carried out by manual adjustment of R_{ext} without using any real-time algorithm, which would guarantee timely correction of R_{ext}. The validity of the CEP and the effects of R_{ext} selection on the biofilm formation for MxCs will be evaluated in detail in this thesis (Sections 4 and 6).

1.2.5. Optimizing Operating Conditions Using Laboratory Experiments

During the operation of an MxC, the principal variables to be optimised and controlled are temperature, pH, substrate flow and concentration, residence time, and external load. Of those listed above, it may be most important to control the external load and a later section will specifically address the control of this variable.

Laboratory experimentation often presents one option for evaluating appropriate (but not optimum) operating conditions, and several research groups use this strategy broadly to evaluate the performance of MxCs under diverse operating conditions. Laboratory experiments frequently provide concrete conclusions about system performance, although this alternative is costly and slow. Furthermore, examining the numerous potential operating conditions may be impractical, due to a large number of possibilities. Therefore, these studies often only present trends of the operating conditions' effect on the performance of the MxC without identifying the optimal operation point. Several studies have analysed the effects of carbon source, pH, organic load, residence time, temperature, and external load on the performance of MFCs and a number of these studies are presented in this section. Note that a deep analysis of these studies goes beyond the scope of this thesis, and therefore only an enumeration of their main results is presented in this section.

One of the first studies on the operating conditions of MFCs was presented by Geun-Cheol et al. (Geun-Cheol et al., 2003), where the effect of pH, external resistance, electrolyte used, and

dissolved oxygen concentration in the cathode compartment on current generation were studied. By analysing MFC results from a 3-year period they determined the rate-limiting factor for different modes of operation. The same research group later presented a study on the effect of residence time on carbon source removal and electricity production in MFCs (Moon, In, Jae, & Kim, 2005). By comparing MFCs with different anode designs, they concluded that the resident time is an important factor to be considered in reactor design. Liu et al. (H. Liu, Cheng, & Logan, 2005) examined the effects of a solution ionic strength, electrode spacing and composition, and temperature on MFC performance. They demonstrated that temperature (32 or 20 ºC) did not have a large impact on current density, while solution ionic strength and electrode spacing directly affected power generation. An in-depth study of the effects of pH on the MFC performance was presented by He et al. (He, Huang, Manohar, & Mansfeld, 2008). By analysing a multi species MFC at several pHs (varying from 5 to 10) they found "that the anodic microbial process preferred a neutral pH". Operation condition effects on performance were also studied by Jadhav & Ghangrekar (2009). They presented results of current generated from a sWW fed MFC operating at different temperatures (20–35 °C and 8–22 °C), pHs (5.5 to 8.5), external resistance (50 Ω, 100 Ω, 500 Ω, or 1000Ω), and organic loads.

1.2.6. Optimizing Operating Conditions Using Model Based Strategies

A second alternative to determine the optimum MxC operating conditions is a model based strategy, where a mathematical model is used to predict the behaviour of the MxC. This modelling alternative can be more advantageous than the experimental one since it is faster and less costly in comparison, however modelling mistakes or wrong hypotheses may lead to errors between model predictions and reality. Therefore, to be successful, this strategy needs to follow a clear methodology of model development, estimation, and validation. A detailed description of the methodology used to develop a model will be presented in chapter 2. So far, to our best knowledge, no work has been reported on model based optimisation of operating conditions for MxCs. However this field has been largely studied for fuel cells and for AD, and some examples of model based optimisation will be enumerated.

Model based optimisation of operating conditions for AD is essential because some model parameters vary over operation due to microorganism metabolic variations. Kim et al. (H.-W.

Kim, Shin, Han, & Oh, 2007) studied the effects of food waste composition on AD from sewage sludge and food waste. By analyzing various substrate mixtures, methane production rate and methane potential through a response surface model, they suggested how to improve the efficiency of the process. Lopez & Borzacconi (2010) used a previously developed AD model to study and evaluate the AD performance on degradation of ruminal contents. Key model parameters were determined using batch experiments, and model simulations were used to find adequate operating conditions for methane production and reactor flow rate.

Model based optimal operating conditions were studied for solid oxide fuel cells in Aguiar et al. (Aguiar, Adjiman, & Brandon, 2004). After developing a dynamic model of the stacked system, the impacts of fuel variations, air inlet temperatures, average current density, and fuel flow configuration on the steady-state performance of the cell were studied. An additional study using a model-based approach was presented by Wu et al. (Wu, Liu, & Fang, 2006). Based on a model developed for hydrogen polymer electrolyte fuel cell, they studied the effects of cell temperature, cathode material, cathode gas pressure, and cathode relative humidity on efficiency of the cells. An optimisation software was used to determine the best operating conditions under different system assumptions.

1.2.7. Choice of External Load

The external load control is challenging because variations in biological activity during MxC operation can change the R_{int} (section 1.1.2.4) and as this variable changes, the MxC optimal external load (R_{ext} for MFCs and $E_{applied}$ for MECs) may change as well. An incorrect selection of R_{ext}, either larger or smaller than the internal resistance, may lead to large losses in power output for MFCs. For commercial operation of MxCs, the task of selecting a proper $E_{applied}/R_{ext}$ becomes an imperative requirement, because R_{int} may vary with changes in operating parameters such as temperature, pH, influent strength, and influent composition. Note that for wastewater treatment, these operating conditions may fluctuate on a daily basis (Eddy, 2003). Chapter 6 will investigate the relationship between the optimum external load (R_{ext} for MFCs and $E_{applied}$ for MECs) and the reactor internal resistance, demonstrating that for MxCs, the optimum external load may not always be the same as R_{int}.

A simple technique often used to estimate the internal resistance of MxCs is to compute the linear slope of a polarization curve (Aelterman et al., 2006). This technique provides a reasonable approximation of R_{int}, although activation and concentration losses may slightly affect the polarization curve's linear slope (Fan et al., 2008). However, to build a polarization curve one needs to disturb the system, changing the external load during operation (often varying it from a large to a small value), so this technique becomes impractical for commercial MxC operation.

A second alternative to maintain the process at its optimum external load is to use non-model based control strategies, often named model-free algorithms. This alternative is often used to control complex systems, which can be difficult to model. Although this option is simple to apply and often does not require much process knowledge, it does not provide any information about the system's behaviour. Variations on the controlled variable may be visible trough the model response, but they cannot be correlated to their causes as can be in a model based approach. Some of these model-free strategies have been applied to MFCs and will be reviewed in this section.

The first model-free application for MFCs was presented by Woodward et al. (L. Woodward, Perrier, Srinivasan, & Tartakovsky, 2009b). Using two continually fed MFCs, the real time maximization of power output (MPPT) was successfully demonstrated. Experimental results showed fast convergence towards the optimal P_{MFC} and stability during temperature perturbations. The algorithm used in this study was the multiunit (MU) developed by Srinivasan (2007). The MU method assumes the presence of two identical units, operated with offset input values (R_{ext} in Woodward et al. (2009b)) between them. The input values for each unit are: $R_{ext,1} = R_{ext} - \Delta/2$ and $R_{ext,2} = R_{ext} + \Delta/2$, while the gradient is estimated by finite differences between both units as:

$$\hat{g}(k) = \frac{P_{MFC,2}(k) - P_{MFC,1}(k)}{R_{ext,2}(k) - R_{ext,1}(k)} \tag{1-18}$$

Finally, the extremum seeking controller is given by:

$$\frac{\partial R_{ext}}{\partial t} = k\hat{g}^{T}(R_{ext}) \tag{1-19}$$

Once the algorithm converges, the maximum distance between the equilibrium point and the optimum is given by Δ. Therefore, a smaller Δ can be used to be closer to the optimum. A detailed description of the MU algorithm can be found in Srinivasan (2007). A main limitation of the MU method presented above is the requirement of two identical units. An improved MU algorithm was presented in Woodward et al. (2009b) where corrections for non-identical units were developed, as previously presented by Woodward et al. (Lyne Woodward, Perrier, & Srinivasan, 2009a). These corrections took account of static differences between the MFCs.

Following these results, Woodward et al. (2010) developed and compared the performance of three different model-free MPPT algorithms for an MFC: perturbation observation (P/O), the gradient method, and MU method with corrections for different units. Based on experimental results from two continuous acetate fed MFCs, the advantages and limitations of each method were illustrated. The P/O and MU methods successfully converged to the optimum for both MFCs and tests involving variations on temperature and influent concentration were performed to compare the methods. Contrarily, due to the curvature of the power curve, the gradient method was unable to converge to one of the MFCs and no further perturbation tests were performed for this method. Although the MU method for non-identical units had more parameters to be tuned, it presented faster convergence than the P/O and was able to track the optimum during process disturbances without changes in the R_{ext}. The authors recommended the use of the P/O algorithm for applications when similarity cannot be guaranteed, while the MU could be used for stack operation, when the same disturbances occur for all reactors at once (e.g. pH and influent temperature variations).

The P/O algorithm applied for MFCs in Woodward et al. (2010) modified R_{ext} with a predetermined amplitude (ΔR) at each iteration. The direction of resistance change was selected by comparing the value of the power output with that at the previous resistance. The method can be expressed as follows:

$$R_{ext}(k+2) = R_{ext}(k+1) + \Delta R sign\left(\frac{P_{MFC}(k+1) - P_{MFC}(k)}{R_{ext}(k+1) - R_{ext}(k)}\right) \quad (1\text{-}20)$$

Once the algorithm converges to an optimum, the R_{ext} will oscillate around this optimum with a maximum distance of ΔR. Therefore, a smaller ΔR can be used to decrease the distance between R_{ext} and the optimal external resistance, but the time of convergence will increase. The long-term performance and stability of the P/O algorithm for MFCs was later evaluated in Pinto et al. (Pinto, Srinivasan, Guiot, & Tartakovsky, 2011a). In this paper, acetate and sWW fed MFCs were operated with the P/O for over 35 days and presented improved Coulombic efficiency and low methane production.

Another example of a model-free algorithm used for MPPT of MFCs was presented in Premier et al. (Premier, Jung Rae, Michie, Dinsdale, & Guwy, 2011). By using acetate-fed batch reactors inoculated with the same AD sludge, they compared the performance of two MFCs: one operated at a fixed R_{ext} (200 Ω) and the other kept at the optimum power by a parsimonious gradient on-line control strategy. This method uses the sign of the power vs. current curve ($\partial P_{MFC}/\partial I_{MFC}$) and the sign of the power variations with time ($\partial P_{MFC}/\partial t$) in a Boolean logic to either increase, reduce, or maintain the R_{ext}. The performance of the on-line controlled MFC was improved enormously (18% of Columbic efficiency against 3%). Furthermore, analysis of the microbial communities after 12 days of operation showed different ecologies in the biofilm and in the suspended biomass for each experiment. These results corroborate with the ones presented in section 1.2.4 and the authors hypothesised that "the control strategy imposed selective pressures favouring electricigenic". Similar results will be presented in the model analysis (sections 4 and 6) of this thesis.

Finally, the P/O algorithm was recently applied for MECs to optimise the applied voltage (Tartakovsky, Mehta, Santoyo, & Guiot, 2011). The method can be expressed as follows:

$$E_{applied}(k+2) = E_{applied}(k+1) + \Delta E sign\left(\frac{I_{MEC}(k+1) - I_{MEC}(k)}{E_{applied}(k+1) - E_{applied}(k)}\right) \qquad (1\text{-}21)$$

1.3. Conclusion

This chapter presented a literature review for modelling and optimisation of MxCs. Relevant concepts of AD and fuel cells modelling techniques were discussed, and a critical overview of the existing MxCs models was presented. Following, pertinent techniques of model based optimisation and process control were examined.

CHAPTER 2: MATERIALS AND METHODS

This section will present the design of MxCs used in this thesis. Furthermore, details of the operating conditions, analytical methods, and inoculation and medium composition for each MxC experiment are shown. Finally, the methodology for model development, the numerical methods used for parameters estimation, and the calculations applied to characterise the experiments are presented.

2.1. MxC Design and Operation

Several identical single-chamber membraneless air-cathode MxCs were constructed using polycarbonate or nylon and stainless steel plates. Each MxC had an anodic chamber volume of 50 mL, while MECs also had a 50 mL H_2 collection chamber on the cathode side.

The anodes were made of 5mm thick carbon felt measuring 10 cm × 5 cm (SGL Canada, Kitchener, ON, Canada). MFC cathodes were made of a gas diffusion electrode (GDE LT 120EW, E-TEK Division, PEMEAS Fuel Cell Technologies, Somerset, NJ, USA) and MEC cathodes were prepared in our lab, made of gas diffusion electrodes with a Ni load of 0.2-0.3 mg cm^{-2}, more details on the cathode preparation technique can be found in Manuel et al. (Manuel, Neburchilov, Wang, Guiot, & Tartakovsky, 2010). The electrodes were separated by a J-cloth (Associated Brands, Mississauga, Canada) with a thickness of 0.7 mm. An external recirculation loop was installed for improved mixing of the anodic liquid. Anodic chamber temperature was controlled by a PID temperature controller (Model JCR-33A, Shinko Technos Co., Ltd., Osaka, Japan) and a heating plate (120V-10W, Volton Manufacturing Ltd, Montreal, Qc, Canada). In the MECs, the pH was controlled at 7 by a PHCN-410 pH controller (Omega Engineering, Stamford CT, USA) and a solution of 0.05N NaOH, which was fed to the recirculation line.

The electrical load of each MFC was controlled individually by an external resistor (R_{ext}). The R_{ext} could be either manually controlled or computer controlled with digital resistors (Innoray, Montreal, QC, Canada) with a variation range from 2.5 Ω to 1000 Ω. All MFC tests that presented computer controlled R_{ext} used the P/O method as presented in Eq. (1-28). The electrical load of each MEC was controlled individually by an adjustable DC power supply (IF40GU,

Kenwood, Japan), used to maintain voltage at a preset value. The MEC voltage could also be computer controlled by the P/O algorithm as presented in section 1.2.6.

Solutions of dilution water, nutrients, and carbon source (acetate or synthetic wastewater) were continuously fed to all MxCs using an infusion pump (model PHD 2000, Harvard Apparatus, Canada) at a rate of 2.5–7 mL d^{-1}. The MxCs were operated at several influent concentrations and a description of each MxC can be found in Table 2-1.

Table 2-1: Operating conditions of the MxCs used in the thesis. External resistances or applied voltages were adjusted after each PT or VS.

Reactor	HRT (h)	Experiment length (d)	Influent	Organic load (mg-*COD* L^{-1})	External load setting
MFC-1	7.5	52	Acetate	310; 620; 1250; 2500	set ~10-25Ω
MFC-2	7.5	60	Acetate	325; 650; 1275; 2550	set ~10-25Ω
MFC-3	7.5	55	Acetate	275; 550; 1100; 2200	set ~40-60Ω
MFC-4	6	35	Acetate	500; 1000; 2000	set to 5Ω
MFC-5	6	35	Acetate	500; 1000; 2000	set to 1000Ω
MFC-6	6	35	Acetate	500; 1000; 2000	P/O algorithm
MEC-1	6	70	Acetate	1000; 1500; 1900	set to 1V
MEC-2	16	38	sWW	2500; 4900; 9000	P/O algorithm
MEC-3	20	33	sWW	550; 6200	P/O algorithm

A simplified MFC diagram is shown in Figure 2.1.

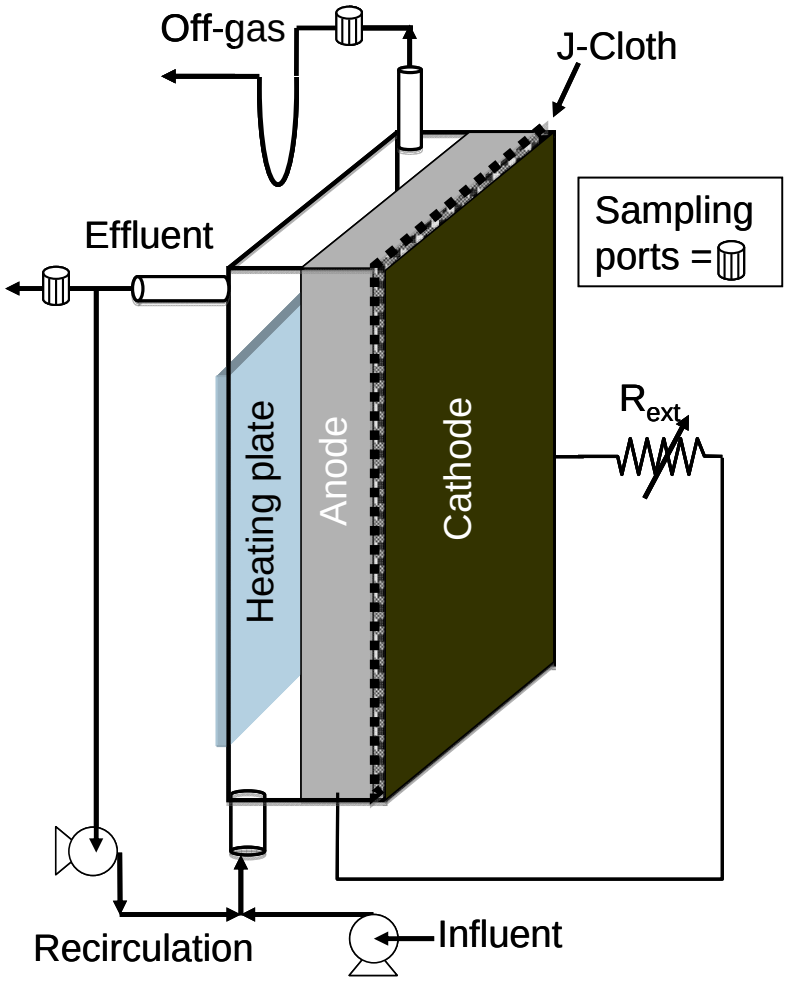

Figure 2.1. A diagram of the MFC set-up showing anode and cathode separated by a J-cloth, heating plate, and sampling ports.

2.2. Analytical Methods

Gas production in the MxC anodic and cathodic chambers were measured on-line using glass U-tube bubble counters interfaced with a data acquisition system. Gas composition was measured using a gas chromatograph (6890 Series, Hewlett Packard, Wilmington, DE) equipped with a 11 m × 3.2 mm 60/80 mesh Chromosorb 102 column (Supelco, Bellefonte, PA, USA) and a thermal conductivity detector. The carrier gas was argon.

Acetate, propionate, and butyrate were analysed on an Agilent 6890 gas chromatograph (Wilmington, DE, USA) equipped with a flame ionization detector and a 1m × 2mm 60/80 mesh Carbopack C column (Supelco, Bellafonte, PA, USA) coated with 0.3% Carbowax 20M and

0.1% H_3PO_4. The carrier gas was helium, which had a flow rate of 20 mL min^{-1}. The injector and the detector were maintained at 200 ºC. The 0.5 µL samples were fortified at a ratio of 1:1 (v/v) using an internal standard of *iso*-butyric acid dissolved in 6% formic acid. Glucose was analysed on an HPLC (Waters Chromatography, Milford, MA, USA) equipped with PDA detector model 2996. The total concentration of volatile fatty acids (VFAs) was calculated with respect to the COD equivalent of each component.

Chemical oxygen demand (COD) of synthetic WW was estimated according to Standard Methods (APHA, 1995). Both total COD (tCOD) and soluble COD (sCOD) values were analysed.

2.3. Inoculum and Media Composition

Each MxC was inoculated with 5 mL of anaerobic sludge with volatile suspended solids of approximately 40-50 g L^{-1} (Lassonde Inc, Rougemont, QC, Canada) and 20 mL of effluent from an existing operating acetate-fed MFC. Prior to MFC-1 inoculation the sludge was heat-treated for 20 min at 100 °C.

The stock solution of acetate-based nutrients was based on the work of Logan et al. (2006) and was composed of (in g L^{-1}): yeast extract (0.8), NH_4Cl (18.7), KCl (148.1), K_2HPO_4 (64), and KH_2PO_4 (40.7). Concentration of acetate in the stock solution was varied in order to obtain the desired organic load by adding sodium acetate (20 to 80 g L^{-1}). Synthetic WW stock solution was composed of (in g L^{-1}): pepticase (50), beef extract (50), yeast extract (30), NH_4HCO_3 (17), K_2HPO_4 (1.75), KH_2PO_4 (1.5). When an MxC was fed with synthetic wastewater, the stock solution had an addition of NaCl (2.8 g L^{-1}) to correct the system conductivity.

A stock solution of the trace elements contained (in g L^{-1}): $FeCl_24H_2O$ (2), H_3BO_3 (.05), $ZnCl_2$ (50), $CuCl_2$ (0.03), $MnCl_24H_2O$ (0.5), $(NH_4)_6Mo_7O_{24}4H_2O$ (0.5), $AlCl_3$ (0.5), $CoCl_26H_2O$ (0.5), $NiCl_2$ (0.5), EDTA (0.5), and concentrated HCl (1 mL). One mL of the trace elements stock solution was added to one L of deionized water, which was fed to the MxCs (dilution water). Deionized water was used for solution preparation, and the chemicals and reagents used were of analytical grade. All acetate solutions were sterilised by filtration (0.22 µm filtration unit) and

maintained at 4 °C, while and synthetic WW solution was frozen and maintained at -6 °C until use.

2.4. Model Development, Estimation, and Validation

In this section, the three stages used in this thesis for a model development will be presented. This methodology was separated in the following sequential phases: (i) model structure selection; (ii) parameters estimation; and (iii) model validation. These stages are comprehensively exemplified in Figure 2.2, and each one will be explained in the following sections.

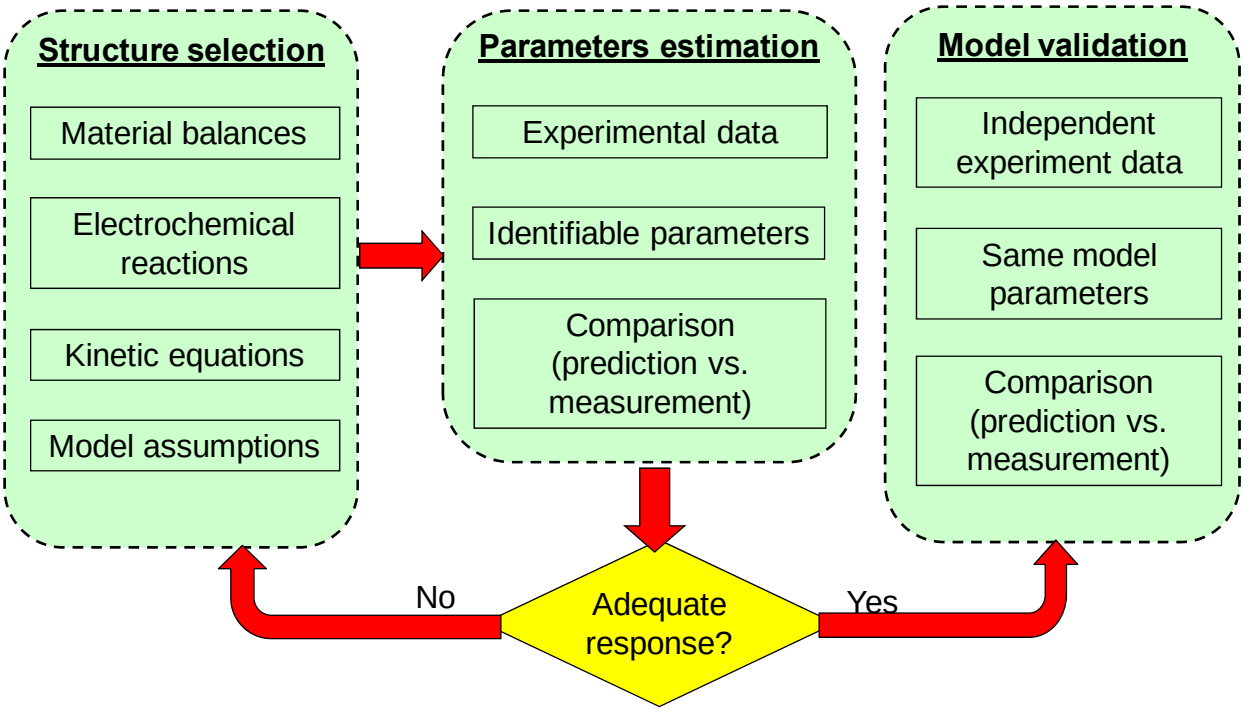

Figure 2.2. Representation of the sequential stages followed for an MxC model development in this thesis.

2.4.1. Model Structure Selection

The model structure selection is the first stage in which mathematical equations are solved to describe/represent the process to be modelled. For an MxC, material and energy balances of the system, reaction kinetics, and electrochemical reactions should be written and integrated in this stage. These balances can be based on previous information gathered from the literature, such as the model concepts presented in section 1 or in simplified assumptions made from experimental observation. The model structure selection is directly related to the model complexity: the more

details are represented by mathematical equations, the more parameters, information, and often longer computation effort are required to solve the model. It is therefore desirable to select the system's main rate-limiting processes (bottlenecks) to be modelled, in order to maintain model simplicity and still represent the aspects of the process that significantly affect its performance.

2.4.2. Parameters Estimation

Once a model structure is selected, there are usually several model parameters left unknown. The next stage is to estimate identifiable unknown parameters. This section reviews some methods to approximate these parameters and some adaptation techniques for those cases in which the model has too many parameters to be estimated with reasonable confidence levels.

Parameter estimation consists of estimating the values of model parameters based on measured or empirical data. In most cases, parameter estimation does not have a unique solution because of the assumed uncertainty of measured or empirical data (often called noise signal) and estimation with a confidence interval is therefore required. The field of parameter estimation is vast and a detailed description of this subject goes beyond the scope of this thesis. The discussion will be limited to an example similar to the MxC model developed here.

The model chosen as an example is a nonlinear continuous time model that can be represented as:

$$\frac{\partial x}{\partial t} = f(x,u,\theta) \tag{2-1}$$

Where θ is the vector with all parameters to be estimated. To estimate these parameters (vector θ), a function that represents the similarity between the model and the experimental data has to be defined. There are several methods to define this function, often called cost or objective function (J). Among the methods available to define the cost function, the least squares is perhaps the most used. This method is the direct algebraic distance (Z. Zhang, 1997) between an observed value (y) and the value given by the model ($\hat{y}$) (Ljung, 1999):

$$J = \frac{1}{N}\sum_{t=1}^{N}(y(t) - \hat{y}(t))^2 \tag{2-2}$$

If the model is nonlinear on parameters, the only possible solution for Eq. (2-2) is to use a minimization algorithm. There are many minimization techniques used to find the "best" fit of θ and each method has its advantages (Dochain & Vanrolleghem, 2001). The minimization methods can be divided into two main groups, those using derivative information and those that are derivative-free. Table 2-2 summarises some of these methods:

Table 2-2: Examples of minimisation algorithms that use or do not use derivative information (Dochain & Vanrolleghem, 2001)

Algorithms Using Derivative Information	Derivative-Free Algorithms
• Steepest descent	• Rosenbrock method
• Gauss-Newton method	• Brent's algorithm
• Levenberg-Marquardt	• Simplex method (Nelder-Mead)
• Quasi-Newton (BFGS, DFP, etc…)	• Secant or DUD algorithm

An important analysis that accompanies the system identification theory is the parameter confidence interval estimation. This analysis shows with a certain degree of confidence that the true value of θ is to be found within a certain interval around the estimate. The larger the number of parameters to be estimated in θ, the larger will be the confidence level of each parameter (Ljung, 1999). Therefore, there is a maximum number of parameters with an acceptable confidence level that can be found for a certain set of input output data. The confidence interval of a set of model parameters can be estimated by the Fisher Information Matrix (FIM), which uses information from the experimental data to define the confidence interval of each estimated parameter. The FIM can be defined as:

$$FIM = \left[\left(\frac{\partial y}{\partial \theta} \right)^T \frac{\partial y}{\partial \theta} \right] \tag{2-3}$$

The FIM can be found by integrating the following sensitivity equations:

$$\frac{\partial y}{\partial \theta} = \frac{\partial y}{\partial x}\frac{\partial x}{\partial \theta} \tag{2-4}$$

$$\frac{d}{dt}\left(\frac{\partial x}{\partial \theta}\right) = \frac{\partial f}{\partial x}\left(\frac{\partial x}{\partial \theta}\right) + \frac{\partial f}{\partial \theta} \tag{2-5}$$

The common problem of a model with too many parameters to be estimated, which usually present large confidence intervals, can be managed by two alternatives: (i) either some parameters should not be estimated, being assumed to be constant, or; (ii) more experimental data from different modes of operation has to be collected. Note that gathering extra experimental data acquired at different experimental conditions is not an easy task, because operational restrictions often limit additional experimental conditions.

Therefore, the selection to estimate only key model parameters is the most common approach for models with several unknowns, and this task can be performed by analysing the model's sensitivity to its parameters (Degenring, Froemel, Dikta, & Takors, 2004). This technique, often called sensitivity analysis, is applied to reduce model complexity and identify parameters that affect the model output more significantly in their neighbourhood domain. Bernard et al. (2001) reported that there is no general methodology to discuss parameter sensitivity, however the usual methods refer to sensitivity for a given system trajectory. This indicates that the reference simulation from which the sensitivity analysis is prepared is extremely important. The relative sensitive analysis method (Dochain & Vanrolleghem, 2001) is an excellent example of model sensitivity measurement. In this method, the sensitivity is measured in terms of the variation of process variables (measured) upon a perturbation of a model parameter. Using finite difference approximation, the sensitive function (SF_{al}) can be expressed as (Dochain & Vanrolleghem, 2001):

$$SF_{al} \approx \frac{\dfrac{\left[c_a(t, p_l + \zeta p_l) - c_a(t, p_l)\right]}{c_a(t, p_l)}}{\zeta p_l / p_l} \tag{2-6}$$

Note that a decrease in the number of parameters to be estimated does not always guarantee small confidence intervals, because the confidence interval is directly related to the measurements available. Therefore after sensitivity analysis, a new FIM has to be built to verify the confidence interval of the remaining parameters to be estimated.

Once model parameters are estimated with a reasonable confidence interval, statistical comparison between model predictions and experimental results are used to assess model performance. Statistical analyses will be described in the following section. Importantly, if the model is unable to predict the experiments with a realistic accuracy, a new model structure must be proposed and new parameters estimated.

2.4.3. Statistical Analysis for Estimation and Validation

After successfully estimating model parameters, statistical analysis is used to determine the model's accuracy. The same numerical methods can also be used in the model validation stage. However, a proper validation step requires the comparison between model predictions and *independent* experimental data, i.e. different data from the one used in parameters estimation. The validation step is often used to verify the validity of the model outside the parameter estimation region.

In the statistical comparison phase, an error function is defined to compare model outputs with experimental results. There is no general methodology to define this error function, but usually it can be based on diverse variations of the mean squared error or the coefficient of determination. In this thesis, two error functions were used: in chapter 3 the mean squared error (*MSE*), while in chapter 5 the adjusted coefficient of determination (R^2). These functions were respectively defined as:

$$MSE = \frac{1}{n_i}\sum_{j=1}^{n_i}\left(\frac{\bar{y}_j^{\exp} - \bar{y}_j^{sim}}{\bar{y}_j^{\exp}}\right)^2 \tag{2-7}$$

$$R^2 = 1 - \frac{1}{n_i}\sum_{j=1}^{n_i}\left(\frac{\bar{y}_j^{\exp} - \bar{y}_j^{sim}}{\max\left(\bar{y}_j^{\exp}, \bar{y}_j^{sim}\right)}\right)^2 \tag{2-8}$$

2.5. Numerical Methods, Characterization, and Calculations

The integration of model equations was performed in MATLAB (Version 7.8, The Mathworks Inc., Natick, MA, USA). Model parameters were estimated by minimizing the following objective function:

$$F_{obj} = \sum_{i=1}^{m} \frac{w_i}{n_i} \left(\sum_{j=1}^{n_i} \left(\bar{y}_{j,i}^{\exp} - \bar{y}_{j,i}^{sim} \right)^2 \right) \quad (2\text{-}9)$$

The measurable variables used in the minimization of the objective function included: (i) sCOD, and (ii) total VFAs concentrations, (iii) CH_4 and (iv) H_2 flow and composition in the H_2-collection compartment, (v) CH_4 flow and composition in the anode compartments, and (vi) current or voltage, hence m = 6. To estimate the selected model parameters, the objective function defined in Eq. (2-9) was minimised using the Nelder-Mead simplex algorithm (Nelder & Mead, 1965) implemented in the fminsearch subroutine of the MATLAB Optimisation Toolbox.

Polarization tests (PT) and voltage scans (VS) were periodically (often weekly) performed for each MFC and MEC respectively. PTs were performed first by disconnecting the external resistance of the MFC for 30 minutes, and then measuring its open circuit potential (OCP) with a multimeter (Fluke 189, Fluke Corp, Everett, WA, USA). Subsequently, R_{ext} was re-connected and progressively decreased from 1000 Ω to 5 Ω every 10 minutes with voltage measurements acquired at the end of each period. The polarization tests were used to build polarization curves, e.g. voltage vs. current plots from where the total (ohmic and solution) R_{int} of the MFC was estimated by the slope of the linear region (Aelterman et al., 2006; Fan et al., 2008). Also, cathode and anode open circuit potentials were measured against an Ag/AgCl reference electrode (222 mV vs. normal hydrogen electrode).

Voltage scans were carried out by stepwise decreasing the applied voltage from 1.2 to 0.2 V, in 0.2 V steps. Once the voltage setting was changed, a 10 min interval was allowed for voltage and current stabilization, then the current was measured using a multimeter (Fluke 189, Fluke Corp, Everett, WA, USA). The MEC internal resistance (i.e., the sum of the charge transfer resistances

and the solution resistance) was estimated using the linear interpolation of the voltage scan in the region of constant voltage drop.

The Coulombic efficiency (*CE*) of the MxC was estimated as:

$$CE = \frac{I^*_{MxC}\Delta t}{\Delta SnF} \tag{2-10}$$

For MFCs, the volumetric power output (P_{out}, mW L_a^{-1}) was calculated using measurements of output voltage, a corresponding value of R_{ext}, and MFC anodic chamber volume (L_a). Maximum volumetric power output ($P_{\max}$) was estimated from the power curves (P_{out} vs. current) obtained during the polarization tests. Since R_{ext} in the PTs was changed stepwise, the accuracy of $P_{\max}$ estimation was improved by using a linear interpolation of the polarization curve in the region of constant voltage drop, $E_{output} = a_0 + a_1 I_{MFC}$, where a_0 and a_1 are the regression coefficients. Based on this interpolation, P_{max} was calculated as described in (Bruce E. Logan, 2008, p. 47):

$$P_{\max} = \frac{a_0^2}{4a_1 L_a} \tag{2-11}$$

Note that, for a MFC with small overpotentials a_0 is close to the OCP estimation and a_1 corresponds to R_{int} (Bruce E. Logan, 2008).

The COD removal efficiency in reactor feed with sWW was calculated as:

$$R_{eff} = 1 - \frac{S + A}{S_0} \tag{2-12}$$

CHAPTER 3: MICROBIAL FUEL CELL MODELLING

This chapter presents the development of a two-population model describing the competition of electricigenic and acetoclastic methanogenic microbial populations for a common substrate in an MFC. Fast numerical solution of the model is provided by using ordinary differential equations to describe biomass growth and retention in the anodic compartment. The model parameters are estimated and validated using experimental results obtained in four continuous flow air-cathode MFCs operated at various external resistances and organic loads. Model analysis demonstrates the influence of operating conditions on MFC performance and suggests ways to maximise MFC power output. The results in chapter 3 were published in Pinto et al. (Pinto, Srinivasan, Manuel, & Tartakovsky, 2010b).

3.1. MFC Model Development

The proposed model focuses on the description of microbial populations and corresponding bio-electrochemical reactions in the anodic compartment of the MFC, while a non-limiting cathode reaction rate is assumed. The charge transfer mechanism from a carbon source to the anode is assumed to involve an intracellular mediator, which exists in the reduced and oxidised forms (e.g. $NADH/NAD^{+}$). Also, extracellular electron transfer via nanowires or direct contact with the anode is assumed. The model considers the existence of electricigenic (attached) and methanogenic (attached or suspended) populations and takes into account acetate as the sole carbon source. The proposed conceptual model is summarised in Fig. 3.1.

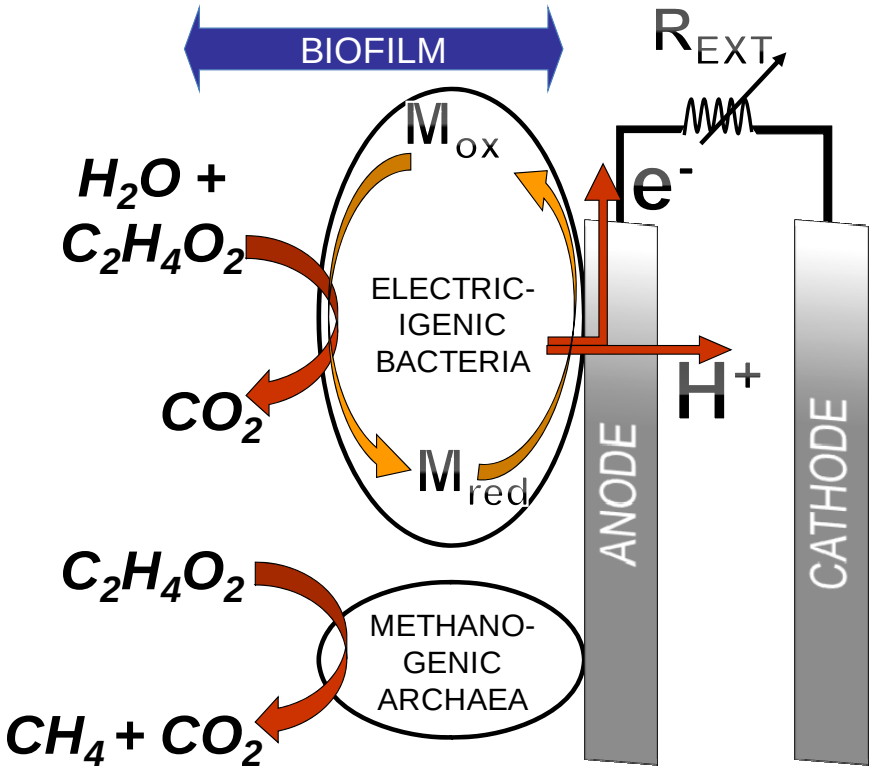

Figure 3.1. Conceptual MFC model showing carbon source (acetate) conversion in the anodic compartment of an MFC by methanogenic and electricigenic microorganisms. M_{red} and M_{ox} denotes reduced and oxidised forms of an intracellular mediator, respectively.

In addition, the following assumptions were made to achieve a fast numerical solution of the model:

1. the carbon source is well distributed in the anodic compartment, therefore ideal mixing is assumed and substrate gradient in the biofilm is neglected;
2. uniform distribution of microbial populations in the anodic compartment biofilm is assumed and biomass retention due to biofilm formation is described by a two phase growth-washout model described below;
3. gas transport (e.g. oxygen, methane) through the porous cathode is neglected;
4. multiplicative Monod kinetics is used to describe growth kinetics of electricigenic microorganisms;
5. a constant pool of intracellular electron transfer mediator in a microorganism is assumed;
6. temperature and pH are considered fully controlled and kept constant.

The conceptual model can be described by the following equations representing acetate and intracellular mediator transformation by the electricigenic microorganisms as well as acetate transformation by the acetoclastic methanogenic microorganisms:

$$C_2H_4O_2 + 2H_2O + 4M_{ox} \rightarrow 4M_{red} + 2CO_2 \quad (3\text{-}1)$$

$$4M_{red} \rightarrow 4M_{ox} + 8e^- + 8H^+ \quad (3\text{-}2)$$

$$C_2H_4O_2 \rightarrow CH_4 + CO_2 \quad (3\text{-}3)$$

The dynamic mass balance equations of the model can be divided into anodic compartment balances and intracellular balances, as described below.

Anodic Compartment Material Balances

For a continuous flow MFC with biofilm retention the influent and effluent flow rates are equal, and the following substrate and microorganisms material balances can be written:

$$\frac{dA}{dt} = -q_e x_e - q_m x_m + D(A_0 - A) \quad (3\text{-}4)$$

$$\frac{dx_e}{dt} = \mu_e x_e - K_{d,e} x_e - \alpha D x_e \quad (3\text{-}5)$$

$$\frac{dx_m}{dt} = \mu_m x_m - K_{d,m} x_m - \alpha D x_m \quad (3\text{-}6)$$

Biofilm formation and retention was simulated using a two-phase biofilm growth model. It was assumed that in the growth phase no biofilm washout occurs so that a batch reactor balance can be used. In the stationary phase, an equilibrium between biofilm growth and washout is reached when biofilm approaches its steady state thickness. Therefore, biofilm washout is equal to net biofilm growth, e.g. a CSTR reactor balance can be used. Similar to the concept presented in section 1.1.1.3, this two-phase biofilm model is described by CSTR material balances with a biomass retention parameter α defined as follows (Mu et al., 2008) :

$$\alpha = \left(\frac{1 + \tanh[K_x(x_e + x_m - X_{MAX})]}{2} \right) \quad (3\text{-}7)$$

Note that the application of Eq. (3-7) is limited to $D > \mu_{max,m}$ and $D > \mu_{max,e}$. Steady state simulation results show that if $D < \mu_{max,m}$ and $D < \mu_{max,e}$, the biomass would grow without limitations, so $(x_m + x_e) > X_{MAX}$ and Eq. (3-7) does not serve the purpose. Furthermore, visual inspection of the MFCs at the end of each test showed that at least some anaerobic sludge used for MFC inoculation remained in the anodic compartment. To account for the existence of these suspended methanogenic microorganisms, slightly different X_{MAX} values were used for electricigenic and methanogenic populations with $X_{MAX,m} > X_{MAX,e}$. Further analysis of the validity of this equation will be presented in section 4.1.

The methane production (mL-CH_4 d^{-1}) in the anode compartment rate was assumed to be directly proportional to the amount of substrate consumed by methanogenic microorganisms, hence

$$Q_{CH4,A} = Y_{CH4} q_m x_m V \tag{3-8}$$

Intracellular Material Balances

Since the intracellular mediator exists either in its oxidised or reduced form and a constant pool of the mediator per electricigenic microorganism is assumed, the following balance equations can be written:

$$M_{Total} = M_{red} + M_{ox} \tag{3-9}$$

$$\frac{dM_{ox}}{dt} = -Y_M q_e + \frac{\gamma}{V x_e} \frac{I_{MxC}}{mF} \tag{3-10}$$

In Eq. (3-10), the rate of oxidised mediator formation from the reduced form is described by Faraday's law, while the consumption rate corresponds to carbon source consumption by the electricigenic microorganisms according to Eq. (3-3). Note that M_{Total} is assumed to be constant, as a part of the electricigens mass.

Kinetic Equations

For electricigenic bacteria, the growth rate was assumed to be limited by concentrations of substrate and the oxidised form of the mediator, while for methanogenic microorganisms the growth rate was limited only by the substrate concentration. Also, the substrate consumption

rates by each microorganism were assumed to be proportional to corresponding growth rates. By using multiplicative Monod kinetics the following equations can be written:

$$\mu_e = \mu_{\max,e} \frac{A}{K_{A,e} + A} \frac{M_{ox}}{K_M + M_{ox}} \quad (3\text{-}11)$$

$$\mu_m = \mu_{\max,m} \frac{A}{K_{A,m} + A} \quad (3\text{-}12)$$

$$q_e = q_{\max,e} \frac{A}{K_{A,e} + A} \frac{M_{ox}}{K_M + M_{ox}} \quad (3\text{-}13)$$

$$q_m = q_{\max,m} \frac{A}{K_{A,m} + A} \quad (3\text{-}14)$$

Electrochemical Equations

MFC voltage can be calculated using theoretical values of electrode potentials and subtracting ohmic, activation, and concentration losses (section 1.1.2.2). By applying Ohm's law to compute the MFC current and ohmic losses ($\eta_{ohm} = I_{MEC} R_{\text{int}}$), the electrochemical balance can be expressed as:

$$E_{output} = E_{thermo} - I_{MFC} R_{\text{int}} - \eta_{conc} - \eta_{act} \quad (3\text{-}15)$$

The MFC current can be found using ohms law ($E_{output} = R_{ext} I_{MFC}$). As presented in sections 1.1.2.3 and 1.1.2.5, activation and concentration losses can be computed separately for the cathode and anode. Due to the assumption that the cathode reaction is non-limiting, these losses at the cathode were assumed to be constant and were included in the calculation of E_{thermo}. The concentration losses at the anode can be calculated by the expression derived in section 1.1.2.5, assuming that the MFC current rate is proportional to the oxidised mediator concentration and that the limiting reference current occurs when all oxidised mediators transfer electrons ($M_{ox} = M_{Total}$):

$$\eta_{conc,A} = \frac{RT}{mF}\ln\left(\frac{I_L^{Reference}}{I_L^{Reference} - I_{MFC}}\right) \approx \frac{RT}{mF}\ln\left(\frac{M_{Total}}{M_{Total} - M_{ox}}\right) = \frac{RT}{mF}\ln\left(\frac{M_{Total}}{M_{red}}\right) \quad (3\text{-}16)$$

The activation losses in Eq. (3-15) can be calculated by the Butler-Volmer equation for symmetric equations (section 1.1.2.3):

$$\eta_{act,A} = \frac{2RT}{mF}\sinh^{-1}\left(\frac{I_{MFC}}{2A_{sur,A}i_0}\right) \quad (3\text{-}17)$$

MFC current can be calculated by combining Eqs. (3-15) to (3-17), and assuming that E_{thermo}, $\eta_{conc,C}$, and $\eta_{act,C}$ in Eq. (3-15) were equal to the experimentally measured value of open circuit potential (E_{OCP}). As shown in Cannarozzo et al. (2007), the concentration losses can be more accurately represented by the addition of boundary conditions at high current densities. To avoid the discontinuity when integrating model equations, the boundary conditions were replaced with a Monod-like term, which limits the calculated MFC current at low values of M_{red}:

$$I_{MFC} = \frac{E_{OCP} - \frac{RT}{mF}\ln\left(\frac{M_{Total}}{M_{red}}\right) - \frac{2RT}{mF}\sinh^{-1}\left(\frac{I_{MFC}}{2A_{sur,A}i_0}\right)}{(R_{ext} + R_{\text{int}})}\frac{M_{red}}{\varepsilon + M_{red}} \quad (3\text{-}18)$$

Note that due to the activation losses, this equation can only be solved numerically, i.e. $\eta_{act,C}=f(I_{MEC})$. If activation losses are neglected a simplified expression that can be solved analytically for current calculation is obtained:

$$I_{MFC} = \frac{E_{OCP} - \frac{RT}{mF}\ln\left(\frac{M_{Total}}{M_{red}}\right)}{(R_{ext} + R_{\text{int}})}\frac{M_{red}}{\varepsilon + M_{red}} \quad (3\text{-}19)$$

3.2. MFC Model Parameters Estimation and Model Revision

Experimental results obtained in MFC-1 and MFC-2 tests were used to estimate model parameters, while two other data sets (MFC-3 and MFC-4) were reserved for model validation.

Importantly, MFC-1 was inoculated with heat-treated sludge. The heat-treatment procedure deactivated methanogenic microorganisms in the inoculum. Consequently, kinetic parameters of the electricigenic microorganisms were estimated using this data set by setting the methanogenic growth rate to zero.

Estimation of model parameters was carried out in several steps. First, Fisher information matrixes (FIM) were used to select identifiable parameters. Because of the limited number of measurable state variables FIM analysis showed that several model parameters cannot be estimated with an acceptable accuracy. The identifiable parameters were $\mu_{max,e}$, $q_{max,e}$, Y_M, $\mu_{max,m}$, and $q_{max,m}$. With a 95% confidence, the confidence intervals found for these parameters were 6.01%, 2.1%, 2.91%, 13.4%, and 13.75%, respectively. Other model parameters were chosen based on available literature data. In particular, all half-rate constants were not identifiable, since to be identified with a reasonable level of confidence these parameters require experimental data acquired from a broad range of substrate concentrations, including tests at low substrate concentration, which were unavailable. Therefore, half-rate constants were also chosen based on available literature values. Once the identifiable model parameters were selected, the parameter estimation procedure was carried out by minimizing the objective function defined in Eq. (2-9) using experimentally measured values of acetate concentration in the effluent, MFC output voltage, and methane production.

The first parameter estimation attempts were carried out using the MFC-1 data set. Large discrepancies between the experimental and simulated values of the MFC voltage were obtained as can be seen from the analysis of MSE values presented in Table 3-1. MFC start-up appeared to be most difficult to model, since for the first 15-20 days of the experiment the simulated output voltage was significantly higher than the measured values. This difference was attributed to the observed variations in the values of E_{OCP} and R_{int} estimated during the MFC experiments. Indeed, during the first days of MFC-1 operation, E_{OCP} and R_{int} were estimated at 0.38 V and 175 Ω respectively, while after 17 days of operation these values stabilised at 0.66 V and 25 Ω. These results agree with the observations of Aelterman et al. (2008), which also demonstrate improved MFC performance after the start-up period.

To improve model accuracy during the start-up period, the E_{OCP} and R_{int} values were linked to the concentration of electricigenic microorganisms. This agrees with the known dependence of cell voltage and internal resistance on the catalyst load (Chaparroa, Gallardo, Folgado, Martín, & Daza, 2009). The following dependence was used to describe the observed changes of internal resistance:

$$R_{\text{int}} = R_{MIN} + (R_{MAX} - R_{MIN})e^{-K_R x_e} \tag{3-20}$$

Similarly, MFC open circuit potential was observed to increase during the start-up period. Cathode and anode OCP measurements against an Ag/AgCl reference electrode showed that the cathode OCP remained at 140-160 mV throughout the tests, while the anode OCP became more negative. This trend was attributed to anode colonization by electricigenic microorganisms, e.g. increasing biocatalyst load, and described by the following dependence:

$$E_{OCP} = E_{MIN} + (E_{MAX} - E_{MIN})e^{-1/K_R x_e} \tag{3-21}$$

The R_{MIN}, R_{MAX}, E_{MIN}, and E_{MAX} values were obtained from the polarization tests. Parameters K_x and K_R were identified using available voltage measurements during the first 20 days of MFC-1 operation.

To evaluate the impact of the proposed dependencies on model accuracy the parameter estimation procedure was repeated. First, Eq. (3-20) was introduced while keeping E_{OCP} constant. Then Eq. (3-21) was introduced while keeping R_{int} constant and finally both Eq. (3-20) and (3-21) were used. The results presented in Table 3-1 clearly show that the accuracy of voltage prediction was improved. In addition, model outputs with activation losses calculated according to Eq. (3-18) were compared with a simplified electrochemical balance, which neglects activation losses (Eq. (3-19)). No significant difference in model accuracy was obtained (Table 3-1) thus confirming that the activation losses could be neglected. Consequently, electrochemical balance Eq. (3-19) was used in all the following calculations.

Table 3-1: A comparison of mean squared errors (*MSE*) calculated for MFC-1 data set at different calculation methods of E_{OCP}, R_{int}, and $\eta_{act,A}$.

state variable	E_{OCP} constant R_{int} constant $\eta_{act,A} = 0$	E_{OCP} constant Using Eq. (3-20) $\eta_{act,A} = 0$	Using Eq. (3-21) R_{int} constant $\eta_{act,A} = 0$	Using Eq. (3-21) Using Eq. (3-20) $\eta_{act,A} = 0$	Using Eq. (3-21) Using Eq. (3-20) Using Eq. (3-18)
voltage	0.43	0.37	0.27	0.14	0.09
substrate	0.36	0.36	0.44	0.44	0.45

Once the model structure was refined by including Eqs. (3-20) and (3-21) and parameters related to electricigenic microorganisms were identified based on the MFC-1 data set, the remaining identifiable parameters related to methanogenic activity ($\mu_{max,m}$ and $q_{max,m}$) were identified using the MFC-2 data set. The resulting values of model parameters are given in Tabel A-1. The estimated values of $\mu_{max,m}$ and $q_{max,m}$ were within the range of parameter values used in ADM1 (D.J. Batstone, Keller, Newell, & Newland, 2000). Also, Tabel A-1 contains values of non-identifiable model parameters that were chosen based on the literature review.

The total mediator fraction per microorganism was assumed to be 5% (Tabel A-1) to avoid numerical problems in the model solution. Although this value was arbitrary, it did not affect model outputs since Eq. (3-16) uses a M_{Total}/M_{red} ratio.

A comparison of model outputs with acetate and voltage measurements during MFC-1 and MFC-2 tests is shown in Figure 3.2*a* to 3.2*d*. Each simulation required less than 2 seconds on a PC with 2.99 GHz dual core processor. Model outputs closely follow experimentally measured acetate concentrations at low and moderate acetate loads. A larger discrepancy was observed at the highest influent acetate concentration around day 40. This was attributed to a power failure during this operating period, which likely led to an overestimation of the influent acetate concentration. Voltage predictions (Fig. 3.2*b*, and 3.2*d*) agreed well with the experimental measurements, both during normal MFC operation and during polarization tests. Voltage changes during the polarization test performed on day 47 are shown in Fig. 3.2*e* in more detail and the predicted changes in M_{red} and M_{ox} during this test are shown in Fig. 3.2*f*. This simulation suggests that MFC operation in the open circuit mode at the beginning of the polarization tests resulted in M_{red} accumulation. Progressive decreases of R_{ext} during the test led to a low level of M_{red}.

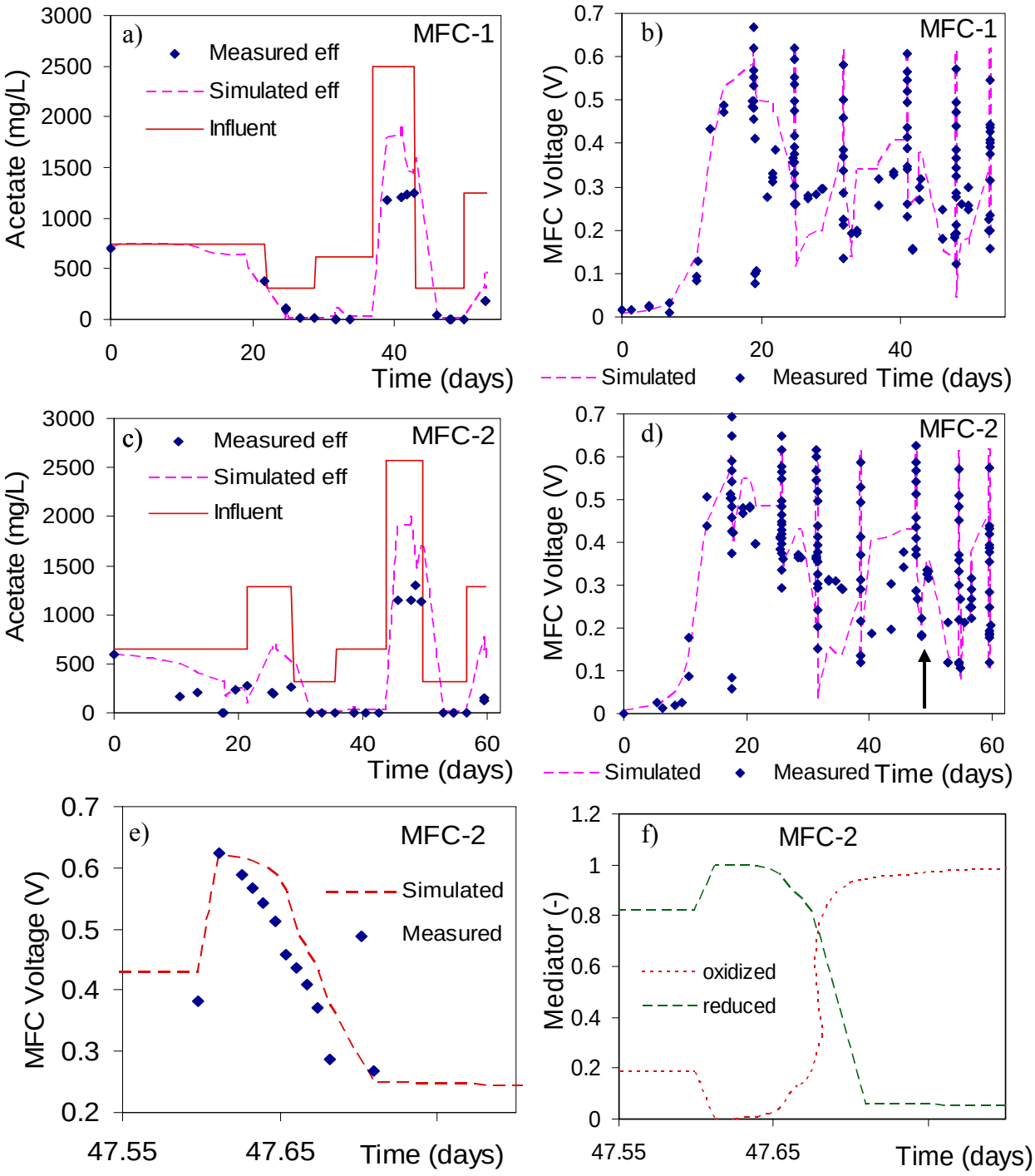

Figure 3.2. Comparison of model outputs with experimentally measured values of acetate and output voltage during MFC-1 (*a, b*) and MFC-2 (*c, d*) operation. MFC-2 output voltage during the polarization test at day 47 (indicated by an arrow in panel *d*) and predicted values of M_{red} and M_{ox} during this polarization test are shown in panels *e* and *f*, respectively.

Statistical analysis of model outputs is provided in Table 3-2.

Table 3-2: *MSE* calculated by comparing experimental results and model outputs for parameter estimation (MFC-1, 2) and model validation (MFC-3, 4) data sets.

state variable	MFC-1	MFC-2	MFC-3	MFC-4
voltage	0.14	0.11	0.036	0.032
substrate	0.44	0.87	0.065	0.053
methane	n/a	23.47	1.00	0.027

n/a – not available (no measurable methane production for MFC-1)

Large MSE values were obtained for methane due to a poor fit between the predicted and measured methane production rates (Table 3-2). This discrepancy can be explained by the low accuracy of methane measurements. Because of the small volume of the anodic compartment (50 mL), methane production rates were between 0.5 and 10 mL d^{-1}. Measuring such small flow rates presented a technical challenge resulting in a large standard deviation of the measurements. Also, we hypothesised that at least part of the methane produced in the anodic compartment was not accounted for because of its diffusion through the cathode.

In more details, model accuracy can be estimated from the analysis of Fig. 3.2*e*, which compares model outputs and measured values of MFC-2 voltage during the polarization test conducted on day 47 of MFC-2 operation. To evaluate model accuracy in a broad R_{ext} range, R_{ext} was changed to between 10 kΩ and 15 Ω during this polarization test. Also, the predicted values of the oxidised and reduced form of the intracellular mediator during this polarization test are shown in Fig. 3.2*f*. As expected, open circuit MFC operation leads to an increase in the reduced mediator form. A decrease in R_{ext} value during the polarization test increases electricigenic activity thus leading to an increase in M_{ox}. After the polarization test, R_{ext} was maintained at 15 Ω for 24 h, which explains the low level of M_{red} and low output voltage after the polarization test. R_{ext} was changed to 35 Ω one day later (not shown).

In the absence of more detailed information, the internal mediator molar mass (γ) and the number of electrons transferred per mol of mediator (m) were assumed to be equal to that of NADH

(Table A-1). However, the electron transfer process is believed to be more complex than the $NADH/NAD^+$ cycle. Since γ, m, and Y_M (yield) values are included in Eq. (3-10), the parameter estimation procedure aimed at estimating Y_M might account for the arbitrary choice of γ and m without affecting model predictions.

3.3. MFC Model Validation

The model was validated using MFC-3 and MFC-4 tests that were not used in the parameter estimation procedure. Importantly, MFC-3 was operated at external resistances, which were overall higher in comparison to those used during MFC-2 operation as described in Table 2-1. MFC-4 was operated at a low external resistance of 5 Ω, which was much lower than the external resistance values used in other tests. Therefore experimental results used for model validation were acquired using different operating conditions thus allowing for model predictive capacity validation. When validating the model, parameters were kept unchanged except for OCP values. These values were calculated for each MFC using polarization curves results. Figure 3.3 shows a comparison of model predictions with the results obtained in MFC-3 and MFC-4 tests.

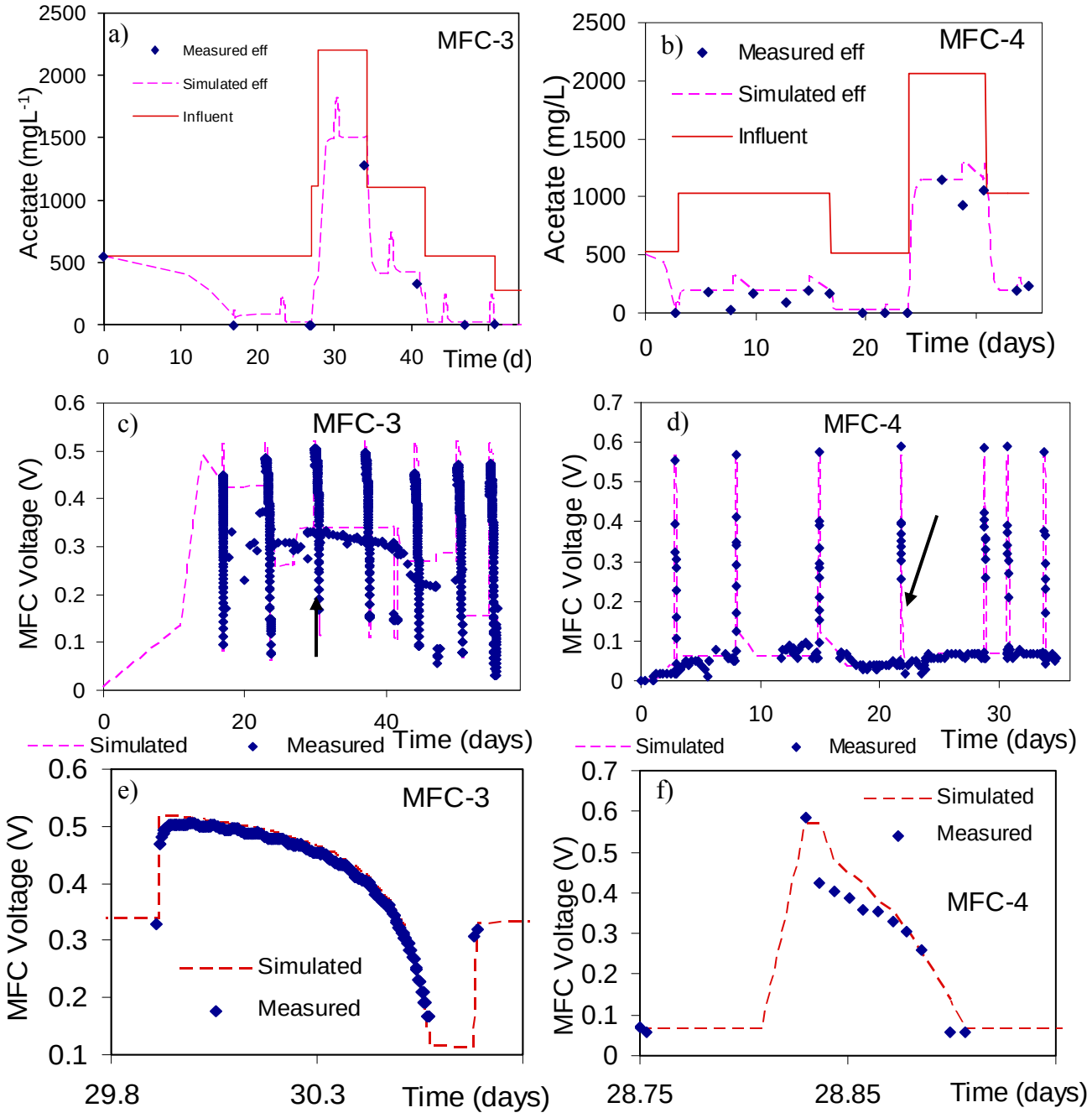

Figure 3.3. Comparison of model outputs with experimentally measured values from MFC-3 (*a*, *c* and *e*); MFC-4 (*b*, *d* and *f*). Polarization curves acquired on day 30 of MFC-3 operation (digital resistor with a step of 2.5 Ω) and on day 28 of MFC-4 operation (manual resistor control) are shown in panels *e* and *f* (days are also indicated by arrows in panels *c* and *d*). In panels *a* and *b*, 'eff' denotes effluent.

For MFC-3, a satisfactory agreement was obtained between measured and predicted output voltages and effluent acetate (Fig 3.3*a*, 3.3*c*, and 3.3*e*). In part this may be due to the similarity

between the operating conditions of MFC-2 and MFC-3, since both MFCs had their external resistance periodically adjusted during the length of the experiment so that R_{ext} remained above the estimated R_{int} value.

As mentioned above, MFC-4 was operated at R_{ext} much below the estimated R_{int} value. Therefore, a comparison between experimental results and model outputs (Figures 3.3*b*, 3.3*d*, and 3.3*f*) for MFC-4 confirmed the predictive capacity of the model. Both experimental measurements and model predictions showed low voltage and low power output due to low external resistance.

A comparison of predicted and measured Coulombic efficiencies and averaged methane production values are presented in Figure 3.4. This comparison was based on MFC operation at pseudo steady-state conditions, e.g. the biomass growth period (first 25 days of MFC operation) and MFC operation at high acetate load were excluded from consideration. Yet, variations in influent acetate concentration resulted in relatively large standard deviations. As discussed above, large standard deviations of methane flow measurements were attributed to difficulties in measuring small amounts of methane produced in the anodic compartment and due to possible losses resulting from methane diffusion through the porous cathode. More accurate methane measurements can potentially be made by significantly increasing the anodic compartment volume and measuring the methane percentage in the cathodic chamber off-gas. Nevertheless, the link between Coulombic efficiency and methane production can be clearly observed, as the highest Coulombic efficiency was observed in MFC-1, which had no methanogens, and in MFC-4, which was operated at R_{ext} = 5 Ω. Coulombic efficiency was lower and methane production was higher in MFC-2 and MFC-3, which were operated at higher R_{ext} values.

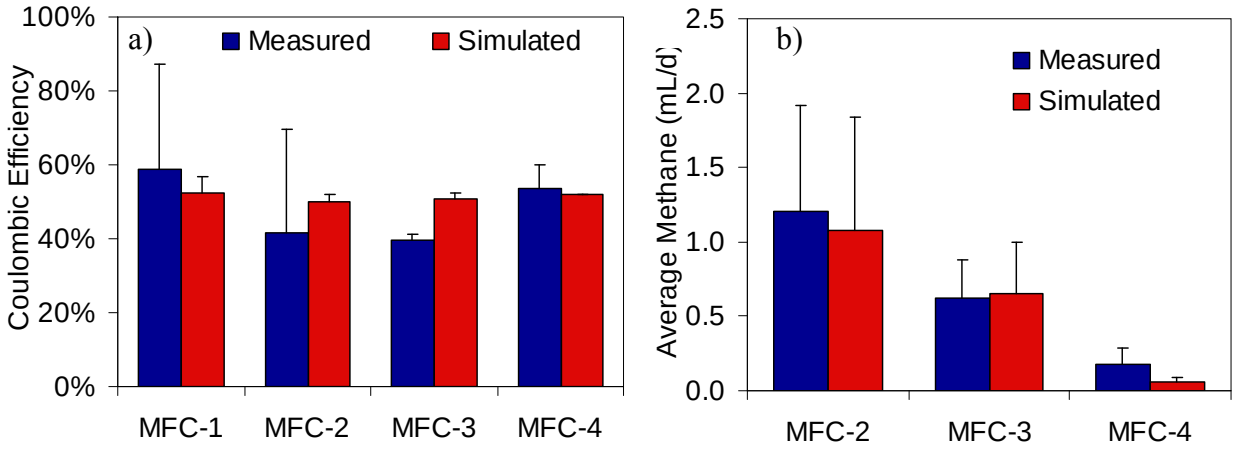

Figure 3.4. Average Coulombic efficiency (*a*) and average methane production (*b*). Data acquired during the biofilm growth phase (first 25 days) and MFC operation at a high acetate load was excluded from calculation.

Statistical analysis of parameter estimation and validation results was performed by comparing MSE values. Analysis of MSE calculations presented in Table 3-2 show that model validation produced MSE values that are smaller than those obtained in the parameter estimation procedure. In part, this difference can be explained by a larger number of voltage measurements during MFC-1 and MFC-2 start-up (Fig. 3.2*b* and *d*), where model predictions are less accurate. Nevertheless, it also confirms excellent predictive capacity of the model. In particular, the model was able to predict MFC dynamics observed in the MFC-4 test, which was operated outside the range of operating conditions used in the parameter estimation procedure.

3.4. The Influence of External Resistance and Organic Load on Microbial Populations

The four MFCs used for model identification and validation were operated at various organic loads and external resistances as outlined in Table 2-1. A comparison of MFC performances suggested that both of these operating parameters significantly affected MFC power output. Obviously, it was maximised when R_{ext} was equal or slightly above the internal resistance value (Aelterman et al., 2008; L. Woodward et al., 2009b). By periodically acquiring polarization curves and adjusting R_{ext} to maintain it at about 5 to 10 Ω above R_{int} during MFC-1 and MFC-2 operation, volumetric power output was maintained at 35-50 mW L_a^{-1}. This dependence was adequately simulated by the model as can be seen from the analysis of mean squared errors in Table 3-2.

In addition to this immediate impact of R_{ext} on MFC power output, it was hypothesised that R_{ext} might also influence the growth and distribution of microbial populations in the anodic compartment. Indeed, the model assumes that the growth rate of electricigenic microorganisms depends on the concentration of the oxidised form of the intracellular mediator (Eq. 3-11). In turn, the M_{ox} concentration depends on the R_{ext} value such that for the same carbon source concentration, a faster growth rate of electricigenic microorganisms is expected for a MFC with lower external resistance. Overall, MFC operation at an optimal ($R_{ext} = R_{int}$) or below optimal resistance is expected to maximise growth of electricigenic microorganisms.

Acetate concentration in the anodic compartment is another factor affecting the distribution of electricigenic and methanogenic microorganisms. Since Monod-like kinetics is used to describe growth of both populations, the growth rates are maximised at high organic loads. Based on the experimental evidence (Esteve-Nunez, Rothermich, Sharma, & Lovley, 2005; Cesar I. Torres et al., 2008a) a smaller value of the half-rate constant is assigned to electricigenic microorganisms (Tabel A-1). Thus, the outcome of the competition between electricigenic and methanogenic populations, and therefore MFC power output, is expected to be dependent on both acetate concentration and external resistance values.

To analyse the impact of these two operating conditions on MFC performance, the model was integrated for a period of 200 days to obtain a steady state solution and the predicted power density was calculated. In these calculations the influent acetate concentration was varied between 10 to 800 mg L^{-1} and R_{ext} was varied between 10 and 800 Ω. The resulting 3D plot is presented in Fig. 3.5*a*.

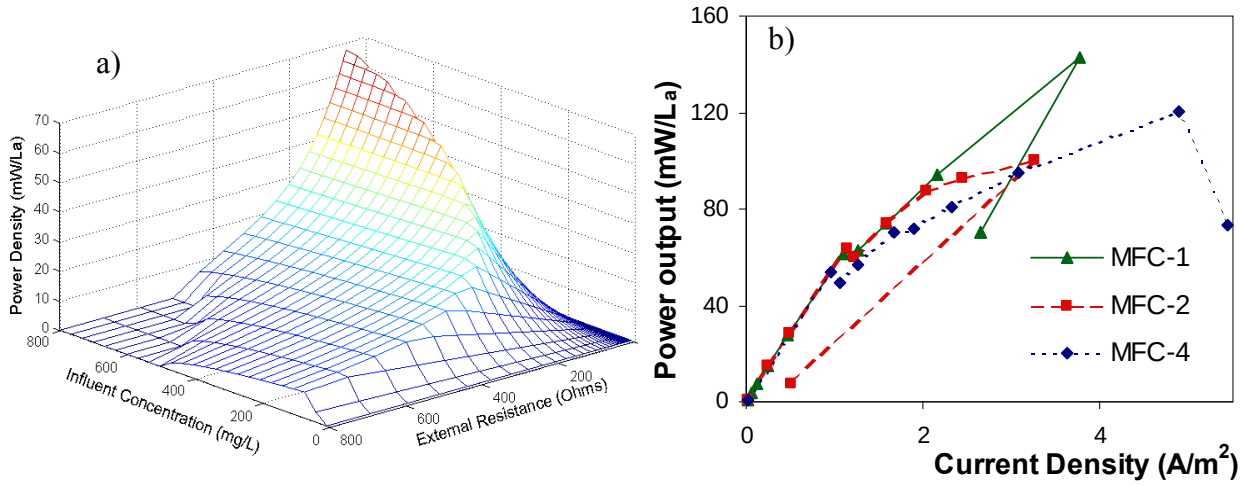

Figure 3.5. (*a*) Predicted steady state power output as a function of operating conditions (acetate concentration and R_{ext}) and (*b*) comparison of power outputs during polarization curves obtained for MFC-1, MFC-2 (close to optimal external resistance), and MFC-4 (low external resistance) tests.

It confirms that both parameters strongly influence the power output and suggests a range of acceptable operating conditions. In particular, a significant decrease in power output is predicted both at very low and very high acetate concentrations. The former can be explained by the combined limitation of the growth rate of electricigenic microorganisms by low concentrations of acetate and M_{ox}, while the latter can be attributed to an increased growth rate of the methanogens. Interestingly, the model analysis predicted high concentrations of electricigenic microorganisms for R_{ext} values that are equal to or less than the internal resistance of the MFC. This result appears to be counterintuitive, as MFC power output is maximised at $R_{ext} = R_{int}$, while a sharp drop is observed if R_{ext} is below its optimal value (Figure 3.5*b*). However, this model prediction was confirmed in the MFC-4 test where R_{ext} was kept below R_{int}, yet high activity of the electricigenic populations was confirmed in the polarization tests. These polarization tests showed that as soon as the MFC external resistance was increased to its optimal value, the power output increases to values comparable to those of MFC-1 and MFC-2, which were always operated close to optimal R_{ext} (Fig. 3.5*b*).

Overall, model analysis suggested that MFC operation under non-optimal conditions (e.g. high external resistance and high organic load) not only leads to a loss in power output, but also favours growth of methanogenic microorganisms accompanied by an increase in acetate

utilization for methane production. This conclusion is in agreement with the results of Aelterman et al. (2008).

Although electricigenic populations are not affected at low R_{ext} values, if one tries to operate an MFC at low R_{ext} to maximise electricigenic growth and the R_{ext} is set below the internal resistance of the MFC, the power production is extremely affected, as shown in Fig 3.5*a* where even a small difference between R_{int} and R_{ext} leads to large power losses. To ensure both high power output and stability of electricigenic populations, periodic adaptation of electric load (external resistance) might be required. This task can be best accomplished by a real time control algorithm, which seeks to maximise power output based on voltage or current measurements. Such maximum power point tracking (MPPT) algorithms are widely used in photovoltaic cell operation and after some adaptation can be used in MFC operation (section 1.2.6). Also, model-based optimisation algorithms can be developed (section 1.2).

3.5. Conclusion

This chapter presented the development of a fast-convergence two-population model of an MFC. The accuracy of model predictions is improved by proposing a dependence of electrochemical parameters (E_{OCP} and R_{int}) on electricigenic biomass density. The accuracy of the parameter estimation procedure and the predictive capacity of the model were confirmed using two independent data sets. Model analysis demonstrates the influence of organic load and R_{ext} on MFC power output and long-term performance. It is demonstrated, that R_{ext} should be at least periodically adjusted to avoid proliferation of methanogens. Overall, the model predictions successfully agree with all experimental data sets and the model provides a convenient tool for off-line process optimisation, an option that will be explored in the next chapter.

CHAPTER 4: MFC MODEL ANALYSIS

The goal of this chapter is to optimise an MFC-based wastewater treatment process in terms of maximizing the amount of wastewater that is cleaned. The MFC mathematical model presented in chapter 3 is used to compare different operating modes and reactor configurations. The following observations are made based on the model analysis: (i) the ratio between the electricigenic and methanogenic populations can be controlled by the electrical load; (ii) co-existence of the two populations decreases reactor performance; (iii) reactors connected in series always improve treatment efficiency, and; (iv) influent and effluent concentrations can be used to define the best series configuration. Furthermore, experimental MFC results are presented to qualitatively demonstrate the applicability of observation (i). This chapter contains results presented in Pinto et al. (Pinto, Perrier, Tartakovsky, & Srinivasan, 2010a; Pinto, Tartakovsky, Perrier, & Srinivasan, 2010c), in addition, a minor part of the experimental results are available in Pinto, Srinivasan, Guiot, and Tartakovsky (2011a).

4.1. Biofilm Retention and Washout

The model analysis will start with a verification of the validity of Eq. (3-7), the biofilm retention constant, as this equation directly affects the composition of the biofilm. Note that all the analysis in chapter 4 considered the biomass concentration in the MFC biofilm, neglecting any suspended acetoclastic methanogenic populations, therefore $X_{MAX,m} = X_{MAX,e}$. First, in the region of Eq. (3-7) validity ($D > \mu_{max,m}$ and $D > \mu_{max,e}$), it will be shown that the total biomass in the system at steady state is always equal to X_{MAX}.

Lemma 1. Let $K_x >> 0$, $A_0 > 0$, $K_{d,m} = 0$, $K_{d,e} = 0$, $D > \mu_{max,m}$ and $D > \mu_{max,e}$. Then no stable equilibrium point exists if $(x_m + x_e) \neq X_{MAX}$.

Proof. First note that if D and A_0 are positive, the steady state solution of Eq. (3-4) assures that A is always different than zero. Also, the dynamics of substrate consumption and oxidised mediator were considered to be much faster than the dynamics of electricigenic and methanogenic microorganisms' growth, because the time constants computed for R_{ext} of 1000 Ω were approximately 30 s, 2 h, 1.5 d, and 90 d, respectively. Thus a pseudo steady state is considered

and only equations (3-5) and (3-6) will be used for further analysis. These equations can be locally linearised to give:

$$\begin{bmatrix} \frac{d\Delta x_e}{dt} \\ \frac{d\Delta x_m}{dt} \end{bmatrix} = \begin{bmatrix} (\mu_e - \alpha D) - 2\alpha(1-\alpha)K_x D x_e & -2\alpha(1-\alpha)K_x D x_e \\ -2\alpha(1-\alpha)K_x D x_m & (\mu_m - \alpha D) - 2\alpha(1-\alpha)K_x D x_m \end{bmatrix} \begin{bmatrix} \Delta x_e \\ \Delta x_m \end{bmatrix} \quad (4\text{-}1)$$

The parameter K_x is used in Eq. (3-7) to ensure that α switches between 0 and 1. So, three cases can be distinguished, i.e. (a) $\alpha = 0$ when $(x_m + x_e) < X_{MAX}$, (b) $\alpha = 1$, $(x_m + x_e) > X_{MAX}$, and (c) α takes a value between 0 and 1 for $(x_m + x_e) = X_{MAX}$.

Consider the case $\alpha = 0$. Since $\mu_{max,m} > 0$, and $A > 0$, the only steady state solution of Eq. (3-5) is $x_m = 0$. Also, any value is allowed for x_e as long as $x_e < X_{MAX}$. By substituting $\alpha = 0$ in Eq. (4-1), it can be seen that at least the second eigenvalue is positive, thereby leading to an unstable solution.

Consider the case $\alpha = 1$. Since $D > \max\{\mu_{\max,m}, \mu_{\max,e}\} > \max\{\mu_m, \mu_e\}$, the only steady state equilibrium point of Eqs. (3-5) and (3-6) is $x_m = 0$ and $x_e = 0$. But, $x_m = 0$ and $x_e = 0$ is inconsistent with the assumption that $\alpha = 1$, which requires $(x_m + x_e) > X_{MAX}$.

So, if ever there is a stable equilibrium point, it should only correspond to $(x_m + x_e) = X_{MAX}$. ■

4.2. Competitive Exclusion and Coexistence: Model Simulation Results

One of the first questions to be answered is related to the co-existence of the two populations. As discussed in section 1.2.4, the "competitive exclusion principle" (Hardin, 1960) suggests the extinction of one of the species when there is a competition for the same substrate in the same ecological niche. This principle was mathematically characterised by Harmand et al. (2008), where it was shown that similar kinetics for growth rate are required to cause this type of exclusion. In the MFC model considered, only the growth rate of electricigenic microorganisms is limited by the mediator concentration. The mediator concentration in turn is influenced by the external resistance; hence the external resistance plays a key role in the type of microorganisms that are present in the MFC. This effect is explained in the following proposition.

Proposition 1. Let the decay rates be negligible and the half-rate constants of the Monod kinetics of the methanogens be greater than that of the electricigens, e.g. $K_{A,m} > K_{A,e}$. Then, the co-existence of the two populations is determined by the expression, $\mu^* = \frac{\mu_{\max,m}}{\mu_{\max,e}} \frac{K_M + M_{ox}}{M_{ox}}$.

Three regions can be distinguished based on the value of μ^*: (I) $\mu^* < 1$, only electricigens exist; (II) $1 < \mu^* < K_{A,m}/K_{A,e}$, both microorganisms coexist, and; (III) $\mu^* > K_{A,m}/K_{A,e}$, only methanogens exist.

Proof. The steady state solution of Eqs. (3-5) and (3-6) present three possible equilibrium points (neglecting the washout solution):

(I) $\mu_e = \alpha D$ and $x_m = 0$ (only electricigenic microorganisms)
(II) $\mu_e = \alpha D$ and $\mu_m = \alpha D$ (coexistence)
(III) $\mu_m = \alpha D$ and $x_e = 0$ (only methanogenic microorganisms)

To study the stability of the equilibrium points (I) to (III), once again the dynamics of substrate consumption and oxidised mediator were assumed to be much faster than the dynamics of bacteria growth. The Eqs. (3-5) and (3-6) can be linearised as in Eq. (4-1).

Now we consider the equilibrium point at (I), for which $\mu_e = \alpha D$ and $x_m = 0$. The Jacobian that corresponds to this solution can be written as:

$$\begin{bmatrix} \frac{d\Delta x_e}{dt} \\ \frac{d\Delta x_m}{dt} \end{bmatrix} = \begin{bmatrix} -2\alpha(1-\alpha)K_x D x_e & -2\alpha(1-\alpha)K_x D x_e \\ 0 & (\mu_m - \mu_e) \end{bmatrix} \begin{bmatrix} \Delta x_e \\ \Delta x_m \end{bmatrix} \quad (4\text{-}2)$$

This equilibrium point is only stable when $\mu_m < \mu_e$. The reverse occurs for the solution of case (III), where stability is only possible when $\mu_e < \mu_m$.

For coexistence to occur (e.g., $\mu_e = \mu_m = \alpha D$), the following condition has to be satisfied:

$$\mu_{max,e}\frac{A}{K_{A,e}+A}\frac{M_{ox}}{K_M+M_{ox}} = \mu_{max,m}\frac{A}{K_{A,m}+A} = \alpha D \qquad (4\text{-}3)$$

Eq. (4-3) can be solved to give:

$$A = \frac{K_{A,m} - K_{A,e}\mu^*}{\mu^* - 1}, \qquad \text{where} \qquad \mu^* = \frac{\mu_{\max,m}}{\mu_{\max,e}}\frac{K_M + M_{ox}}{M_{ox}} \qquad (4\text{-}4)$$

If the above expression gives a positive value of A, coexistence is possible. On the contrary, negative values of A indicate that one of the microorganisms would be extinct. Therefore, coexistence is possible only between $1 < \mu^* < K_{A,m}/K_{A,e}$.

In particular, when $\mu^* < 1$ it can be shown that $\mu_e > \mu_m$ for any values of A and only solution (I) is stable. Meanwhile, for $K_{A,m}/K_{A,e} < \mu^*$ one can see that $\mu_e < \mu_m$ for any values of A and only solution (III) is stable. ■

The relationship between A and μ^* is represented in Fig.4.1:

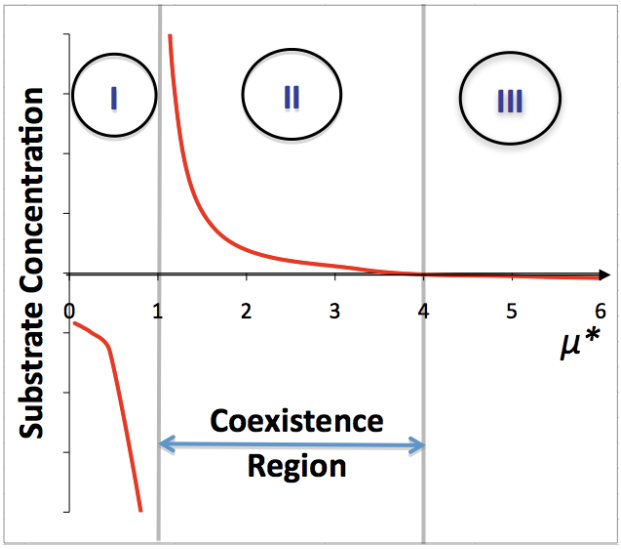

Figure 4.1. Regions of coexistence and single population existence. Region (I) with values of $\mu^* < 1$ represents only electricigenic microorganisms, while region (II) where $1 < \mu^* < 4$ represents coexistence and (III) $\mu^* > 4$ represents only methanogenic microorganisms.

To illustrate this proof, the influence of the external resistance on the populations at steady state is presented in Figure 4.2. The R_{ext} varied between 10 to 5000 Ω, while the influent concentration was 1000 mg L^{-1}. Three regions can be distinguished in this figure: (I) only electricigenic microorganisms (low R_{ext}); (II) coexistence (intermediate R_{ext}), and; (III) only methanogenic microorganisms (e.g. anaerobic reactor, with high R_{ext}). Calculation with zero decay rate constants produced qualitatively the same results, supporting the hypothesis that decay rates can be neglected.

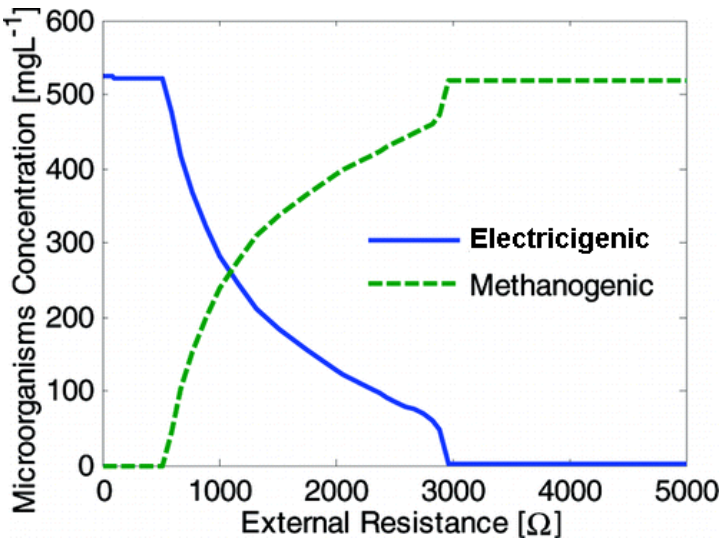

Figure 4.2. Predicted concentration of electricigenic and methanogenic populations as a function of R_{ext}.

The results presented in Figure 4.2 were qualitatively confirmed in other experimental work. Aelterman et al. (2008), observed low methane production and stable power output in an MFC operated at an R_{ext} set close to the R_{int} of the MFC. Furthermore, as seen in section 1.2.4, Chae et al. (2010) concluded that electricity production was increased and methane production was decreased in MFCs only at an R_{ext} close to R_{int}, or when a methanogenesis inhibitor was added to the anodic chamber. At the end of this chapter, MFC experimental results that qualitatively confirm this proposition will be presented.

4.3. Variation of Substrate Consumption with External Load and Effluent Concentration

Coexistence depends on the difference between the growth rates of the methanogenic and the electricigenic populations, while treatment capacity depends on the substrate consumption of these microorganisms. From Eq. (3-4), it can be seen that the consumption rate depends on the desired effluent substrate concentration and the concentration of each microbial population. As seen in the previous section, the latter is determined by the external resistance (electric load) of the MFC. So, the effect of external load and effluent concentration on the consumption rate is studied in this section.

Proposition 2. If $\frac{q_{max,e}\mu_{max,m}}{q_{max,m}\mu_{max,e}} \leq 1$, then coexistence always leads to lower substrate consumption.

Proof. This result can be proved by comparing the substrate consumption rates (q) for each region. For a given A, q_m = constant and q_e is maximised when $M_{ox} = M_{Total}$, e.g., at low R_{ext}:

$$q_e^{\max} = q_{max,e}\frac{A}{K_{A,e}+A}\frac{M_{Total}}{K_M+M_{Total}}X_{MAX} \tag{4-5}$$

$$q_m^{\max} = q_{max,m}\frac{A}{K_{A,m}+A}X_{MAX} \tag{4-6}$$

For the coexistence region, the substrate consumption rate is (q_c):

$$q_c^{\max} = q_{max,e}\frac{A}{K_{A,e}+A}\frac{M_{ox}}{K_M+M_{ox}}x_e + q_{max,m}\frac{A}{K_{A,m}+A}(X_{MAX}-x_e) \tag{4-7}$$

The coexistence only occurs when $\mu_e = \mu_m = \alpha D$, then Eq. (4-3) is valid. Substituting the same gives:

$$q_c^{\max} = \left[\frac{q_{max,e}\mu_{max,m}}{q_{max,m}\mu_{max,e}}\frac{x_e}{X_{MAX}} + \left(1-\frac{x_e}{X_{MAX}}\right)\right]q_{max,m}\frac{A}{K_{A,\,m}+A}X_{MAX} \tag{4-8}$$

$$\frac{q_c^{\max}}{q_m^{\max}} = \left[1+(\kappa-1)\lambda\right] \tag{4-9}$$

Eq. (4-9) is always smaller than 1, because of the definition of $\kappa = \frac{q_{max,e}\mu_{max,m}}{q_{max,m}\mu_{max,e}} \leq 1$ and the definition of $\lambda = x_e/X_{MAX}$., which varies between 0 and 1. Thus, if $\kappa < 1$, then $q_c^{max} \leq q_m^{max}$. ■

Proposition 2 can be illustrated by the following example presented in Fig. 4.3, where the influence of external resistance on the substrate consumption rate is shown. For this example two

constant effluent substrate concentrations (low and high) were selected. At low effluent substrate concentrations, an MFC with small external resistance (electricigens only) consumes the most organic matter, while for high concentrations the best cleaning performance is reached at high resistance (methanogens only). Fig. 4.3 also shows that the coexistence always leads to poorer substrate consumption.

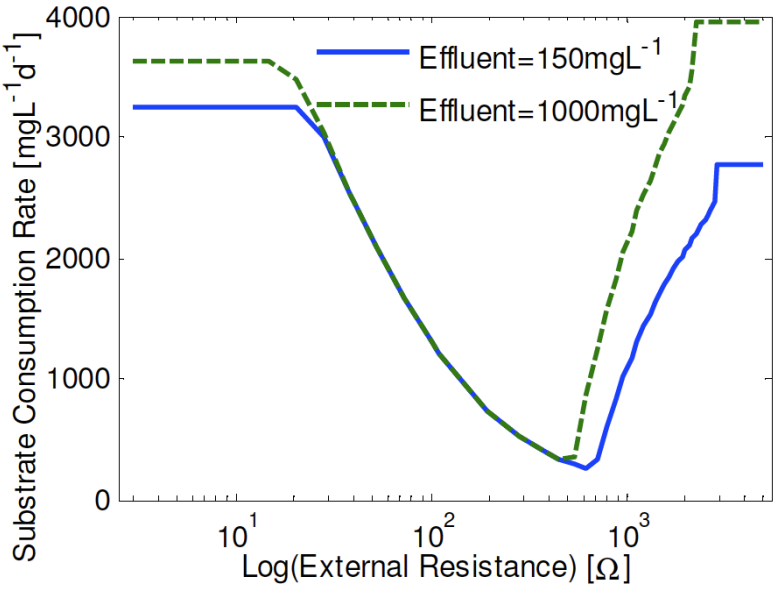

Figure 4.3. Steady state substrate consumption rate for MFCs operated at low (150 mg L^{-1}) and high (1200 mg L^{-1}) effluent concentrations.

To analyse this aspect further, the influence of the consumption rate on the effluent substrate concentration (A) is presented in Fig. 4.4. Three values of R_{ext} are chosen that correspond to (I) only electricigens, (II) coexistence, and (III) only methanogens. The influent concentration was varied from 150 to 2500 mg L^{-1}. It can be seen that the methanogens perform better for higher substrate concentrations while the electricigens do better at lower concentrations. As confirmed in Proposition 2, the coexistence always results in a decreased substrate consumption rate.

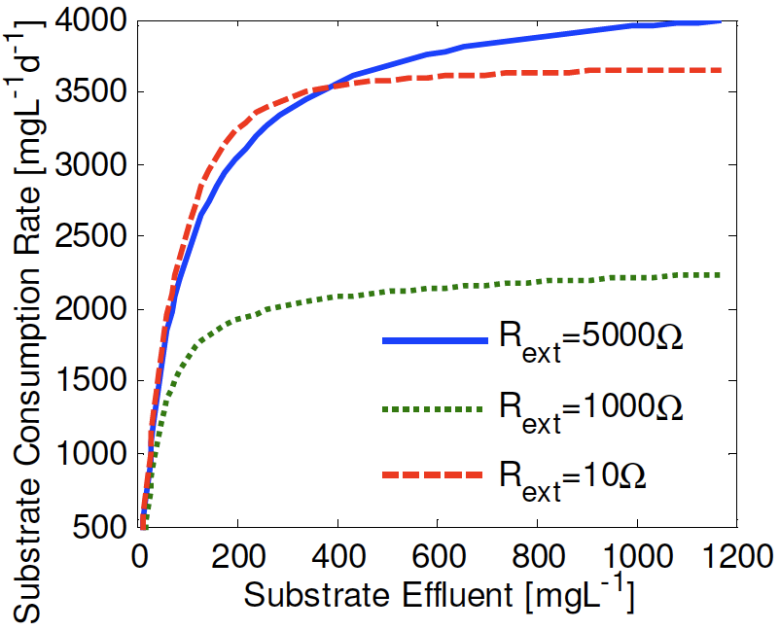

Figure 4.4. Steady state substrate consumption rate for MFCs colonised by either electricigens (R_{ext} = 10Ω), both populations (R_{ext} = 1000Ω), or methanogens (R_{ext} = 5000Ω).

The intersection point of the two curves in Fig. 4.4 can be expressed as follows:

$$\overline{A} = \frac{K_{A,\,m} - K_{A,\,e}\overline{q}}{\overline{q} - 1}, \qquad \text{where} \qquad \overline{q} = \frac{q_{\max,m}}{q_{\max,e}} \frac{K_M + M_{ox}}{M_{ox}} \frac{x_m}{x_e} \tag{4-10}$$

If $x_m = x_e = X_{MAX}$ and $M_{ox} = M_{Total}$, for the given set of model parameters $\overline{A}$ can be computed as 354 mg L^{-1}. So, for $A < \overline{A}$ the electricigens have a higher substrate consumption rate than methanogens and vice versa. As R_{ext} increases, M_{ox} decreases and the value of $\overline{A}$ increases. Furthermore, the lower the R_{ext} is, the larger the substrate consumption rate for electricigens.

4.4. Optimisation of Substrate Consumption by Staging

4.4.1. Staging

As discussed in section 1.2.3, staging may be an interesting option for improving the treatment capacity of MFCs, since the substrate consumption in these CSTR bioreactors is described by Monod kinetics. A staging unit with two MFCs is presented in the following figure.

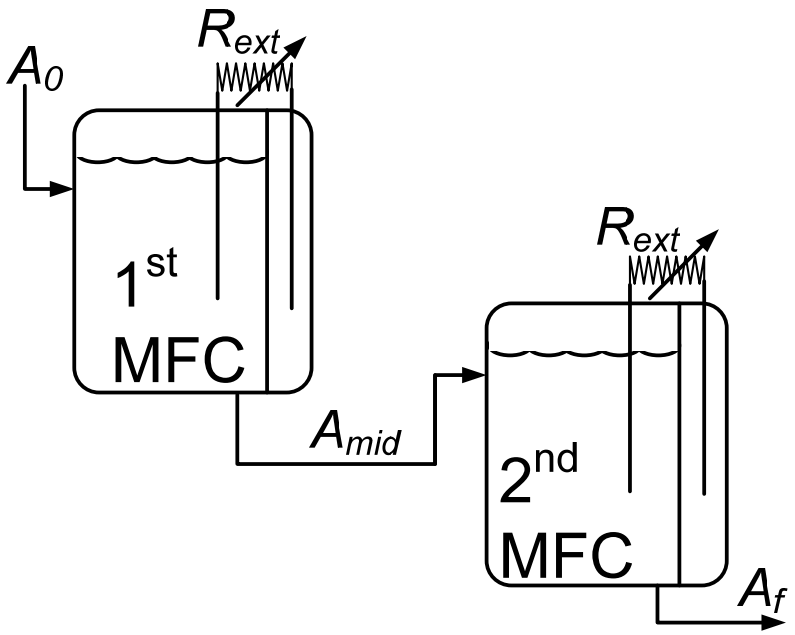

Figure 4.5. A simplified diagram of the design of two MFCs placed in series (staging technique).

The advantages and disadvantages of a staging strategy for improving the treatment capacity (flow rate for a given effluent concentration) of the MFC will be studied in this section. First, it is shown mathematically that if two MFC reactors were present, staging would always lead to better performance than running the reactors in parallel.

Proposition 3. Given a fixed influent concentration and an effluent concentration, operating two MFCs in series leads to a higher treatment performance than operating them in parallel.

Proof. Consider the two MFCs to have only acetoclastic methanogens (anaerobic reactor) and to have the same volume. This analysis would be similar for MFCs with electricigens. Let A_f be the MFC-specified desired effluent concentration. The flow rate of the parallel configuration (F_P) at steady state is given by:

$$F_P = \frac{2V}{(A_0 - A_f)} q_{max,m} \frac{A_f}{K_{A,m} + A_f} X_{MAX} \tag{4-11}$$

For the MFCs in series, let A_{mid} be the effluent concentration of the first reactor and the influent concentration of the second. Then, the flow rate (F_S) is given by:

$$F_S = \frac{Vq_{max,m}}{(A_0 - A_{mid})} \frac{A_{mid} X_{MAX}}{K_{A,m} + A_{mid}} = \frac{Vq_{max,m}}{(A_{mid} - A_f)} \frac{A_f X_{MAX}}{K_{A,m} + A_f} \tag{4-12}$$

The above equation can be solved to give:

$$A_{mid} = \frac{A_f (A_f + A_0) + \sqrt{A_f^2 (A_f + A_0)^2 + 4A_0 K_{A,m} A_f (K_{A,m} + 2A_f)}}{2(K_{A,m} + 2A_f)} \tag{4-13}$$

For the series configuration to be better than the parallel one, $F_S > F_P$:

$$\frac{1}{(A_{mid} - A_f)} > \frac{2}{(A_0 - A_f)}, \text{ e.g., } \quad A_{mid} < \frac{(A_0 + A_f)}{2} \tag{4-14}$$

So, the proposition can be proved if it can be shown that:

$$\frac{A_f (A_f + A_0) + \sqrt{A_f^2 (A_f + A_0)^2 + 4A_0 K_{A,m} A_f (K_{A,m} + 2A_f)}}{2(K_{A,m} + 2A_f)} < \frac{(A_0 + A_f)}{2} \tag{4-15}$$

Moving A_f $(A_f + A_0)/2(K_{A,m} + 2A_f)$ to the right hand side, removing the denominators and re-arranging gives:

$$A_f^2 (A_f + A_0)^2 + 4A_0 K_{A,m} A_f (K_{A,m} + 2A_f) < (A_0 + A_f)^2 (K_{A,m} + A_f)^2 \tag{4-16}$$

Eq. (4-16) can be further simplified to:

$$4A_0 A_f < (A_0 + A_f)^2 \tag{4-17}$$

Which is obviously true since $(A_f - A_0)^2 > 0$. Therefore, $A_{mid} < (A_f + A_0)/2$ and so, $F_S > F_P$. ■

Staging performance will change if the growth kinetics is described by Haldane kinetics (Andrews, 1968), which includes microorganism inhibition at higher substrate concentrations. As described in section 1.1.1.1, Haldane kinetics was not considered for MFCs.

4.4.2. Optimising a Two-Stage Process

The optimisation problem addressed in this section is the following, given: (i) two MFCs of prefixed volume; (ii) a fixed influent concentration, and; (iii) a constraint on the effluent concentration, choose (i) the interconnection structure between the MFCs, and (ii) the external resistance of each MFC in order to maximise the treatment capacity (as flow rate) of the MFCs.

From a substrate consumption point of view, the choice of external resistance can be considered binary. This is in fact justified by proposition 2, where the coexistence always leads to lower substrate consumption rates. For operation with methanogens, which necessitates high external resistance, R_{ext} = 5000 Ω was selected. It should be emphasised, that MFC operation at high external resistance essentially converts an MFC into an anaerobic reactor. For simulations with electricigens, a low external resistance of 10 Ω was chosen. Thus, the interconnection structure and external resistance are binary variables, which in turn lead to the following six interconnection configurations:

MP - Two MFCs with high external resistance in parallel (methanogens)
EP - Two MFCs with low external resistance in parallel (electricigens)
MM - Two MFCs in series, both with high external resistance (methanogens)
ME - Two MFCs in series, the first with high external resistance followed by the second with low external resistance (methanogens and electricigens)
EM - Two MFCs in series, the first with low external resistance followed by the second with high external resistance (electricigens and methanogens)
EE - Two MFCs in series, both with low external resistance (electricigens)

Thus, the optimisation problem is purely a combinatorial one. So, the flow rates for all six configurations would be evaluated and the best is selected. The configurations ME and EM can be considered as cogeneration systems since electricity and methane are produced in the same

configuration. Furthermore, the results presented in this section do not take into account the price of electricity and methane, which could affect the choice of reactor configuration.

Here it is shown mathematically which configuration is the best for each case.

Proposition 4. Let $A_0 > A_f$, $q^* = \frac{q_{\max,m}}{q_{\max,e}} \frac{K_M + M_{Total}}{M_{Total}}$, $A^* = \frac{K_{A,m} - K_{A,e} q^*}{q^* - 1}$ and $\hat{A} = \frac{A^*(A^* K_{A,e} + 2A^* A_f - A_f^2)}{A_f (K_{A,e} + A^*)}$.

If $A_f > A^*$, then the configuration MM will have the largest treatment capacity.
If $A_f < A^*$ and $A_0 > \hat{A}$ then the configuration ME will have the largest treatment capacity.
If $A_f < A^*$ and $A_0 < \hat{A}$ then the configuration EE will have the largest treatment capacity.

Proof. Assume that the oxidised mediator is at the maximum level ($M_{ox} = M_{Total}$) for all reactors with electricigens. The treatment capacity for each configuration can be written as:

$$F_{MM} = \frac{VX_{MAX}}{(A_{midMM} - A_f)} \frac{q_{max,m} A_f}{K_{A,m} + A_f} = \frac{VX_{MAX}}{(A_0 - A_{midMM})} \frac{q_{max,m} A_{midMM}}{K_{A,m} + A_{midMM}} \quad (4\text{-}18)$$

$$F_{ME} = \frac{VX_{MAX}}{(A_{midME} - A_f)} \frac{q_{max,e} A_f}{K_{A,e} + A_f} \frac{M_{Total}}{K_M + M_{Total}} = \frac{VX_{MAX}}{(A_0 - A_{midME})} \frac{q_{max,m} A_{midME}}{K_{A,m} + A_{midME}} \quad (4\text{-}19)$$

$$F_{EM} = \frac{VX_{MAX}}{(A_{midAM} - A_f)} \frac{q_{max,m} A_f}{K_{A,m} + A_f} = \frac{VX_{MAX}}{(A_0 - A_{midEM})} \frac{q_{max,e} A_{midEM}}{K_{A,e} + A_{midEME}} \frac{M_{Total}}{K_M + M_{Total}} \quad (4\text{-}20)$$

$$F_{EE} = \frac{VX_{MAX}}{(A_{midEE} - A_f)} \frac{q_{max,e} A_f}{K_{A,e} + A_f} \frac{M_{Total}}{K_M + M_{Total}} = \frac{VX_{MAX}}{(A_0 - A_{midEE})} \frac{q_{max,e} A_{midEE}}{K_{A,e} + A_{midEE}} \frac{M_{Total}}{K_M + M_{Total}} \quad (4\text{-}21)$$

From the definition of A^* and q^* one can find that $\frac{q_{\max,e} M_{Total}}{K_M + M_{Total}} = q_{\max,m} \frac{K_{A,e} + A^*}{K_{A,m} + A^*}$, then each of Eqs. (4-18) to (4-21) can be arranged such that:

$$F_{12} = \frac{VX_{MAX} q_{\max,m}}{K_{A,m} + A^*} \frac{A_f}{(A_{mid} - A_f)} \frac{K_{A2} + A^*}{K_{A2} + A_f} = \frac{VX_{MAX} q_{\max,m}}{K_{A,m} + A^*} \frac{A_{mid}}{(A_0 - A_{mid})} \frac{K_{A1} + A^*}{K_{A1} + A_{mid}} \quad (4\text{-}22)$$

where A_{mid} is the intermediate concentration between the first and second MFC, and the subscripts 1 and 2 denote the first and the second MFC respectively.

From Eq. (4-22), it can be seen that

$$A_f = A_{mid} \frac{(A_{mid} - A_f)}{(A_0 - A_{mid})} \frac{K_{A1} + A^*}{K_{A1} + A_{mid}} \frac{K_{A2} + A_f}{K_{A2} + A^*} \tag{4-23}$$

Note that all concentrations and half saturation constants are positive, i.e. $K_{A1} > 0$, $K_{A2} > 0$, $A_0 > 0$, $A_{mid} > 0$, and $A_f > 0$. From Eq. (4-23) it can be seen that $(A_{mid} - A_f) / (A_0 - A_{mid}) > 0$. Therefore, it can be deduced that $sign(A_{mid} - A_f) = sign(A_0 - A_{mid})$. Since the sign is not changed by the addition of two quantities of the same sign, $sign(A_{mid} - A_f + A_0 - A_{mid}) = sign(A_0 - A_f) = sign(A_{mid} - A_f) = sign(A_0 - A_{mid})$. Due to the assumption $A_0 > A_f$, $sign(A_0 - A_f)$ is positive. Consequently, $A_{mid} > A_f$ and $A_{mid} < A_0$.

Now, differentiating the first equality of (4-22) with respect to K_{A1} and the second equality with respect to K_{A2} we obtain:

$$\frac{\partial F_{12}}{\partial K_{A1}} = \frac{\partial F_{12}}{\partial A_{mid}} \frac{\partial A_{mid}}{\partial K_{A1}} = -\frac{F_{12}}{(A_{mid} - A_f)} \frac{\partial A_{mid}}{\partial K_{A1}} \tag{4-24}$$

$$\frac{\partial F_{12}}{\partial K_{A2}} = \frac{\partial F_{12}}{\partial A_{mid}} \frac{\partial A_{mid}}{\partial K_{A2}} = F_{12} \left[\frac{K_{A,1}}{A_{mid}(K_{A,1} + A_{mid})} + \frac{1}{(A_0 - A_{mid})} \right] \frac{\partial A_{mid}}{\partial K_{A2}} \tag{4-25}$$

Note that A_f is a constant, Eq. (4-23) can be differentiated with respect to K_{A1} and K_{A2}, yielding:

$$\frac{\partial A_{mid}}{\partial K_{A1}} = \frac{\dfrac{(A^* - A_{mid})}{(K_{A1} + A^*)(K_{A1} + A_{mid})}}{\dfrac{K_{A1}}{A_{mid}(K_{A1} + A_{mid})} + \dfrac{1}{(A_0 - A_{mid})} + \dfrac{1}{(A_{mid} - A_f)}} \tag{4-26}$$

$$\frac{\partial A_{mid}}{\partial K_{A2}} = \frac{\dfrac{(A_f - A^*)}{(K_{A2} + A_f)(K_{A2} + A^*)}}{\dfrac{K_{A1}}{A_{mid}(K_{A1} + A_{mid})} + \dfrac{1}{(A_0 - A_{mid})} + \dfrac{1}{(A_{mid} - A_f)}} \tag{4-27}$$

Since $A_0 > A_{mid} > A_f$, the following can be concluded from Eqs. (4-24) to (4-27),

$$sign\left(\frac{\partial F_{12}}{\partial K_{A1}}\right) = -sign\left(\frac{\partial A_{mid}}{\partial K_{A1}}\right) = sign\left(A_{mid} - A^*\right) \tag{4-28}$$

$$sign\left(\frac{\partial F_{12}}{\partial K_{A2}}\right) = sign\left(\frac{\partial A_{mid}}{\partial K_{A2}}\right) = sign\left(A_f - A^*\right) \tag{4-29}$$

Now, three areas of operation can be depicted and the following conclusions can be affirmed:

- Consider the case when $A_f > A^*$. Since $A_{mid} > A_f$, $A_{mid} > A^*$. Under this assumption, $\partial F_{12}/\partial K_{A1} > 0$ and $\partial F_{12}/\partial K_{A2} > 0$. Therefore, to maximise F_{12}, a maximum K_{A1} and K_{A2} must be selected. Then, $K_{A,m} > K_{A,e}$ leads to an optimum configuration MM.
- Consider the case when $A_f < A^*$ and $A_{mid} > A^*$. Under this assumption, $\partial F_{12}/\partial K_{A1} > 0$ and $\partial F_{12}/\partial K_{A2} < 0$. Now, to maximise F_{12}, a maximum K_{A1} and a minimum K_{A2} must be selected. Then, $K_{A,m} > K_{A,e}$ leads to an optimum configuration ME.
- Consider the case when $A_f < A^*$ and $A_{mid} < A^*$. Under this assumption $\partial F_{12}/\partial K_{A1} < 0$ and $\partial F_{12}/\partial K_{A2} < 0$. To maximise F_{12}, a minimum K_{S1} and K_{S2} must be selected. Then, the optimum configuration is indeed EE.

The condition $A_{mid} < A^*$, can be represented in terms of A_0 instead of A_{mid}. For this, Eq. (4-23) is rearranged to obtain:

$$A_0 = A_{mid}\left(1 + \frac{(A_{mid} - A_f)}{A_f}\frac{K_{A1} + A^*}{K_{A1} + A_{mid}}\frac{K_{A2} + A_f}{K_{A2} + A^*}\right) \tag{4-30}$$

When $A_{mid} = A^*$

$$A_0 = \frac{A^*(A^*K_{A2} + 2A^*A_f - A_f^2)}{A_f(K_{A2} + A^*)} \tag{4-31}$$

Also the $\partial A_0/\partial A_{mid} > 0$ as seen below:

$$\frac{\partial A_0}{\partial A_{mid}} = 1 + (A_0 - A_{mid})\left(\frac{K_{A1}}{A_{mid}(K_{A1} + A_{mid})} + \frac{1}{(A_{mid} - A_f)}\right) > 0 \tag{4-32}$$

So, the inequality $A_{mid} < A^*$ can be written in terms of A_0 as:

$$A_0 < \frac{A^*(A^*K_{A2} + 2A^*A_f - A_f^2)}{A_f(K_{A2} + A^*)} \tag{4-33}$$

The inequality $A_{mid} < A^*$ is valid only when $A_f < A^*$. However, when $A_f < A^*$, $\partial F_{12}/\partial K_{A2} < 0$, which leads to the second MFC always containing electricigenic microorganisms. So, using $K_{A2} = K_{A,e}$ gives $A_0 < \hat{A}$. ■

The next step was to compare the six different configurations with model simulations. All calculations were done at steady state using the model presented in chapter 3. Figure 4.6*a* shows the dependence of flow at steady state on the effluent substrate concentration for $A_0 = 1000$ mg L^{-1}. The operation of reactors in parallel can be analysed using this figure. As expected, the treatment capacity was larger for an MFC occupied by electricigens when substrate effluent concentration was low. When the treatment requirements were less strict, an MFC with methanogens presented a larger treatment capacity. For the two MFCs in parallel, with a specific substrate effluent concentration, the maximum treatment capacity could be found simply by multiplying the treated flow by the number of MFCs in parallel.

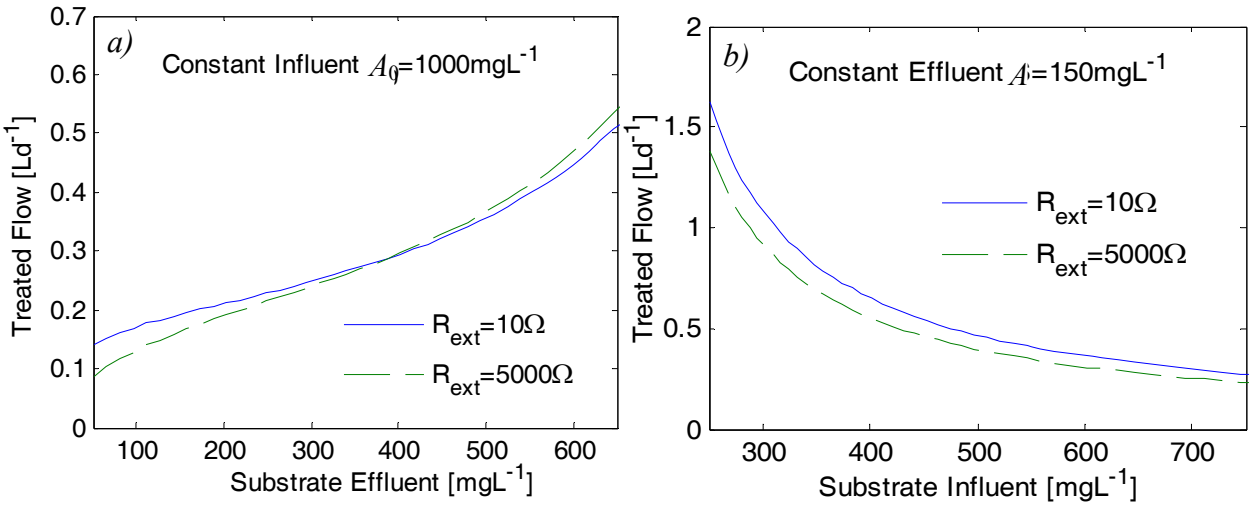

Figure 4.6. Treatment capacity of MFCs at steady state for diverse treatment requirements. (*a*) Treatment capacity of the two MFCs connected in parallel and operated at an influent concentration of 1000 mg L^{-1}. (*b*) Treatment capacity of the second MFC of the two MFCs connected in series at an effluent concentration was kept at 150 mg L^{-1}. The treatment capacity of the first MFC in series is the same as in MFCs in parallel (panel (*a*)).

The treatment capacity of MFCs operating in series was also graphically computed. For this, another curve that links the substrate influent concentration with the flow for a given fixed effluent concentration is required. This curve is represented in Figure 4.6*b*. When Figures 4.6*a* and 4.6*b* are plotted on the same figure, the crossing points represent the treatment capacity of each configuration in series (MM, ME, EM, or EE).

The treatment capacity for all configurations analysed above was computed for numerous influent and effluent concentrations. These results are summarised in Figure 4.7, where the design that presents the largest treatment capacity is indicated in each region:

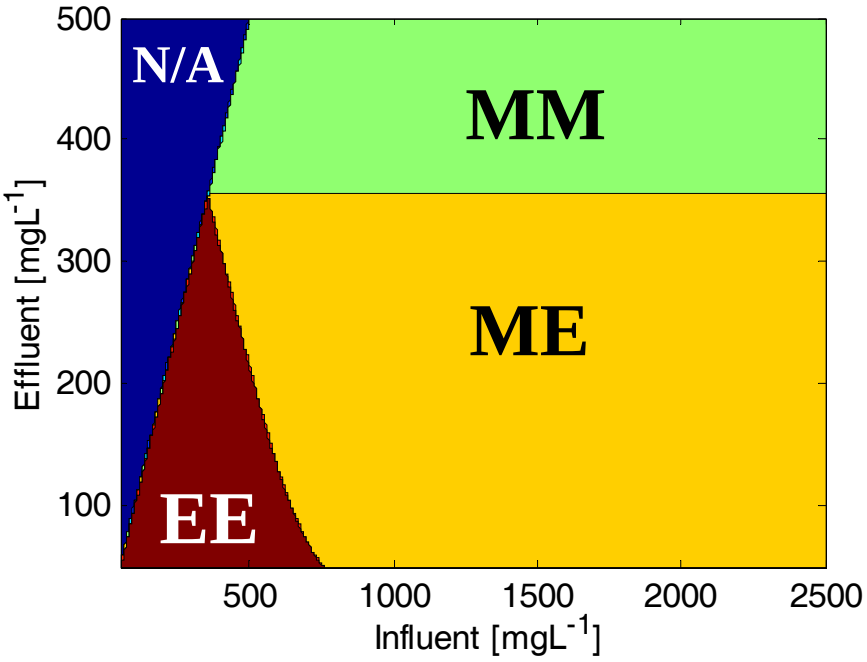

Figure 4.7. Regions with the largest treatment capacity. Area denoted by N/A represents a section where the effluent is larger or the same as the influent (unfeasible region). Notations: MM: two MFCs in series, both with high external resistance (methanogens); ME: two MFCs in series, the first with high external resistance followed by the second with low external resistance (methanogens and electricigens), and; EE: two MFCs in series, both with low external resistance (electricigens).

As shown in proposition 4, the configuration in series with the first MFC operating as a methanogenic reactor and second MFC in electricigenic mode represent the best treatment capacity for most of the wastewater treatment operating regions ($A_f < A^*$ and $A_{mid} > A^*$). This configuration has the methanogens consuming substrate at large substrate concentrations and electricigens polishing the effluent concentration to a specific requirement. When the effluent requirements are less strict ($A_f > A^*$), the configuration with two methanogenic MFCs in series is the best. For low concentrations of influent ($A_f < A^*$ and $A_{mid} < A^*$), two electricigenic MFCs in series present the best results. As expected from the development made in proposition 4, the boundary between configuration MM and ME occurs when the effluent is A^*. In addition, the curve that describes $A_{mid} = A^*$ represents the frontier between regions EE and ME in Fig. 4.7.

An additional challenge for the electricity production design is the control of R_{ext}. While the selection of a low R_{ext} enhances electricigenic concentration, an R_{ext} smaller than the R_{int} of the

MFC strongly decreases the power output. As discussed in section 1.2.7, the best choice for such design would be matching R_{ext} with R_{int}.

As previously mentioned, an MFC that only contains methanogens operates as an anaerobic reactor. In this case, all the extra material involved in building an MFC can be excluded (anode, cathode, external load, etc.). However, the flexibility offered by an MFC presents a great advantage for moving from one population to another, simply by adjusting the external load. Yet, the slow dynamics of microorganism growth presents a restriction, such that it takes time to switch between populations. However, this same limitation may also minimise the effect of population elimination, e.g. even at extreme values of R_{ext}, both populations may coexist for an extremely long time, one of them at very low concentrations.

4.5. Competitive Exclusion and Coexistence: Experimental Validation

In this section, experimental MFC results aimed to confirm proposition 1 are presented. These experiments evaluated the impact of the external resistance on the long-term performance of a MFC and demonstrated the real-time optimisation of the external resistance. For this purpose, acetate-fed MFCs were operated at external resistances, which were above, below, or equal to the internal resistance of a corresponding MFC. A P/O algorithm was used for the real-time optimal selection of the external resistance. MFC operation at the optimal external resistance resulted in increased power output, improved Coulombic efficiency, and low methane production. These results along with sWW fed MFC experiments were published in Pinto, Srinivasan, Guiot, and Tartakovsky (2011a). Note that the sWW fed MFC results are not presented in this thesis.

4.5.1. The Impact of External Resistance on MFC Performance

The effect of R_{ext} on long-term MFC performance was studied by simultaneously operating acetate fed MFC-4, 5, and 6 at low, high, and optimal R_{ext} settings, respectively, for 30-35 days (Table 2-1). The selected R_{ext} values were significantly different (e.g. high R_{ext} corresponded to 1000 Ω and low R_{ext} corresponded to 5 Ω, Table 2-1). The long length of the experimets reduced the impact of MFC performance variability due to the microbiological nature of the process on the comparison of MFC power outputs and other performance parameters at each mode of operation. Throughout the tests, variations in influent acetate concentration were simultaneously imposed for all MFCs. The profile of acetate influent concentration is shown in Figure 4.8*a*.

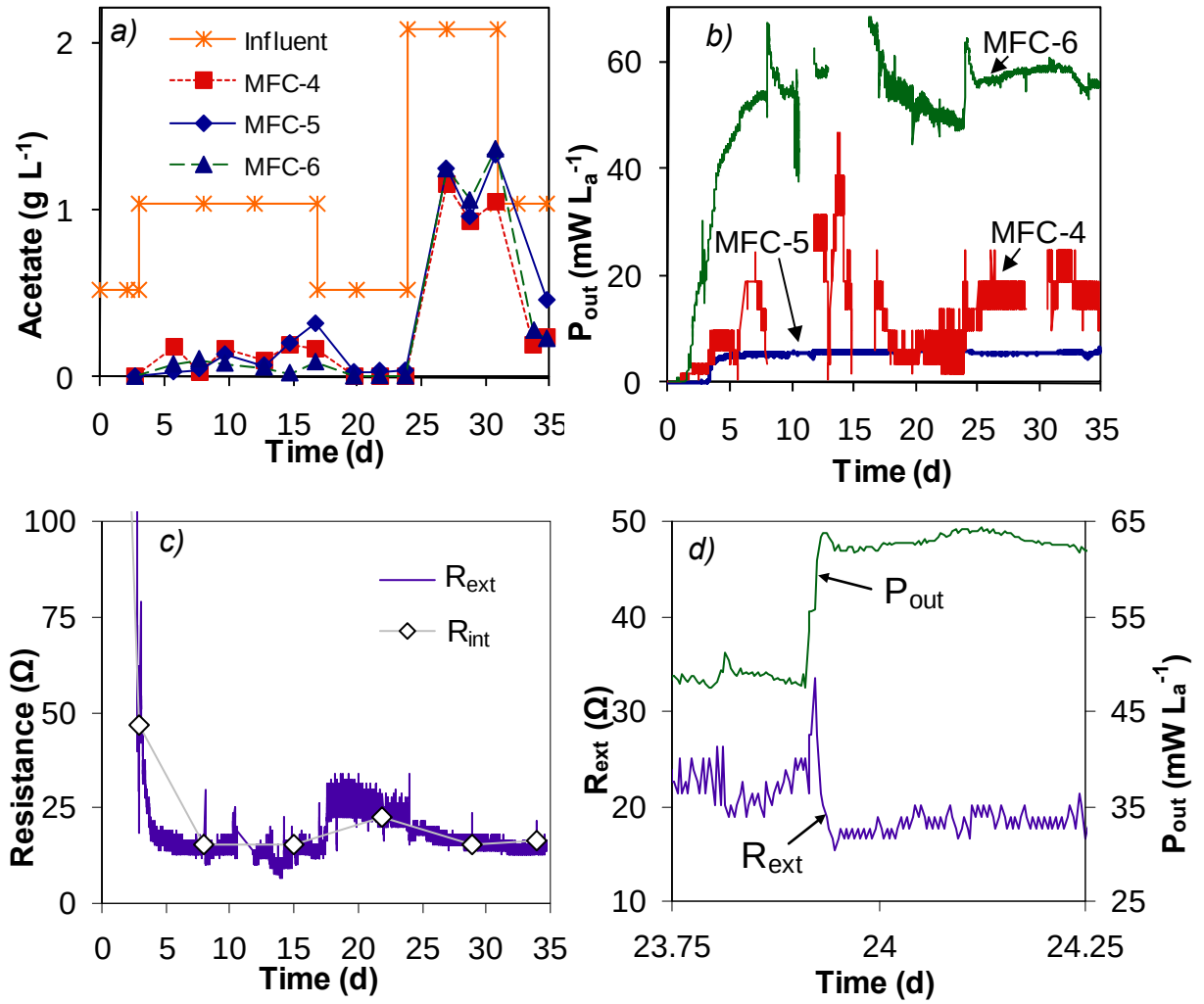

Figure 4.8. (*a*) Acetate concentration in the influent and effluent, and (*b*) power production for MFC-4, MFC-5, and MFC-6 against time; (*c*) R_{ext} and R_{int} values for MFC-6 (MFC-4 and MFC-5 R_{ext} values were always kept at 5 Ω and at 1000 Ω, respectively); (*d*) R_{ext} and P_{out} values during an increase in the MFC-6 influent concentration at t=23.9 days.

Acetate concentration measurements in the effluent streams showed similar substrate removal in all MFCs, as can be seen from the values presented in Fig. 4.8*a*. At steady state, the effluent acetate concentration varied from 20 to 160 mg L^{-1}. At the same time, power outputs were quite different. Fig. 4.8*b* summarises power production observed throughout the tests. This figure shows that in all MFCs, power output began to increase after approximately 3 days of operation, reaching steady state values after 7-10 days. Power outputs at steady state strongly depended on R_{ext} selection with power outputs around 15, 6, and 58 mW L_a^{-1}, observed for MFC-4 (low R_{ext}), MFC-5 (high R_{ext}), and MFC-6 (optimal R_{ext}), respectively. Note that on day 13, the cathode of

MFC-6 was punctured and replaced by a new cathode, made of the same material. Following the replacement, MFC-6 power output approached 135 mW L_a^{-1} for about two days before returning to its previous level. This period was excluded from Fig. 4.8*b*. Also, due to technical problems, MFC-4 voltage was not recorded between days 8 to 12, 14.5 to 16.5, and 28.5 to 30.5.

Figure 4.8*c* presents changes in R_{ext} of MFC-6 imposed by the P/O algorithm over time. At start-up, R_{ext} values maintained by the algorithm were above 400 Ω, then after about 5 days of operation, R_{ext} sharply decreased to values below 40 Ω. This figure also shows R_{int} values estimated for MFC-6 during polarization tests. As expected, the P/O algorithm provided timely adjustment of R_{ext} to maintain it close to R_{int} values, such that the R_{ext} oscillated around the optimum value equal to the internal resistance of MFC-6. The profile of R_{int} change in the MFC-4 test was similar to that observed for MFC-6, rapidly decreasing to 15-30 Ω after the first 6 days of MFC operation, while R_{int} of MFC-5 remained at around 200 Ω for most of the test. These results corroborate with the development of equation 3-20, where the MFC R_{int} was assumed to decrease with the biofilm colonization.

While the growth of electricigenic microorganisms during the start-up period resulted in relatively slow changes in R_{int}, the variations in operating conditions had an almost immediate impact on R_{int} and therefore on MFC performance. The P/O algorithm's ability to track fast variations of operating conditions (e.g. influent composition) during MFC-6 operation is illustrated in Figure 4.8*d*. Here, the influent acetate concentration was increased from 0.5 to 2 g L^{-1} on day 24. This increase in acetate concentration caused a decrease of R_{int} and, accordingly, the MPPT algorithm decreased the R_{ext} value thus maximizing power output under new operating conditions.

Figure 4.9 presents estimations of current density and Coulombic efficiency (*CE*) for MFC-4, MFC-5, and MFC-6. As expected, MFC-5, which was operated at a high R_{ext}, always had a low current density and a low *CE*, while MFC-4 and MFC-6 showed larger values. MFC-4, which was operated at the lowest R_{ext}, was expected to have the highest Coulombic efficiency. However, current densities (Fig. 4.9*a*) and *CE* (Fig. 4.9*b*) of MFC-6, which was operated at an optimal R_{ext}, on average were slightly higher than that of MFC-4. *CE* calculations showed a more pronounced

difference between MFC-4 and MFC-6, however this difference could be attributed to the variability of the effluent acetate measurements. Also, MFC-6 featured the shortest start-up time, as can be seen from the comparison of current densities in Fig. 4.9*a*.

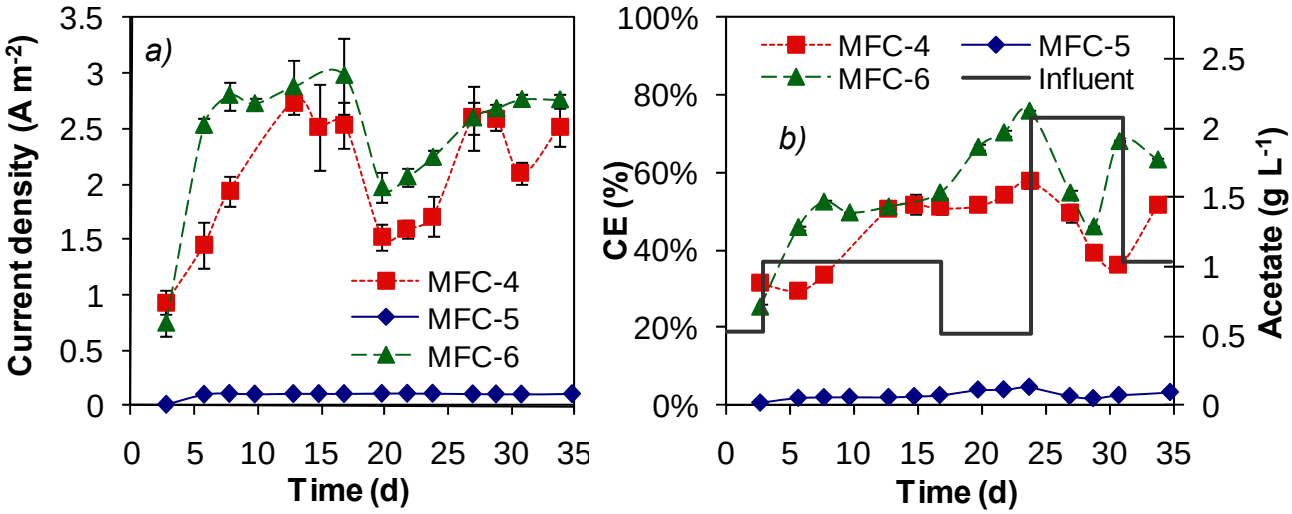

Figure 4.9. Current density (*a*) and Coulombic efficiency (*b*) measured during MFC operation at various acetate loads.

Polarization tests provided additional information for the comparison of MFC performances. Figure 4.10*a* shows the evolution of the cathode and anode open circuit potentials (OCP) over time. As expected, cathode OCP values were similar for all MFCs and remained constant throughout the experiment. Following the start-up, anode OCP values decreased for all MFCs, with the fastest decrease observed for MFC-4 (low R_{ext}), followed by MFC-6 (optimal R_{ext}). MFC-5, which was operated at a high R_{ext}, was the last to reach a steady state value of the anode potential. Nevertheless, the anode OCP values for all MFCs were similar after 15 days of testing. It can be hypothesised that this pattern of anode OCP decrease over time was reflective of anode colonization by the electricigenic microorganisms (see Eq. (3-20)). Indeed, lower values of R_{ext} facilitate the electron transfer process thus providing growth advantages to the electricigenic microorganisms. Consequently MFC-4 operated at the lowest R_{ext} featured the fastest rate of the electricigenic biofilm formation. However, MFC operation at a R_{ext} below R_{int} results in low power output, thus requiring R_{ext} optimisation.

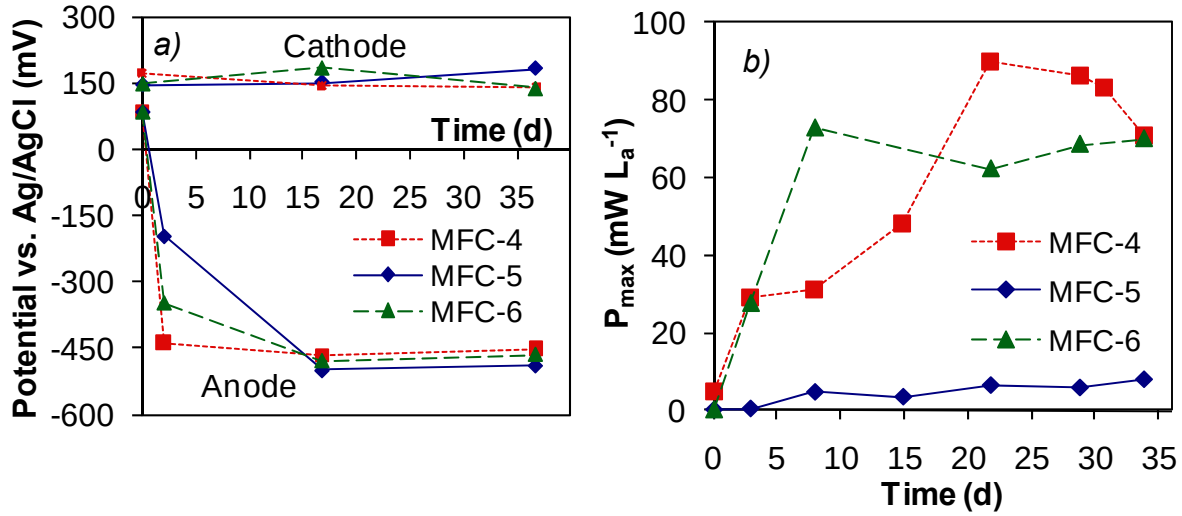

Figure 4.10. The evolution of the cathode and anode OCP values over time (*a*), and maximum power densities (*b*) observed in the polarization tests.

When maximal power outputs were estimated from the polarization test results, it was observed that MFC-5 always had low P_{max}, never exceeding 9 mW L_a^{-1}. Maximal power outputs estimated for MFC-4 and MFC-6 increased during the first 15-20 days of the experiment (Fig. 4.10*b*). A maximal power output of 95 mW L_a^{-1} was estimated based on the polarization test for MFC-6 on day 15, which was carried out shortly after the cathode replacement in this MFC. As mentioned above, the cathode replacement resulted in higher than usual power output between days 13 and 15. On average, MFC-6 maximal power output remained around 70 mW L_a^{-1}, which agreed well with the power densities measured during the MFC-6 test (Fig. 4.8*b*). At the same time, power output of MFC-4 during normal operation was very low because of the choice of R_{ext}. The selection of R_{ext} for MFC-4 (R_{ext} = 5 Ω) and MFC-5 (R_{ext} = 1000 Ω) was confirmed by the polarization tests. After the start-up period, R_{int} in MFC-4 varied between 15 and 25 Ω, while in MFC-5 R_{int} varied between 50 and 200 Ω. Thus, MFC-4 was operated at $R_{ext} << R_{int}$, and MFC-5 was operated at $R_{ext} >> R_{int}$ throughout the test, as intended.

Besides power output comparison, methane production in the anodic compartment of each MFC was measured throughout the tests and was used to compare the long-term effects of R_{ext} selection on methane production. Since the MFCs were inoculated with anaerobic sludge, methane production was observed at the beginning of the operation in all MFCs. The methane production

in MFC-5 increased over time, while it decreased in MFC-4 and MFC-6. To compare electricity and methane production for MFC-4, MFC-5, and MFC-6, steady state values were calculated using experimental results obtained between day 7 and 30 of MFC operation, when constant organic load was applied. These results can be depicted in figure 4.11.

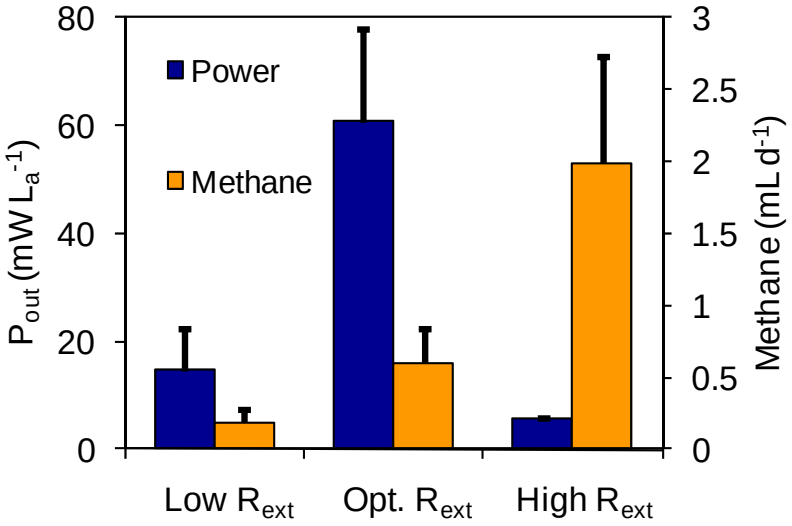

Figure 4.11. The average steady state power and methane production for MFC-4, 5, and 6, respectively kept at low, high, and optimum R_{ext}.

It should be acknowledged that methane flow measurements were complicated by the small volume (50 mL) of the anodic compartments and low methane production rates, in the range of several mL per day. Measurements of such small flow rates resulted in large standard deviations. Nevertheless, the overall trends were clear, showing significantly higher methane production in MFC-5 operated at high R_{ext}. In contrast, methane production in MFC-4 and in MFC-6 was very low. Importantly, methane and electricity production in the MFCs can be hypothesised to be proportional to the concentration of acetoclastic methanogenic and electricigenic microorganisms' populations in the biofilm, respectively.

The model prediction presented in proposition 1 are in perfect agreement with the findings presented in this section, where acetate fed MFCs were inoculated with the same anaerobic sludge and consumed comparable quantities of carbon source. They were operated at low, high, or optimal R_{ext} settings, leading to Coulombic efficiencies remarkably different (Fig. 4.9*b*). High

R_{ext} led to, essentially, an anaerobic reactor with low Coulombic efficiency and significant methane production. At the same time, both MFC-4 (low R_{ext}) and MFC-6 (optimal R_{ext}) featured high Coulombic efficiency, and by the end of the 30 day test, methane production in these MFCs declined to near zero values. Considering that MFC operation at R_{ext} values below R_{int} leads to a sharp drop in power output, it is sufficient to maintain R_{ext} at an optimal value in order to minimise methane production and maximise power production.

4.6. Conclusion

This chapter presented analysis of the two-population MFC model presented in chapter 3. The model predicts the concentration of electricigenic and methanogenic microorganisms, and shows that MFC external resistance (electric load) and organic load affect steady state distribution of microbial populations. Steady state analysis of the model shows three possible scenarios of microorganism distribution: (I) only electricigenic microorganisms; (II) coexistence, and; (III) only methanogenic microorganisms. Furthermore, methanogens have higher substrate consumption rates at higher substrate effluent concentrations than the electricigenic, while the reverse occurs at lower substrate concentrations. The coexistence scenario always leads to lower substrate consumption rates.

In addition, MFC staging was proven to always present better treatment capacity than parallel MFCs. Diverse designs for a staging unit with two MFCs were simulated to compare the maximum organic load treating capacity. The best design is a function of the dominant microbial population in each MFC, selected according to its external load. Regions with the best design were drawn as a function of influent and effluent concentrations. For the largest and most common region of operation, two MFCs in series, the first with high external resistance followed by a second with low external resistance, presented the best results.

Finally, an experimental comparison of MFC performance at an optimal R_{ext} value with MFCs operated at either high ($R_{ext} >> R_{int}$) or low ($R_{ext} << R_{int}$) external resistances qualitatively confirmed the long-term effects of external resistance on the concentration of the microorganisms in the MFC biofilm and showed that real-time resistance optimisation led to significantly higher power outputs with less methane production.

CHAPTER 5: MICROBIAL ELECTROLISYS CELL MODELLING

This section presents a multi-population dynamic model of a Microbial electrolysis cell (MEC). The model describes the growth and metabolic activity of fermentative, electricigenic, acetoclastic methanogenic, and hydrogenophilic methanogenic microorganisms and is capable of simulating hydrogen production in a MEC fed with complex organic matter, such as wastewater. The model parameters were estimated with the experimental results obtained in continuous flow MECs fed with acetate or synthetic wastewater. Following successful model validation with an independent data set, the model was used to analyse and discuss the influence of applied voltage and organic load on hydrogen production and COD removal. These results were published in Pinto, Srinivasan, Scapa, and Tartakovsky (2011b).

5.1. MEC Model Development

The main objective of the MEC model is to simulate the hydrogen production from wastewater in a simple, easily identifiable dynamic model which provides a fast convergence numerical solution and can be conveniently used in process design, control, and optimisation. The model equations presented here are based on the two-population MFC model presented in chapter 3 and on the anaerobic digestion model proposed by Bernard et al. (2001). Since a model complexity is directly associated with the number of microbial populations considered in its material balances, a minimal number of microorganisms that can adequately describe the experimental results have to be selected to provide model simplicity.

The anaerobic degradation of wastewater in the anodic compartment of a MEC was assumed to be described by a single hydrolysis and fermentation step of complex organic matter conversion to acetate (Bernard et al., 2001). Thus, all VFAs are represented by acetate, which is a significant simplification of the complexity of the multi-step anaerobic digestion process (Lettinga, 1995). This modelling simplification has been demonstrated to be sufficient for an acceptable description of the methane formation dynamics in anaerobic reactors (Bernard et al., 2001; Jeyaseelan, 1997; Moletta et al., 1986). Furthermore, the conversion of organic substrate into H_2 was considered to be negligible. Acetate is assumed to be consumed by both acetoclastic methanogenic and electricigenic microorganisms as in chapter 3. Finally, the model accounts for H_2 consumption by hydrogenotrophic methanogens (Hu, Fan, & Liu, 2008; Wang et al., 2009).

The MECs used for the experiments employed a 3D carbon felt anode, which occupied most of the anode compartment and offered a good support for the formation of an anaerobic biofilm (Yang, Tsukahara, Sawayama, & Maekawa, 2004). Due to the high porosity of the anode and considerably high recirculation rates, homogeneous distribution of the carbon source and the degradation products throughout the anode was assumed. To avoid the use of a distributed parameter model to describe carbon source and product distribution within the biofilm, the model was further simplified by assuming a layered biofilm structure, as proposed by Rauch et al. (1999) and using biofilm retention constants as presented in section 3.1 (α definition) in the biomass material balances. The existence of three biofilm layers was considered, as shown in Figure 5.1. The outer biofilm layer (Layer 1) was assumed to contain fermentative microorganisms converting wastewater to acetate, and acetoclastic methanogens converting acetate to methane. An inner biofilm, Layer 2, was assumed to contain the electricigenic and acetoclastic methanogenic microorganisms. Finally, the abundance of H_2 in a close proximity to the cathode was assumed to result in the existence of the third biofilm layer adjacent to the cathode and entirely populated by hydrogenotrophic methanogens (Layer 3 in Fig. 5.1).

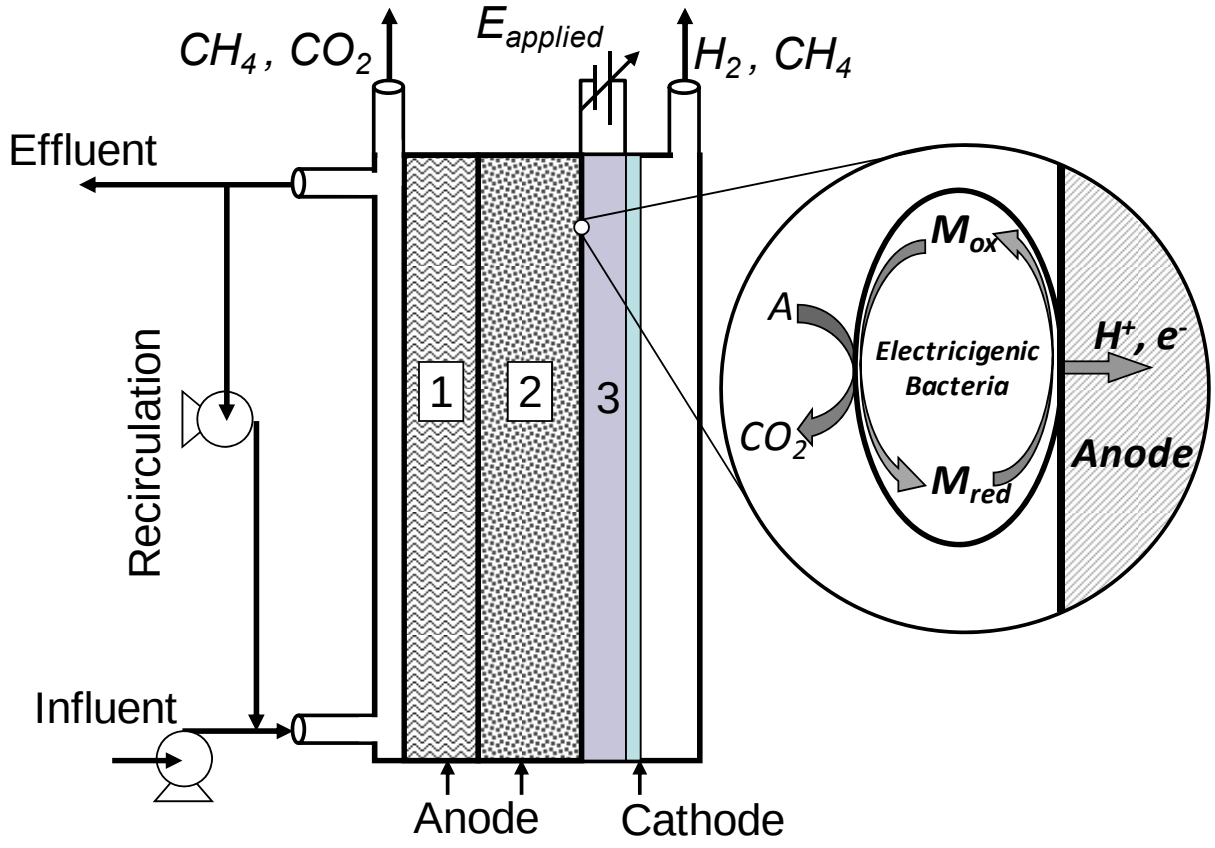

Figure 5.1. A simplified diagram of a continuous flow MEC with three biofilm layers. Layer 1 represents the outer anodic biofilm, containing fermentative and acetoclastic methanogenic microorganisms, layer 2 represents the inner biofilm, occupied by electricigenic and methanogenic (acetoclastic) microorganisms, and layer 3 represents the cathode biofilm populated by hydrogenotrophic methanogenic microorganisms. The conceptual acetate conversion in the anodic layer 2 by electricigenic microorganisms is shown in detail. M_{red} and M_{ox} denotes reduced and oxidised forms of an intracellular mediator, respectively.

Other simplifying assumptions included ideal mixing in the anodic compartment, the existence of a constant pool of intracellular electron transfer mediator in electricigenic microorganisms, and the absence of biomass growth in the anodic liquid. Also, temperature and pH were considered fully controlled and maintained at constant levels.

Stoichiometric Equations and Material Balances

Organic substrate transformation to acetate by fermentative microorganisms (x_f) is assumed to occur in a single step as discussed above. Such transformation can be illustrated by the transformation of glucose into acetate ($C_6H_{12}O_6 \rightarrow 3C_2H_4O_2$), or, in general:

$$S \rightarrow \text{n}A \tag{5-1}$$

Acetate consumption by electricigenic microorganisms (x_e) is described by Eqs. (3-1) and (3-2) as seen in section 3.1. The acetate consumption by the acetoclastic methanogenic microorganisms (x_m), which results in methane and carbon dioxide formation in biofilm Layer 1 and 2 (Fig. 5.1) is described by Eq. (3-3).

Hydrogen consumption by the hydrogenotrophic methanogenic microorganisms (x_h) is described as:

$$CO_2 + 4H_2 \rightarrow CH_4 + 2H_2O \tag{5-2}$$

For a continuous flow MEC with equal influent and effluent flow rates, the following material balance equations can be written:

Substrate Material Balances

$$\frac{dS}{dt} = -q_f x_f + D(S_0 - S) \tag{5-3}$$

$$\frac{dA}{dt} = -q_e x_e - q_m (x_{m,1} + x_{m,2}) + D(A_0 - A) + Y_{COD} q_f x_f \tag{5-4}$$

Outer Biofilm (Layer 1) Material Balances

$$\frac{dx_f}{dt} = \mu_f x_f - K_{d,f} x_f - \alpha_1 x_f \tag{5-5}$$

$$\frac{dx_{m,1}}{dt} = \mu_m x_{m,1} - K_{d,m} x_{m,1} - \alpha_1 x_{m,1} \tag{5-6}$$

Inner Biofilm (Layer 2) Material Balances

$$\frac{dx_e}{dt} = \mu_e x_e - K_{d,e} x_e - \alpha_2 x_e \tag{5-7}$$

$$\frac{dx_{m,2}}{dt} = \mu_m x_{m,2} - K_{d,m} x_{m,2} - \alpha_2 x_{m,2} \tag{5-8}$$

Cathodic Biofilm (Layer 3) Material Balance

$$\frac{dx_h}{dt} = \mu_h x_h - K_{d,h} x_h - \alpha_3 x_h \tag{5-9}$$

The biofilm retention in the anodic compartment is described by assuming that biomass growth in each biofilm layer is limited by the maximum attainable biomass concentration (X_{MAX}) and that the biofilm approaches its steady state thickness in the stationary phase (Mu et al., 2008; Wanner & Gujer, 1986). Therefore, in the growth phase, no biofilm washout occurs so that a batch reactor balance is used. When biofilm reaches its maximum biomass concentration a CSTR reactor balance is used. This approach is similar to the one presented in section 3.1, however the mathematical definition of the biofilm retention constant was changed, now using a hybrid model the biofilm retention constants α are defined as follows:

$$\begin{cases} \alpha_1 = \dfrac{\mu_f x_f - K_{d,f} x_f + \mu_m x_{m,1} - K_{d,m} x_{m,1}}{x_f + x_{m,1}}, & if \quad x_f + x_{m,1} \geq X_{\max,1} \\ \alpha_1 = 0, & otherwise \\ \alpha_2 = \dfrac{\mu_e x_e - K_{d,e} x_e + \mu_m x_{m,2} - K_{d,m} x_{m,2}}{x_e + x_{m,1}}, & if \quad x_f + x_{m,2} \geq X_{\max,2} \\ \alpha_2 = 0, & otherwise \\ \alpha_3 = \mu_h - K_{d,h}, & if \quad x_h \geq X_{\max,3} \\ \alpha_3 = 0, & otherwise \end{cases} \tag{5-10}$$

The methane production rate in the anode compartment ($Q_{CH4,A}$ expressed in mL-CH_4 d^{-1}) corresponding to biofilm Layers 1, 2, and the methane production rate from H_2 in Layer 3 ($Q_{CH4,C}$) is described by:

$$Q_{CH4,A} = Y_{CH4} q_m (x_{m,1} + x_{m,2}) V \quad (5\text{-}11)$$

$$Q_{CH4,C} = Y_{H2/CH4} Y_h \mu_h x_h V \quad (5\text{-}12)$$

The hydrogen production rate (in mL-H_2 d^{-1}) can be described by:

$$Q_{H2} = Y_{H2} \left(\frac{I_{MEC}}{m_{H2} F} \frac{RT}{P} \right) - Y_h \mu_h x_h V \quad (5\text{-}13)$$

Intracellular Material Balances

The intracellular balances for the electricigenic microorganisms were described in the same manner as in chapter 3, so oxidised and reduced mediators balance were described by Eqs. (3-9) and (3-10).

Kinetic Equations

The fermentative microorganisms were assumed to follow Monod kinetics equations, being limited by the organic substrate concentration:

$$\mu_f = \mu_{\max,f} \frac{S}{K_{S,f} + S} \quad (5\text{-}14)$$

$$q_f = q_{\max,f} \frac{S}{K_{S,f} + S} \quad (5\text{-}15)$$

The growth of the hydrogenotrophic methanogens in biofilm Layer 3 (Fig. 1) was assumed to depend on the H_2 concentration in water. Considering the low solubility of H_2 in water (approximately 1.5 mg L^{-1} at 30°C) and close proximity of the biofilm Layer 3 to the cathode, a zero-order growth kinetics was assumed. When no H_2 was produced (i.e. at a zero current), the

concentration of dissolved H_2 is assumed to rapidly decline to zero leading to no growth. This dependence can be represented by:

$$\mu_h \begin{cases} \mu_{\max,h} \ if \ I_{MEC} > 0 \\ 0 \qquad if \ I_{MEC} = 0 \end{cases} \tag{5-16}$$

The kinetics equations for electricigenic and acetoclastic methanogenic microorganisms were identical to the ones presented in section 3.1 (Eqs. (3-11) to (3-14)).

Electrochemical Equations

The MEC electrochemical balance can be written based on the concepts presented in sections 1.1.2 and 3.1:

$$-E_{applied} = E_{CEF} - \eta_{ohm} - \eta_{conc,A} - \eta_{conc,C} - \eta_{act,A} - \eta_{act,C} \tag{5-17}$$

Ohm's law can be applied in Eq. (5-17) to compute ohmic losses ($\eta_{ohm} = I_{MEC} R_{\text{int}}$). For MECs, concentration losses at the cathode will be neglected due to the small size of hydrogen molecules resulting in a large diffusion coefficient of hydrogen in the gas diffusion electrode used as a cathode. The concentration losses at the anode were calculated using the Eq. (3-16). Furthermore, since MECs operate at high over-potential at the cathode (Bruce E. Logan et al., 2008), the $\eta_{act,A}$ were assumed to be much smaller than $\eta_{act,C}$ and were neglected. The cathodic activation losses can be calculated by the Butler-Volmer equation. Assuming that the reduction and oxidation transfer coefficients that express the activation barrier symmetry are identical, the Butler-Volmer equation can be approximated as suggested by section 1.1.2.3:

$$\eta_{act,C} = \frac{RT}{\beta m F} \sinh^{-1}\left(\frac{I_{MEC}}{A_{sur,A} i_0} \right) \tag{5-18}$$

Therefore, the MEC current can be calculated by combining the electrochemical balance equations:

$$I_{MEC} = \frac{E_{CEF} + E_{applied} - \frac{RT}{mF}\ln\left(\frac{M_{Total}}{M_{red}}\right) - \frac{RT}{\beta mF}\sinh^{-1}\left(\frac{I_{MEC}}{A_{sur,A} i_0}\right)}{R_{\text{int}}} \quad (5\text{-}19)$$

Due to the activation losses at the cathode, the I_{MEC} calculation requires a numerical solution of the nonlinear Eq. (5-19), as $\eta_{act,C} = f(I_{MEC})$. Because the solution of Eq. (5-19) could result in negative I_{MEC} values if $E_{applied}$ is smaller than the sum of η_{act}, η_{conc}, and E_{CEF}, only non-negative values of I_{MEC} were considered.

Finally to improve the MEC model accuracy during the start-up period, the R_{int} values were linked to the concentration of electricigenic microorganisms, as presented in Eq. (3-20) in section 3.2.

5.2. Parameter Estimation

In spite of a number of simplifying assumptions used in model formulation, the dynamic model presented above includes 36 parameters, which had to be estimated for the numerical solution of the model. The task of parameter estimation was solved by problem decomposition. First, values were assigned to physical constants (Tables A-1 and A-2). Next, kinetic and stoichiometric parameters estimated in chapter 3 were adopted as initial values and then adjusted using experimental results obtained during MEC operation with acetate (MEC-1 test). Model parameters related to fermentative microorganisms were first adopted from ADM1 (D. J. Batstone et al., 2002a) and then adjusted using experimental results obtained during the MEC-2 test, where sWW was used as a carbon source.

In the MEC-1 test, only some model parameters could be estimated with acceptable accuracy since the measurable state variables were limited to the measurements of current, hydrogen and methane production, and acetate concentration in the effluent. After analyzing the Fisher information matrix (FIM), the maximal substrate consumption rate ($q_{max,e}$), mediator yield (Y_M), and counter-electromotive force (E_{CEF}) were considered to be identifiable. The confidence

intervals (95% confidence level) of these parameters were found to be 9.7%, 6.9%, and 4.2%, respectively.

Because current measurements were most accurate, the weight constants (w_i) required for the parameter estimation procedure (Eq. (2-9)) were selected as to provide higher weight to current measurements (Tabel A-3). A lower weight constant was assigned to the acetate values because of a significant standard deviation of these measurements. The lowest w_i were assigned to the gas measurements because of the low accuracy of the bubble counter system for measuring gas flow rates. The resulting values of model parameters are given in Tabel A-2. As mentioned above, the non-identifiable model parameters were chosen based on chapter 3 results and Batstone et al. (2002a).

Figure 5.2 presents a comparison of model outputs with the experimental results obtained in MEC-1. It should be noted that since in this test acetate was used as a carbon source, the fermentative activity was not simulated ($x_f = 0$). Furthermore, because the test was carried out in a MEC that was in operation for over one month prior to the test start-up, initial conditions for biomass density were set close to the maximum attainable biomass density (e.g. $x_h \approx X_{max,3}$). Methane production in the anodic compartment was not observed, apparently because the acetoclastic methanogens were already out-competed by the electricigenic microorganisms during MEC operation preceding the test (see results in sections 4.2 and 4.5).

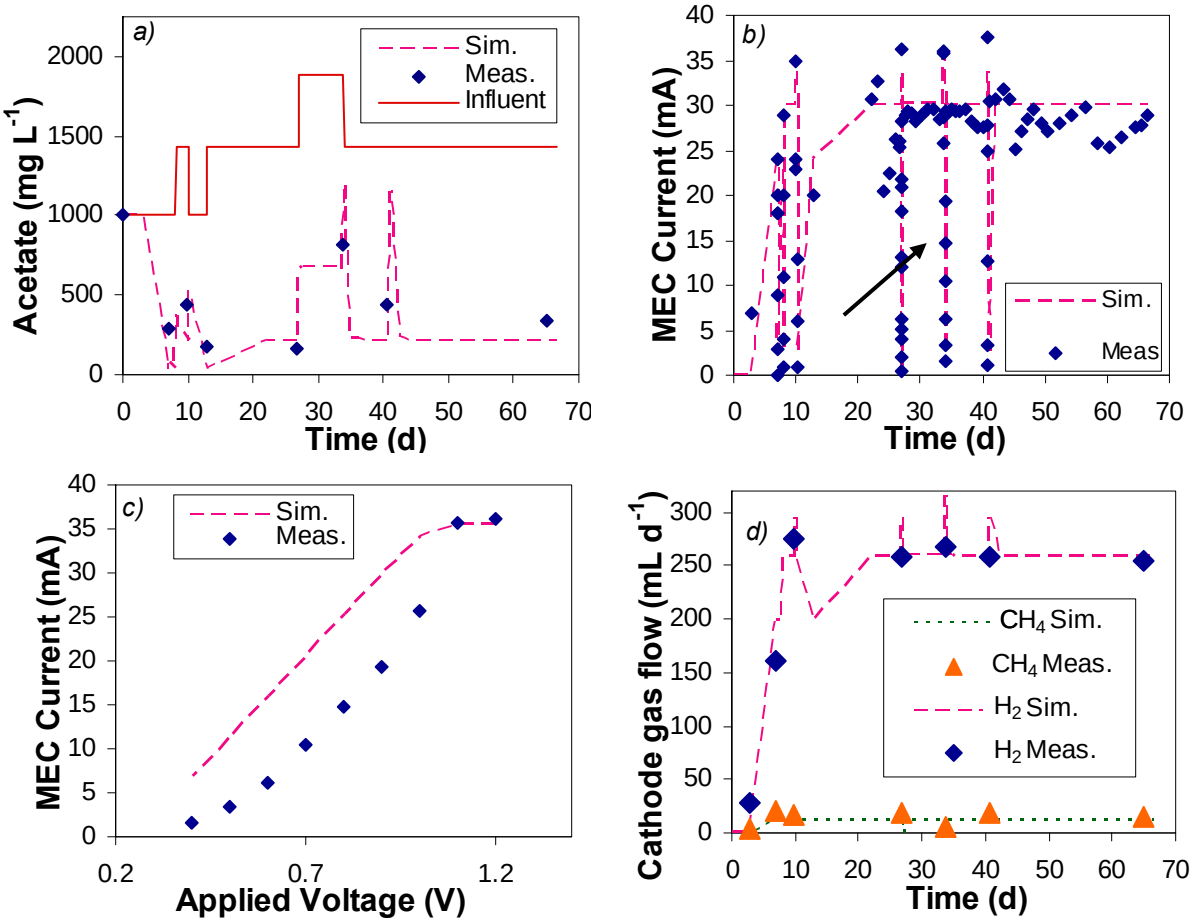

Figure 5.2. Comparison of model outputs with experimentally measured values in MEC-1 fed with acetate (*a*-acetate, *b*-current, and *d*-gas production in the cathode compartment). Panel *c* presents a detailed plot of MEC current vs. voltage during the voltage scan at day 33.9 (indicated by an arrow in panel *b*).

The simulation required less than 30 s on a PC with 2.99 GHz dual core processor. An acceptable agreement was obtained between measured and predicted effluent acetate (Fig 5.2*a*), current (Fig. 5.2*b*), and gas production (Fig. 5.2*d*) values. Further confirmation of the model capacity to describe process dynamics can be seen from the comparison of model outputs and experimentally measured values of current during one of the voltage scans, as shown in Fig 5.2*c*.

Once model parameters related to the electricigenic microorganisms were estimated, the MEC-2 data set was used to estimate kinetic and stoichiometric parameters of the fermentative and acetoclastic methanogenic microorganisms. Once again the FIM was used to select identifiable

parameters based on an acceptable interval of confidence. The following parameters were selected for the parameter estimation procedure (notations are provided in Table 1): $q_{max,f}$ $q_{max,m}$, E_{CEF}, and Y_{COD}. The respective confidence intervals were 11.8%, 35.4%, 19.0%, and 18.9%. The counter electromotive force (E_{CEF}) was re-estimated because this parameter is related to the cathode potential, which can vary from electrode to electrode.

In the MEC-2 test, the measurable state variables included the values of current, sCOD, and VFAs concentration in the effluent, as well as the measurements of hydrogen and methane production in the anode and H_2 collection compartments. The values of model parameters obtained after the parameter estimation procedure are given in Tabel A-2. The estimated values of $q_{max,f}$ and $q_{max,m}$ were within the range of parameters used in ADM1 (D. J. Batstone et al., 2002a). Also, the E_{CEF} values estimated for MEC-1 and MEC-2 were close to the values reported in the literature (R. A. Rozendal et al., 2006).

Figure 5.3 presents a comparison of model predictions with the measurable state variables in the MEC-2 test. Acetate (Fig. 5.3*b*) and sCOD (Fig. 5.3*a*) model outputs generally follow experimental measurements, although a certain underestimation can be seen. Nevertheless, this underestimation was acceptable considering the larger standard deviations of sCOD and acetate measurements in comparison to I_{MEC} measurements. Model predictions of I_{MEC} closely followed the measured values for most of the tested sWW loads with the exception of the highest load, when I_{MEC} values were underestimated (Fig. 5.3*c*). Process dynamics were predicted reasonably well as can be seen from Fig. 3*d*, where I_{MEC} predictions and experimental measurements are shown for a voltage scan with 10 min intervals between applied voltage changes. Interestingly, both predicted and measured values of I_{MEC} approached a maximum at around 1 V and then decreased. This behaviour was related to carbon source limitation at higher applied voltages. Indeed, voltage scans were started at the lowest applied voltage (e.g. 0.2 - 0.6 V) resulting in decreased acetate consumption evidenced by acetate peaks in Fig. 5.3*a*. Progressive increase of the applied voltage during the scan led to increased current, but also to increased acetate consumption. The acetate concentration decreased over the course of the voltage scan until it reached a rate-limiting level. Consequently, by the end of the voltage scan I_{MEC} slightly decreased in spite of increasing applied voltage. Gas production measurements were followed reasonably

well in spite of large fluctuations in measured H_2 and CH_4 production (Fig.5.3*e* and 5.3*f*, respectively). Once again, voltage scans led to short-term drops in hydrogen production during the first part of each voltage scan when the applied voltage was low.

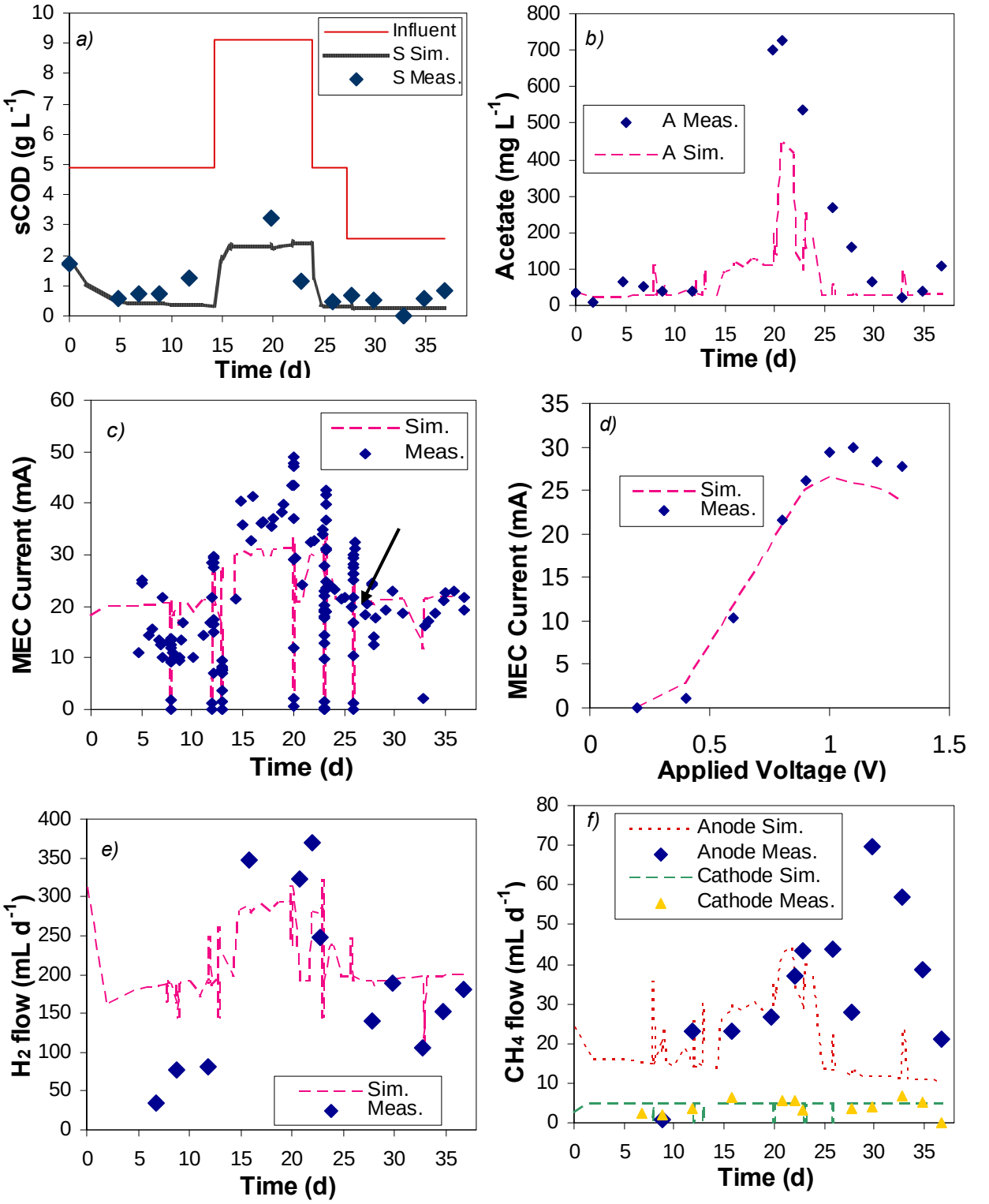

Figure 5.3. Comparison of model outputs with experimentally measured values in MEC-2 fed with sWW (*a*-sCOD, *b*-acetate, *c*-current, *e*-H_2 production, and *f*- CH_4 production in the anode and cathode compartments). MEC current during the voltage scan at day 12 is presented in panel *d* (indicated by an arrow in panel *c*).

A statistical measure of the model accuracy was provided by calculating the adjusted coefficients of determination (R^2) of model outputs. R^2 values calculated both for MEC-1 and MEC-2 data sets are provided in Table 5-1. Regardless of the low weight constants assigned to H_2 measurements, the R^2 values corresponding to H_2 measurements were above 0.8, possibly because H_2 production was directly proportional to current (Eq. (5-13)) and the current measurements were followed quite well by the model as can be seen from Figs. 5.2*b* and 5.3*c*. Overall, R^2 calculations confirmed a reasonable agreement between experimentally measured and calculated state variables.

Table 5-1: A comparison of R^2 values calculated for the MEC data sets used for parameters estimation and model validation.

State variable	*MEC-1*	*MEC-2*	*MEC-3*
Effluent sCOD	n/a	0.69	0.65
Effluent VFA	0.73	0.64	0.70
Current	0.82	0.78	0.82
H_2 flow-Cathode	0.85	0.85	0.65
CH_4 flow-Cathode	0.70	0.83	0.81
CH_4 flow-Anode	n/a	0.66	0.57

n/a - not available

5.3. Model Validation

Model validation was carried out using the results obtained in MEC-3, which was fed with sWW. Notably, the organic load profiles in MEC-2 and MEC-3 tests were different (Figs 5.3*a* and 5.4*a*), thus eliminating any possible correlation between the two data sets. During the model validation procedure, all model parameters were kept unchanged apart from the internal resistance value (R_{MIN} in Tabel A-2), which was re-estimated using the voltage scan technique (see section 2.4) and was found to be higher (35 Ω vs. 20 Ω) than in the MEC-2 test.

Fig. 5.4 presents a comparison between the predicted and measured state variables in the MEC-3 test. A satisfactory agreement was obtained, especially between predicted and measured values of current and hydrogen flow (Fig. 5.4*c* and 5.4*e*), which confirmed the predictive power of the

model. Fig. 5.4*d* compares I_{MEC} model predictions and measurements during a voltage scan performed on day 10 at a high COD load. Although the maximal current was predicted correctly, it was only reached at 1.2 V because the model overestimated the acetate concentration at the time of the test. Nevertheless, in general the predicted effluent concentrations of sCOD and acetate followed the measurements with acceptable accuracy (Fig. 5.4*a*, and 5.4*b*). Once again, H_2 and CH_4 measurements had relatively large standard deviations related to the difficulty of measuring gas flow rates as low as 10 – 40 mL d^{-1}. Nevertheless, the trends in H_2 and CH_4 production were correctly predicted, although CH_4 presence in the anode compartment was underestimated for the second part of the experiment (Fig. 5.4*f*). R^2 calculations (Table 5-1) confirmed acceptable accuracy of model predictions. Importantly, similar R^2 values were obtained both for MEC-2 (parameter estimation) and MEC-3 (model validation) data sets, which confirmed the predictive capacity of the model.

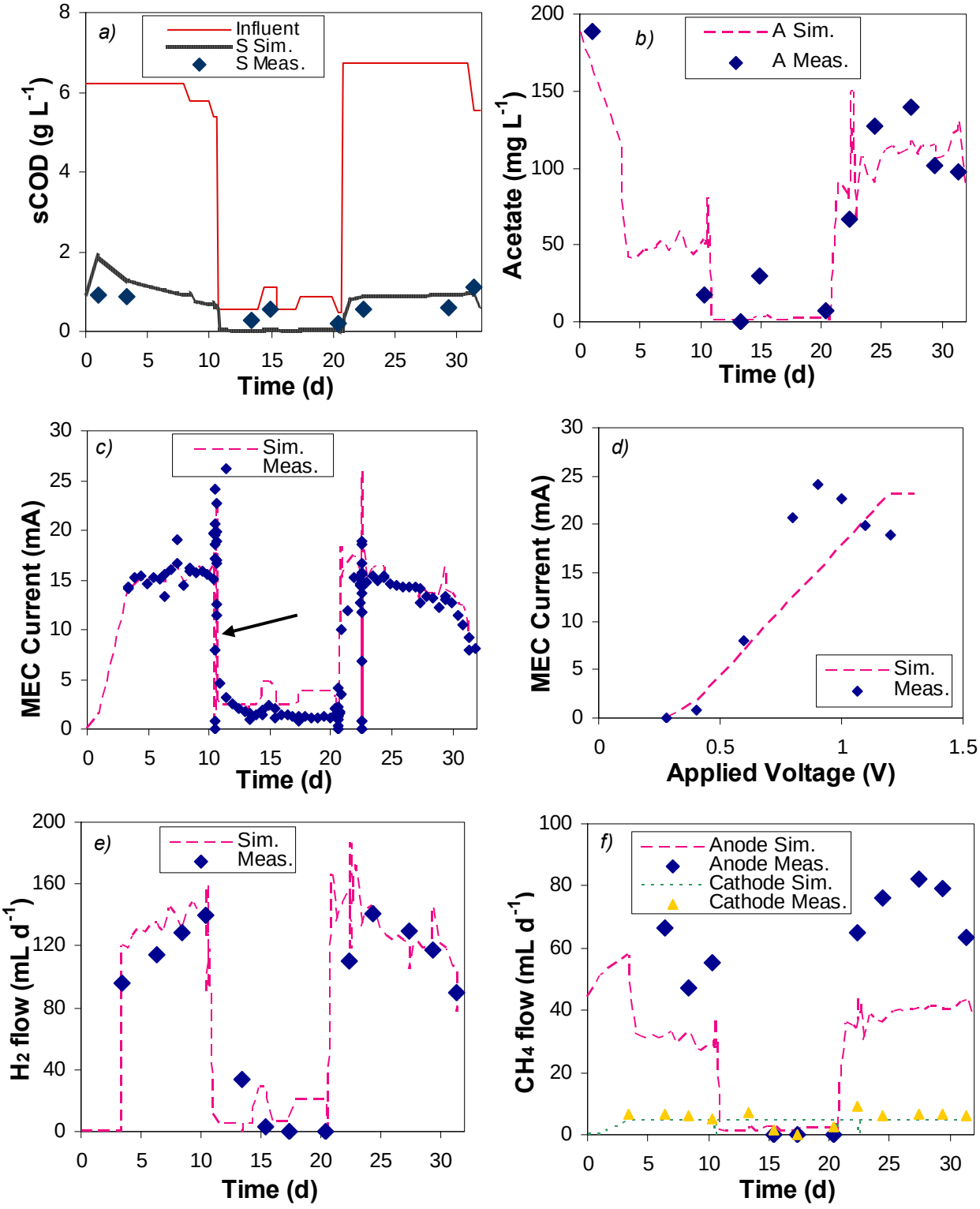

Figure 5.4. Model validation based on the experimental results obtained in sWW fed MEC-3 (*a*-sCOD, *b*-acetate, *c*-current, *e*-H_2 production, and *f*- CH_4 production). The voltage scan presented in panel *d* was performed on day 10 as indicated by the arrow in panel *c*.

5.4. The Influence of Applied Voltage and Organic Load on the Efficiency of the MEC

In this section the first application of the multi-population model described above for predicting H_2 production and COD removal in a MEC operated at various applied voltages and influent COD concentrations is demonstrated. The model analysis presented in this section is performed by integrating the model equations for a period of 200 days and analyzing MEC performance at the end of this period, i.e. steady state analysis is presented. In these calculations, the applied voltage was varied between 0 and 1.2 V, the influent sCOD concentration was varied between 200 - 5000 mg L^{-1} with no acetate in the influent, and the influent flow rate was kept at 150 mL d^{-1}.

Figure 5.5*a* shows the effect of applied voltage and influent COD concentrations on H_2 production. As expected, H_2 production is maximised at the highest applied voltage of 1.2 V. This prediction agrees both with the previously reported results (Bruce E. Logan et al., 2008; R. A. Rozendal et al., 2006) and with the experiments described above. Analysis of Eq. (5-19) shows that no current can be produced at applied voltages below the sum of $\eta_{act,C}$, $\eta_{conc,A}$, and E_{CEF}. Above this threshold the electricigenic microorganisms are able to transfer electrons to the anode resulting in a measurable current and H_2 production. The dependence of I_{MEC} on applied voltage is further illustrated in Fig 5.5*b*, which shows the predicted levels of oxidised (M_{ox}) and reduced (M_{ox}) forms of the intracellular mediator. As the applied voltage increases, the concentration of M_{ox} augments until it reaches its maximum value equal to M_{Total}. Since I_{MEC} is dependent on M_{ox}, it also increases. Once the maximum M_{ox} concentration is reached, no further increase in I_{MEC} can be achieved even if the applied voltage is increased. It should be mentioned that MEC operation at excessively high applied voltages results in energy losses and might lead to the onset of water electrolysis at around 1.8 V (R. A. Rozendal et al., 2006).

Influent COD concentration is another important factor influencing H_2 production that should be considered in MEC design and operation. Model predictions shown in Fig. 5.5*a* suggest that the high rates of H_2 production require a sufficient organic load. This can be related to the Monod kinetics of the fermentative microorganisms (Eq. (5-15)). At low COD concentrations less acetate is produced. The shortage of acetate for the electricigenic microorganisms results in lower current and therefore in a reduced H_2 flow.

COD removal efficiency (Eq. (2-5)) is an essential parameter, which determines the overall performance of the MEC. Fig. 5.5*c* shows how $E_{applied}$ and influent wastewater concentration affect this parameter. As one can see from this plot, when influent concentration increases, the removal efficiency decreases because maximal substrate consumption rates are reached by all microbial populations. The applied voltage has a significant impact on R_{eff}. At a low $E_{applied}$, electricigenic microorganisms are not able to transfer electrons (M_{ox} = 0, Fig. 5.5*b*) and do not grow and metabolise. Accordingly, the acetoclastic methanogenic microorganisms proliferate and consume acetate. Since the acetoclastic methanogens co-exist with the fermentative microorganisms in Layer 1 (Fig. 5.1), at a low $E_{applied}$, a new equilibrium between the microbial populations is reached. As the applied voltage increases, biofilm Layer 2 becomes mostly occupied by the electricigenic microorganisms and the acetate consumption rate becomes M_{ox} – limited, as can be seen from Eq. (3-13). This leads to a lower removal efficiency, as shown in Fig. 5.5*d*. As M_{ox} augments with larger applied voltages, more acetate is consumed by the electricigenic microorganisms in biofilm Layer 2. This increase in acetate consumption in Layer 2 leads to a lower acetate availability in Layer 1. Accordingly, the ratio of the fermentative microorganisms in Layer 1 increases resulting in a more efficient COD removal. The maximum removal efficiency is reached when biofilm Layer 2 is occupied by the electricigenic microorganisms, $M_{ox} = M_{Total}$, and biofilm Layer 1 is mainly occupied by the fermentative microorganisms. It can be concluded that MEC operation at relatively high values of $E_{applied}$, maximises COD removal and H_2 production.

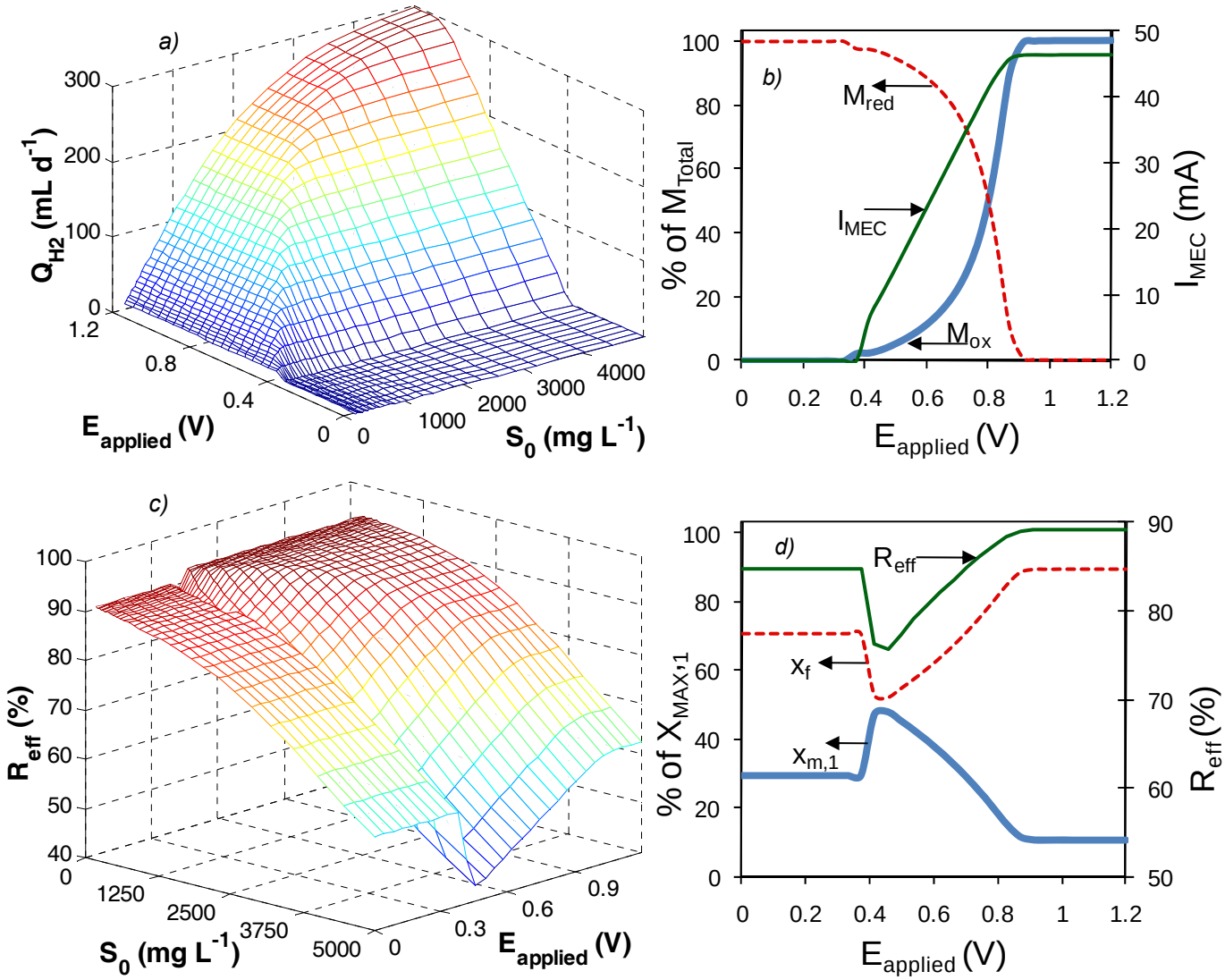

Figure 5.5. The predicted dependency of H_2 production (*a*) and removal efficiency (*c*) on applied voltage and influent COD concentration. The predicted changes in mediator and biomass concentrations are shown in panels (*b*) and (*d*).

5.5. Conclusion

This chapter presented a fast-convergence multi-population dynamic model of MECs fed with wastewater. Four microorganism populations were assumed to be present in the anode, one to account for the degradation of organic substrate (fermentative), a second one to report the production of current (electricigens), and the two last to account for the methane production at the anode (acetoclastic methanogens) and at the cathode (hydrogenotrophic methanogens). Different biofilm layers were assumed to contain one or more microbial populations. MEC experimental data sets fed with acetate and sWW were used for estimation of identifiable model parameters. An independent MEC data set fed with sWW was used for model validations, confirming the model's predictive capacity. Finally, the influence of applied voltage and influent concentration on the effluent concentration and hydrogen production was analysed with the model showing high-performance operating conditions for an MEC.

CHAPTER 6: MXC MODEL ANALYSIS

The goal of this chapter is to optimise the product generation of MxCs, either electricity or hydrogen, by selecting optimum operating current, with the influent flow (organic load) being adjusted to guarantee a given treatment capacity. Analysis of a unified multi-population model of MFCs and MECs reveals that the ratio between different microbial populations in the anodic biofilm is determined by the current. The optimal operating current for an MFC varies considerably with internal resistance. On the other hand, the optimal current for an MEC may vary with the internal resistance or it may always be close its maximum limit, depending on the definition of the objective function of the MEC. The results in chapter 6 can be seen in Pinto et al. (Pinto, Srinivasan, & Tartakovsky, 2011c; Pinto, Tartakovsky, & Srinivasan, 2011d).

6.1. A Unified MxC Model

This section presents a model derived from the MFC and MEC models presented in chapters 3 and 5, respectively. For the sake of simplicity, the model presented here will not take into account the conversion of organic matter to acetate. This version of the model will consider only the existence of electricigenic and methanogenic microbial populations, and will be used for the analysis and optimisation purposes of this thesis.

For a MxC operating with the same influent and effluent flow rates, the following substrate and microorganisms material balances can be written for the anode compartment:

$$\frac{dA}{dt} = -q_e x_e - q_m x_m + \frac{F_{in}}{V}(A_0 - A) \tag{6-1}$$

$$\frac{dx_e}{dt} = \mu_e x_e - \alpha x_e \tag{6-2}$$

$$\frac{dx_m}{dt} = \mu_m x_m - \alpha x_m \tag{6-3}$$

$$x_e M_{Total} = \left(M_{red} + M_{ox}\right) x_e \tag{6-4}$$

$$x_e \frac{dM_{ox}}{dt} = -Y_M q_e x_e + \frac{I_{MxC}\gamma}{VmF} \tag{6-5}$$

Note that the substrate consumptions (q_e and q_m) and the growth rates (μ_e and μ_m) are defined in Eqs. (3-13), (3-14), (3-11), and (3-12) respectively. The effect of biomass formation and retention in each biofilm layer is based on a two-phase biofilm growth concept presented in chapter 5. Therefore, the biofilm retention constant can be defined here as:

$$\alpha = \begin{cases} \dfrac{\mu_e x_e + \mu_m x_m}{(x_m + x_e)} & if \quad (x_m + x_e) \geq X_{\max} \\ 0 & otherwise \end{cases} \tag{6-6}$$

For the MEC mode, the hydrogen production rate in mL-H_2 d^{-1} was computed as in Eq. (5-13). The electrochemical balance was used to calculate the current for MFCs and MECs. In both cases, activation, ohmic, and concentration losses are considered. Activation losses were assumed to be constant and were included in the open circuit potential (MFC) or counter electromotive force (MEC) constants. The concentration losses at the cathode were neglected, while the concentration losses at the anode ($\eta_{conc,A}$) were calculated using Eq. (3-16):

$$E_{output} = +E_{OCP} - \frac{RT}{mF}\ln\left(\frac{M_{total}}{M_{red}}\right) - I_{MFC}R_{\text{int}} \tag{6-7}$$

$$E_{applied} = -E_{CEF} + \frac{RT}{mF}\ln\left(\frac{M_{total}}{M_{red}}\right) + I_{MEC}R_{\text{int}} \tag{6-8}$$

Note that in Eqs. (6-7) and (6-8) the current has a positive value.

Finally, due to environmental requirements, it is important to control the effluent concentration in a WW treatment plant, despite fluctuations in wastewater flow or composition. Thus, it is common in such processes to manipulate the incoming treatment flow to maintain the effluent concentration at a certain required level (typically using a PI controller) with the aid of a buffer

tank. So, the effluent concentration (A) was maintained at a set-point by the following control law:

$$F_{in} = F_0 + K_i \int_0^t \left(A_{ref} - A\right)dt + K_p\left(A_{ref} - A\right) \tag{6-9}$$

6.2. Coexistence

The coexistence of electricigenic and methanogenic microbial populations and the CEP (Hardin, 1960) in the biofilm of the MxC will be analysed in this section. The previous analysis of the MFC model (chapter 4) demonstrated that the CEP principle was partially valid for MFCs, depending on the choice of external resistance. This effect and the possible biofilm compositions for the unified MxC model as a function of its operating current are analysed in the following proposition.

Proposition 5. To study the equilibrium points of the MxC biofilm composition, let the current to the reactor be controlled at a constant value I_{MxC}. The equilibrium point, that is stable, satisfies the following conditions: (i) If $I_{MxC} = 0$, then only methanogens exist; (ii) if $0 < I_{MxC} \leq \overline{I_{MxC}}$ then there is coexistence, and; (iii) if $I_{MxC} > \overline{I_{MxC}}$, then only electricigens exist.

where, for a given value of effluent A at which the reactor is controlled $\overline{M}_{ox} = \dfrac{K_M}{\left(\dfrac{\mu_{\max,e}\left(K_{A,m} + A\right)}{\mu_{\max,m}\left(K_{A,e} + A\right)} - 1\right)}$ and $\overline{I_{MxC}} = \dfrac{\overline{M}_{ox} X_{MAX}}{\left(K_M + \overline{M}_{ox}\right)}\left(\dfrac{Vm F Y_M q_{\max,e} A}{\gamma\left(K_{A,e} + A\right)}\right)$.

Proof. The steady state solution of Eqs. (6-2) and (6-3) present four possible equilibrium points:

(*I*) $x_m = 0$, and $x_e = 0$ (wash-out solution)

(II) $\mu_m = \alpha$, $x_m = X_{MAX}$, and $x_e = 0$ (only methanogenic microorganisms)

(*III*) $\mu_e = \alpha$, $x_e = X_{MAX}$, and $x_m = 0$ (only electricigenic microorganisms)

(*IV*) $\mu_e = \alpha$, $\mu_m = \alpha$, and $(x_m + x_e) = X_{MAX}$ (co-existence)

To study the stability of the equilibrium points (*I*) to (*IV*), the dynamics of oxidised mediator was considered to be much faster than the dynamics of bacteria growth (pseudo-steady state). Thus only Eq. (6-2) and (6-3) will be used for further analysis. First, consider the equilibrium point (*I*), for which $\alpha = 0$, since $(x_m + x_e) < X_{MAX}$. Under this condition, Eq. (6-2) and (6-3) can be linearised to:

$$\begin{bmatrix} \frac{d\Delta x_e}{dt} \\ \frac{d\Delta x_m}{dt} \end{bmatrix} = \begin{bmatrix} \mu_e & 0 \\ 0 & \mu_m \end{bmatrix} \begin{bmatrix} \Delta x_e \\ \Delta x_m \end{bmatrix} \tag{6-10}$$

Because μ_m and μ_e are positive, this equilibrium point, i.e. the wash-out solution, is unstable.

For equilibrium points (*II*) to (*IV*), the steady state solution of oxidised mediator balance (Eq. (6-5)) provides an association between M_{ox}, x_e, and I_{MxC}:

$$I_{MxC} = \frac{M_{ox} x_e}{\left(K_M + M_{ox}\right)} \left(\frac{Vm F Y_M q_{\max,e} A}{\gamma \left(K_{A,e} + A\right)} \right) \tag{6-11}$$

Furthermore, the biofilm retention constant, α, defined in Eq. (6-6), is not equal to zero. Then Eq. (6-2) and (6-3) can be linearised to give:

$$\begin{bmatrix} \frac{d\Delta x_e}{dt} \\ \frac{d\Delta x_m}{dt} \end{bmatrix} = \begin{bmatrix} \frac{(\mu_e - \mu_m)x_m^2 + \left(\frac{\partial \mu_e}{\partial x_e} - \frac{\partial \mu_m}{\partial x_e}\mu_m\right)(x_e + x_m)x_e x_m}{(x_e + x_m)^2} & \frac{(\mu_e - \mu_m)x_e^2 + \left(\frac{\partial \mu_e}{\partial x_m} - \frac{\partial \mu_m}{\partial x_m}\right)(x_e + x_m)x_e x_m}{(x_e + x_m)^2} \\ \frac{(\mu_m - \mu_e)x_m^2 + \left(\frac{\partial \mu_m}{\partial x_e} - \frac{\partial \mu_e}{\partial x_e}\right)(x_e + x_m)x_e x_m}{(x_e + x_m)^2} & \frac{(\mu_m - \mu_e)x_e^2 + \left(\frac{\partial \mu_m}{\partial x_m} - \frac{\partial \mu_e}{\partial x_m}\mu_e\right)(x_e + x_m)x_e x_m}{(x_e + x_m)^2} \end{bmatrix} \begin{bmatrix} \Delta x_e \\ \Delta x_m \end{bmatrix} \tag{6-12}$$

Now we consider the equilibrium point at (*II*), for which $x_e = 0$. The Jacobian that corresponds to this solution can be written as:

$$\begin{bmatrix} \frac{d\Delta x_e}{dt} \\ \frac{d\Delta x_m}{dt} \end{bmatrix} = \begin{bmatrix} \mu_e - \mu_m & 0 \\ \mu_m - \mu_e & 0 \end{bmatrix} \begin{bmatrix} \Delta x_e \\ \Delta x_m \end{bmatrix} \tag{6-13}$$

This equilibrium point is only stable when $\mu_e < \mu_m$. From this stability condition and the definition of μ_e and μ_m (Eqs. (6-2) and (6-3)), one can see that this equilibrium point is stable for $M_{ox} < \overline{M}_{ox}$. Furthermore, from Eq. (6-11) and $x_e = 0$, one can find that $I_{MxC} = 0$ whenever methanogens occupy the biofilm.

The reverse occurs for the solution of case (*IV*), when $x_m = 0$, where stability is only possible when $\mu_m < \mu_e$ due to the following Jacobian:

$$\begin{bmatrix} \frac{d\Delta x_e}{dt} \\ \frac{d\Delta x_m}{dt} \end{bmatrix} = \begin{bmatrix} 0 & \mu_e - \mu_m \\ 0 & \mu_m - \mu_e \end{bmatrix} \begin{bmatrix} \Delta x_e \\ \Delta x_m \end{bmatrix} \tag{6-14}$$

In terms of oxidised mediator, $M_{ox} > \overline{M}_{ox}$. Since $x_e = X_{MAX}$, whenever electricigenic microorganisms occupy the biofilm, $I_{MxC} > \overline{I_{MxC}}$.

For coexistence to occur (i.e., $\mu_m = \mu_e = \alpha$), the following Jacobian can be found:

$$\begin{bmatrix} \frac{d\Delta x_e}{dt} \\ \frac{d\Delta x_m}{dt} \end{bmatrix} = \begin{bmatrix} \frac{\left(\frac{\partial \mu_e}{\partial x_e} - \frac{\partial \mu_m}{\partial x_e}\mu_m\right) x_e x_m}{(x_e + x_m)} & \frac{\left(\frac{\partial \mu_e}{\partial x_m} - \frac{\partial \mu_m}{\partial x_m}\right) x_e x_m}{(x_e + x_m)} \\ \frac{\left(\frac{\partial \mu_m}{\partial x_e} - \frac{\partial \mu_e}{\partial x_e}\right) x_e x_m}{(x_e + x_m)} & \frac{\left(\frac{\partial \mu_m}{\partial x_m} - \frac{\partial \mu_e}{\partial x_m}\mu_e\right) x_e x_m}{(x_e + x_m)} \end{bmatrix} \begin{bmatrix} \Delta x_e \\ \Delta x_m \end{bmatrix} \tag{6-15}$$

Note that because the control loop keeps the acetate concentration constant at A_{ref}, μ_m is a constant and all its partial derivatives are equal to zero. Assuming that current (I_{MxC}) is constant, from the steady state solution of Eq. (6-5) one can observe that the product $q_e x_e$ is always constant. Furthermore, from the definition of q_e and μ_e, one can see that $\mu_e x_e$ is also a constant. Since $\mu_e x_e$ is a constant, $\partial \mu_e / \partial x_e = -\mu_e / x_e$. Therefore the Jacobian in Eq. (6-15), can be represented as:

$$\begin{bmatrix} \frac{d\Delta x_e}{dt} \\ \frac{d\Delta x_m}{dt} \end{bmatrix} = \begin{bmatrix} \frac{-\mu_e x_m}{(x_e + x_m)} & 0 \\ \frac{\mu_e x_m}{(x_e + x_m)} & 0 \end{bmatrix} \begin{bmatrix} \Delta x_e \\ \Delta x_m \end{bmatrix} \tag{6-16}$$

This equilibrium point is stable since μ_e is positive. Furthermore, because of the coexistence condition ($\mu_e = \mu_m$), one can find that this equilibrium point is only stable for $M_{ox} = \overline{M}_{ox}$. Therefore by substituting $x_e = (X_{MAX} - x_m)$ and $M_{ox} = \overline{M}_{ox}$ in Eq. (6-11), one can find that the equilibrium point in Eq. (6-16) is only stable when $0 < I_{MxC} \leq \overline{I_{MxC}}$. ■

Figure 6.1 is presented to illustrate the above proof. By using the model parameters presented in Tables A-1and A-2, and by setting the internal resistance to 20 Ω, this figure presents steady state results of microorganisms and mediator concentrations against I_{MxC}, which varied between 0 to 30 mA, while the effluent concentration was maintained at 100 mg L^{-1} by the control loop. Note that, $\overline{M}_{ox}$ and $\overline{I_{MxC}}$ were computed as 2.8% of M_{Total} and 4.6 mA, respectively and that the results for MFC and MEC were the same, which can be seen on the plot as the curves coincide. In Fig. 6.1*a*, two stable regions can be distinguished, i.e. at low currents ($0 < I_{MxC} \leq \overline{I_{MxC}}$) coexistence (*IV*) occurs ($x_e + x_m = X_{MAX}$ and $M_{ox} = \overline{M}_{ox}$), and at higher currents ($I_{MxC} > \overline{I_{MxC}}$) only electricigenic microorganisms (*III*) are present in the MxC (i.e. $x_e = X_{MAX}$ and $M_{ox} > \overline{M}_{ox}$). The last stable region, when only methanogenic microorganisms (*II*) are present in the biofilm, only occurs at $I_{MxC} = 0$. The development of the oxidised and reduced mediators with I_{MxC} can be depicted in Fig. 6.1*b*. At currents below $\overline{I_{MxC}}$, the oxidised mediator concentrations remain constant at $\overline{M}_{ox}$, a value much lower than its reduced form. Once the current of the MxC becomes larger than $\overline{I_{MxC}}$, the oxidised form of the mediator increases until reaching its maximum concentration (M_{Total}).

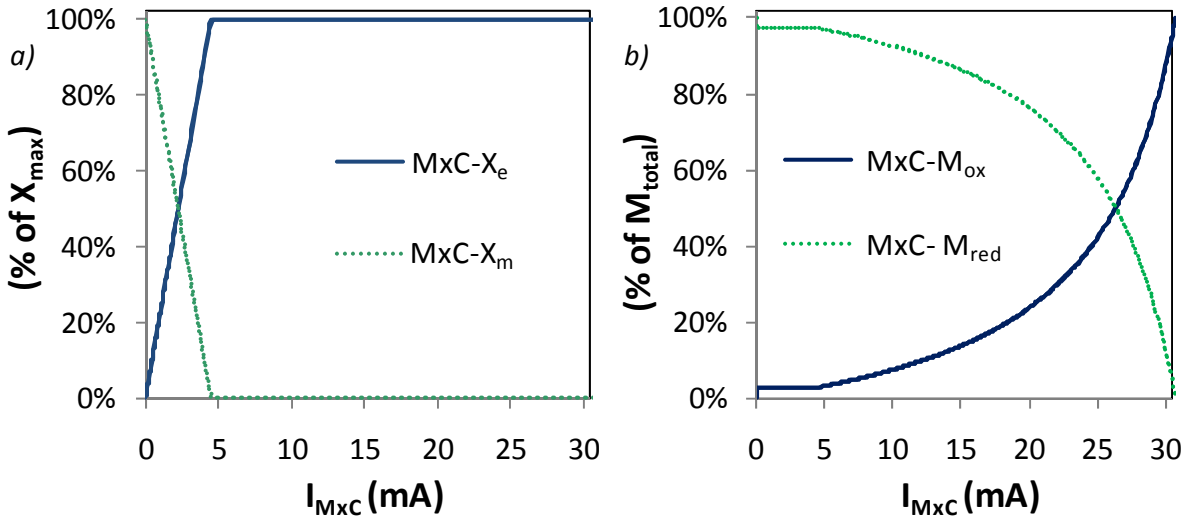

Figure 6.1. Steady state predicted concentration of (*a*) electricigenic and methanogenic populations in the biofilm, and (*b*) oxidised and reduced mediators concentration as a function of I_{MxC} for MFCs and MECs (curves overlap for MEC and MFC).

Although the biofilm and mediator concentrations of MFCs and MECs present the same behaviour when analysed in terms of current, the difference in the electrochemical balances (Eqs. (6-7) and (6-7)) lends itself to a different interpretation when viewed in terms of voltage. Figure 6.2 presents the results for MFC and MEC when the current, microorganism, and mediator concentrations are plotted against reactor voltage (E_{output} and $E_{applied}$).

For an MFC, as the output voltage increases from zero to its OCP, the MFC current decreases from its maximum until zero (Fig. 6.2*a*). Note the effect of concentration losses, which "bend" the curve at low voltages. At low output voltages, only electricigenic microorganisms occupy the biofilm (Fig. 6.2*c*) and the oxidised mediator concentration (Fig. 6.2*e*) is high, reaching its maximum (M_{Total}) at the zero E_{output}. With the increase in E_{output}, the oxidised mediator decreases until reaching $\overline{M}_{ox}$. At this point, the biofilm becomes populated by both microorganism populations and the mediator concentration remains constant. At open circuit, when no current flows between the electrodes, the MFC operates as an anaerobic digester with only methanogens present in the biofilm.

The MEC presents different behaviour. Because of the additional applied voltage that is required for H_2 formation in the cathode, at low applied voltages no current is present. The I_{MEC} only starts to be produced after a threshold value of $E_{applied}$, which increases until a maximum current is reached (Fig. 6.2*b*). As expected, no current leads to a biofilm occupied only by methanogenic microorganisms. As the current increases, the oxidised from of mediator remains at $\overline{M}_{ox}$, while a coexistence biofilm is present. Note that during the coexistence regime, the concentration of electricigenic microorganisms increases linearly with the current, as can be seen in Eq. (6-11) once $M_{ox} = \overline{M}_{ox}$.

Further increases in the applied voltage lead to a biofilm only populated with electricigenic microorganisms and a mediator concentration larger than $\overline{M}_{ox}$. Furthermore, the maximum MEC current is defined by the maximum M_{ox}: once $M_{ox} = M_{Total}$ the current cannot increase, even with a further increase in applied voltage.

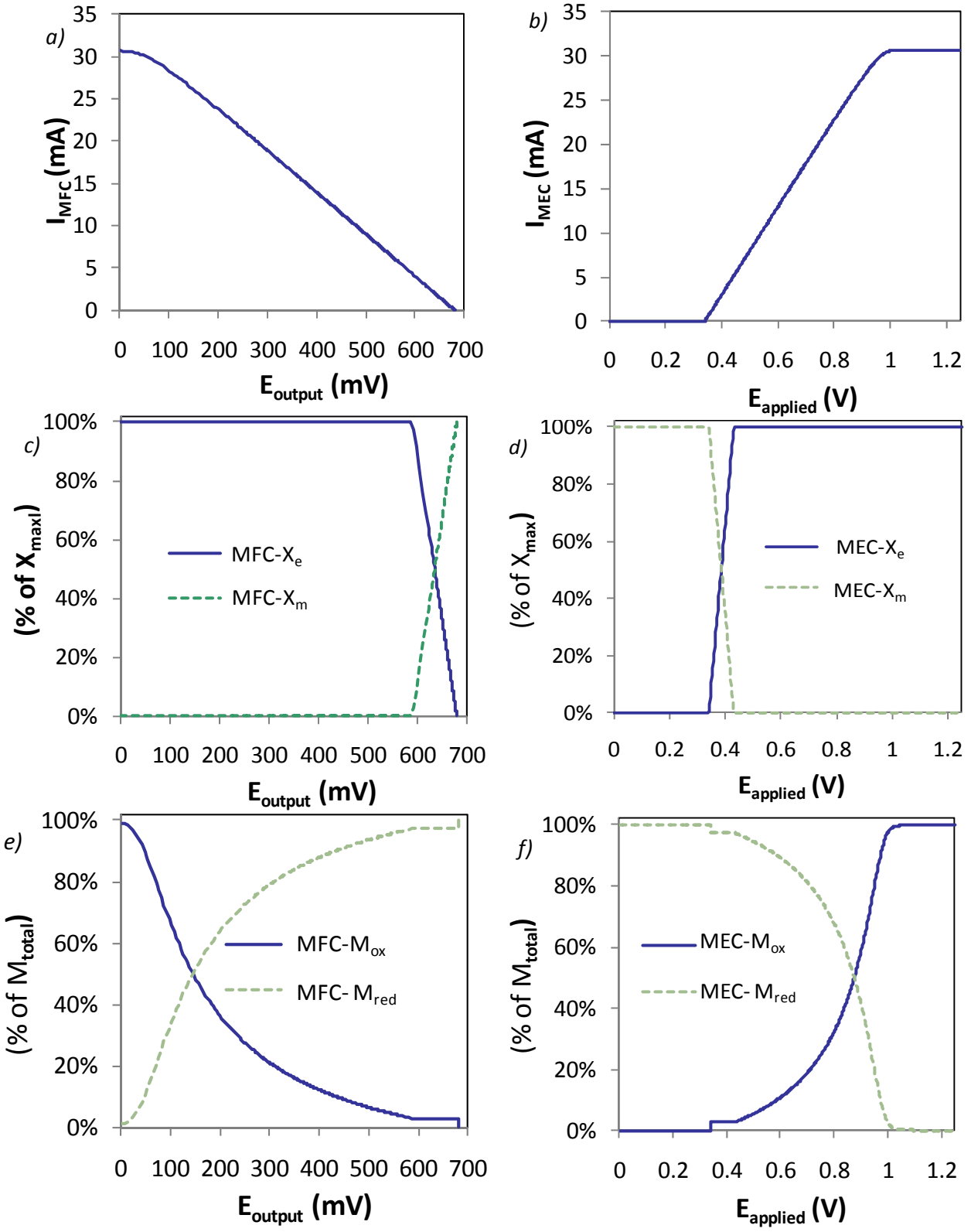

Figure 6.2. Steady state predicted concentration of (*a-b*) reactor current (*c-d*), electricigenic and methanogenic populations in the biofilm, and (*e-f*) mediator concentration as a function of E_{output} (MFC in panels *a*, *c*, *e*) or $E_{applied}$ (MEC in panels *b*, *d*, *f*).

6.3. Energy Productivity Optimisation

The production of the products of MxCs (electricity and H_2) can be maximised by an appropriate choice of operating conditions, while the treatment constrains are respected. In this section, objective functions will be defined for the electricity and H_2 production in MxCs.

6.3.1. Productivity Definition

In MFCs, the power produced is the objective function that can be optimised. Thus, the productivity of MFCs can be defined as:

$$P_{MFC} = I_{MFC} E_{output} \tag{6-17}$$

In MECs, power is applied to produce hydrogen. The first objective function that one may think of is the H_2 production (Q_{H2}). However, the amount of hydrogen produced increases monotonically with the applied power, i.e., there is no optimum. On the other hand, by using the hydrogen enthalpy of combustion, one can find the total energy produced by the MEC by subtracting the energy produced from the burning H_2 from the energy used to produce this hydrogen. Therefore, in this section, a MEC productivity function will be defined as the difference between the H_2 energy (in watts) minus the power produced by the applied voltage:

$$P_{MEC} = \left(\Delta H_{H2} \rho_{H2} Q_{H2}\right) - P_{applied} \tag{6-18}$$

Using Eqs. (5-13) and (6-18) the productivity of the MECs can be further simplified as:

$$P_{MEC} = \left(\frac{\Delta H_{H2} \rho_{H2} Y_{H2} RT}{m_{H2} FP}\right) I_{MEC} - E_{applied} I_{MEC} = I_{MEC}\left(\xi - E_{applied}\right) \tag{6-19}$$

Both productivity functions were simulated for several currents in Figure 6.3 using the parameters presented in the appendix (Tables A-1and A-2), while the internal resistance of the reactors was maintained at 20 Ω.

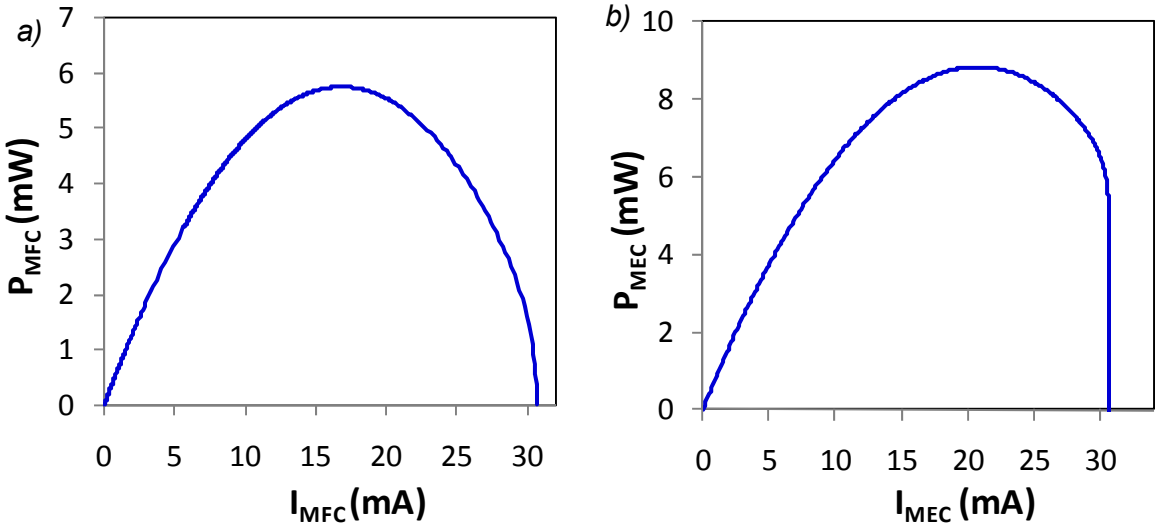

Figure 6.3. Steady state productivity of the MxCs as a function of (*a*) I_{MFC} and (*b*) and I_{MEC}.

Note that due to the action of the PI controller, both productivities are independent of the influent concentration. As expected, both productivities present an optimum, which will be analysed next. First, the optimum productivity for MxCs is mathematically characterised.

Lemma 2. The optimum productivity for the MxCs can be described by the following unified expression: $I_{MxC} = \frac{E_{MxC}}{2R_{\text{int}}} - \frac{\eta_{conc,A}}{2R_{\text{int}}} - \frac{1}{2R_{\text{int}}}\frac{\partial \eta_{conc,A}}{\partial I_{MxC}}$

where $E_{MxC} = E_{OCP}$ for MFCs and $E_{MxC} = \left(\xi + E_{CEF}\right)$ for MECs.

Proof. The optimum productivities can be found when $\partial P_{MFC}/\partial I_{MFC}$ and $\partial P_{MEC}/\partial I_{MEC}$ are equal to zero:

$$\frac{\partial P_{MFC}}{\partial I_{MFC}} = \left(E_{output} + I_{MEC}\frac{\partial E_{output}}{\partial I_{MEC}} \right) \tag{6-20}$$

$$\frac{\partial P_{MEC}}{\partial I_{MEC}} = \xi - E_{applied} - I_{MEC}\frac{\partial E_{applied}}{\partial I_{MEC}} \tag{6-21}$$

So the optimal productivity of MxCs corresponds to:

$$\frac{\partial E_{output}}{\partial I_{MFC}} = \frac{-E_{output}}{I_{MFC}} \tag{6-22}$$

$$\frac{\partial E_{applied}}{\partial I_{MEC}} = \frac{\xi - E_{applied}}{I_{MEC}} \tag{6-23}$$

Furthermore, using the definition of $\eta_{conc,A}$, Eqs. (6-7) and (6-8) can be rewritten as:

$$E_{output} = E_{OCP} - \eta_{conc,A} - R_{\text{int}} I_{MFC} \tag{6-24}$$

$$E_{applied} = -E_{CEF} + \eta_{conc,A} + R_{\text{int}} I_{MEC} \tag{6-25}$$

Eqs. (6-24) and (6-25) can be differentiated with respect to the current, and this result must be equal to the results of Eqs. (6-22) and (6-23), leading to:

$$\frac{\partial E_{output}}{\partial I_{MFC}} = -\frac{\partial \eta_{conc,A}}{\partial I_{MFC}} - R_{\text{int}} = \frac{-E_{OCP} + \eta_{conc,A} + I_{MFC} R_{\text{int}}}{I_{MFC}} \tag{6-26}$$

$$\frac{\partial E_{applied}}{\partial I_{MEC}} = \frac{\partial \eta_{conc,A}}{\partial I_{MEC}} + R_{\text{int}} = \frac{\xi + E_{CEF} - \eta_{conc,A} - I_{MEC} R_{\text{int}}}{I_{MEC}} \tag{6-27}$$

Finally, by using the definition of E_{MxC} for MFCs and MECs, and by rearranging Eqs. (6-26) and (6-27) one can find a unified optimum current function for MxCs:

$$I_{MxC}^{opt}\left(2R_{\text{int}} + \frac{\partial \eta_{conc,A}}{\partial I_{MxC}}\right) = E_{MxC} - \eta_{conc,A} \tag{6-28}$$

By analysing the gradient of this optimum ($\partial \eta_{conc,A}/\partial I_{MxC}$), analytical solutions for optimum MxC productivity will be expressed next.

6.3.2. Analytical Expressions for Optimal MxC Productivity

In the following proposition, an analytical expression for the optimum productivity for MxCs will be derived.

Proposition 6. The optimum steady state of the productivity of MxCs is given by the following analytical expressions:

$$I_{MxC}^{opt} = \begin{cases} I_{\text{int}}^{opt} - \dfrac{\overline{E}_{conc}}{2R_{\text{int}}} \approx I_{\text{int}}^{opt}, & if \quad I_{\text{int}}^{opt} < \overline{I_{MxC}}^{*} \\ I_{\text{int}}^{opt}\left(1 + \dfrac{I_{\text{int}}^{opt}\left(2I_{\max} - I_{\text{int}}^{opt}\right)E_z}{\left(I_{\max} - I_{\text{int}}^{opt}\right)^2}\right) \approx I_{\text{int}}^{opt}, & if \quad \overline{I_{MxC}}^{*} < I_{\text{int}}^{opt} < I_{\max} \\ I_{\max}\left(1 - \sqrt{\dfrac{I_{\text{int}}^{opt}E_z}{\left(I_{\text{int}}^{opt} - I_{\max}\right)}}\right) \approx I_{\max}, & if \quad I_{\max} < I_{\text{int}}^{opt} \end{cases}$$

Furthermore, if $I_{\text{int}}^{opt} \le \overline{I_{MxC}}^{*}$, then there is coexistence in the biofilm, while if $\overline{I_{MxC}}^{*} < I_{\text{int}}^{opt}$, the biofilm is occupied only by electricigenic microorganisms.

where $\overline{E}_{conc} = \dfrac{RT}{mF}\ln\left(\dfrac{M_{Total}}{M_{Total} - \overline{M}_{ox}}\right)$, $E_z = \dfrac{E_c}{E_{MxC}}$,

$E_c = \dfrac{RTK_M}{mF\left(K_M + M_{Total}\right)}$, $I_{\max} = \dfrac{VmFY_M}{\gamma}\dfrac{q_{\max,e}AX_{\max}}{\left(K_{A,e} + A\right)}\dfrac{M_{Total}}{K_M + M_{Total}}$,

$I_{\text{int}}^{opt} = \dfrac{E_{MxC}}{2R_{\text{int}}}$, and $\overline{I_{MxC}}^{*} = \dfrac{\overline{M}_{ox}X_{\max}}{\left(K_M + \overline{M}_{ox}\right)}\left(\dfrac{VmFY_M q_{\max,e}A}{\gamma\left(K_{A,e} + A\right)}\right) + \dfrac{\overline{E}_{conc}}{2R_{\text{int}}}$.

Proof: The expression of the gradient ($\partial\eta_{conc,A}/\partial I_{MxC}$) in Eq. (6-28) varies depending on whether (i) only methanogenic microorganisms are present, (ii) coexistence, or (iii) only electricigenic

microorganisms are present. So, the analysis has to be performed independently for these three regions.

First, in the methanogenic region (No R_{ext} – OCP and low $E_{applied}$), one can see that $I_{MxC} = 0$. Once there is no current, the productivity is zero and the MxC operates as an anaerobic digester, only producing methane. Clearly, a non-zero value of the productivity can be obtained in other regions. So, the optimum is never in the methanogenic region for MxCs.

In the coexistence region, as shown in proposition 5, M_{ox} is constant ($\overline{M}_{ox}$) and the concentration losses become constant ($\eta_{conc,A} = \overline{E}_{conc}$). Then the gradient equals zero ($\partial \eta_{conc,A}/\partial I_{MxC} = 0$) and using the definition of I_{int}^{opt} , Eq. (6-28) can be rewritten as:

$$I_{MxC}^{opt} = I_{\text{int}}^{opt} - \frac{\overline{E}_{conc}}{2R_{\text{int}}} \tag{6-29}$$

The coexistence is defined by the condition $I_{MxC}^{opt} \le \overline{I_{MxC}}$. This condition can be represented as a function of I_{int}^{opt} as: $I_{\text{int}}^{opt} \le \overline{I_{MxC}}^{*}$.

Finally, for the electricigenic region, $\overline{I_{MxC}}^{*} < I_{\text{int}}^{opt}$, from the steady state solution of Eq. (6-5) and using the definition of I_{max}, one can find a M_{ox} expression function of current (with $x_e = X_{MAX}$):

$$M_{ox} = \frac{M_{Total} K_M I_{MxC}}{K_M I_{\max} + M_{Total}\left(I_{\max} - I_{MxC}\right)} \tag{6-30}$$

By substituting Eq. (6-30) in the concentration losses ($\eta_{conc,A}$) yields:

$$\eta_{conc,A} = \frac{RT}{mF} \ln\left(\frac{I_{\max}\left(K_M + M_{Total}\right) - M_{total} I_{MxC}}{\left(I_{\max} - I_{MxC}\right)\left(K_M + M_{Total}\right)} \right) \tag{6-31}$$

Note that the logarithmic term is zero when $I_{MxC} = 0$ and infinite when $I_{MxC} = I_{max}$. So, the logarithmic term can be approximated by $\frac{K_M}{(K_M + M_{Total})}\frac{I_{MxC}}{(I_{\max} - I_{MxC})}$. Therefore, using this approximation and the definition of E_c, Eq. (6-28) can be simplified as:

$$I_{MxC}^{opt} = \frac{E_{MxC}}{2R_{\text{int}}} - \frac{E_c I_{MxC}^{opt}}{2R_{\text{int}}\left(I_{\max} - I_{MxC}^{opt}\right)} - \frac{E_c I_{\max} I_{MxC}^{opt}}{2R_{\text{int}}\left(I_{\max} - I_{MxC}^{opt}\right)^2} \tag{6-32}$$

The optimum MxC current can be found by rearranging the previous equation and by using the definitions of I_{int}^{opt} and E_z:

$$f\left(I_{MxC}, E_z\right) = \left(I_{\text{int}}^{opt} - I_{MxC}\right)\left(I_{\max} - I_{MxC}\right)^2 - E_z I_{\text{int}}^{opt} I_{MxC}\left(2I_{\max} - I_{MxC}\right) = 0 \tag{6-33}$$

Note that E_z is a small value. The roots of this cubic equation will be found first by considering, $E_z = 0$ and then doing a variational analysis around this point. For $E_z = 0$, it is clear that the roots are $I_{MxC} = I_{\text{int}}^{opt}$ or $I_{MxC} = I_{\max}$.

From variational analysis, the three roots can be defined as:

$$I_{MxC} = I_{\text{int}}^{opt} + \frac{\left.\frac{\partial f}{\partial E_z}\right|_{\substack{E_z=0 \\ I_{MxC}=I_{\text{int}}^{opt}}} \Delta E_z}{\left.\frac{\partial f}{\partial I_{MxC}}\right|_{\substack{E_z=0 \\ I_{MxC}=I_{\text{int}}^{opt}}}} \tag{6-34}$$

$$I_{MxC} = I_{\max} \pm \sqrt{\frac{-\left.\frac{\partial f}{\partial E_z}\right|_{\substack{E_z=0 \\ I_{MxC}=I_{\max}}} \Delta E_z}{\left.\frac{1}{2}\frac{\partial^2 f}{\partial I_{MxC}{}^2}\right|_{\substack{E_z=0 \\ I_{MxC}=I_{\max}}}}} \tag{6-35}$$

The three optimum currents can be found as:

$$I_{MxC}^{opt} = I_{\text{int}}^{opt}\left(1 + \frac{I_{\text{int}}^{opt}\left(2I_{\max} - I_{\text{int}}^{opt}\right)E_z}{\left(I_{\max} - I_{\text{int}}^{opt}\right)^2}\right) \tag{6-36}$$

$$I_{MxC}^{opt} = I_{\max}\left(1 \pm \sqrt{\frac{I_{\text{int}}^{opt} E_z}{\left(I_{\text{int}}^{opt} - I_{\max}\right)}}\right) \tag{6-37}$$

If $I_{\text{int}}^{opt} < I_{\max}$, these two roots arising from Eq. (6-37) become imaginary and only Eq. (6-36) presents a meaningful optimum. On the contrary, considering the case when $I_{\max} < I_{\text{int}}^{opt}$, Eq. (6-36) and the positive sign for the square root in Eq. (6-37) provide solutions that are larger than I_{max} (the maximum possible current) and should not be considered. Therefore, the only meaningful solution corresponds to the negative square root in Eq. (6-37). Note that the analytical expression is approximate, and does not provide in the neighbourhood of $I_{\text{int}}^{opt} = I_{\max}$. Third order variations should then be considered. ■

The optimum external resistance and applied voltage, which are the controlled parameters in MFCs and MECs respectively, can be found from the electrochemical balance as:

$$R_{ext}^{opt} = \frac{E_{OCP} - \frac{RT}{mF}\ln\left(\frac{I_{\max}\left(K_M + M_{Total}\right) - M_{Total}I_{MFC}^{opt}}{\left(I_{\max} - I_{MFC}^{opt}\right)\left(K_M + M_{Total}\right)}\right) - I_{MFC}^{opt}R_{\text{int}}}{I_{MFC}^{opt}} \tag{6-38}$$

$$E_{applied}^{opt} = -E_{CEF} + \frac{RT}{mF}\ln\left(\frac{I_{\max}\left(K_M + M_{Total}\right) - M_{Total}I_{MEC}^{opt}}{\left(I_{\max} - I_{MEC}^{opt}\right)\left(K_M + M_{Total}\right)}\right) + I_{MEC}^{opt}R_{\text{int}} \qquad (6\text{-}39)$$

Proposition 6 can be confirmed by the following example. Figure 6.4 presents the steady state productivities for MFCs and MECs (P_{MxC}) against current (I_{MxC}). All model parameters as in Tables A-1and A-2 are used, except for the internal resistances of the MxCs. The parameters $\overline{I_{MxC}}^*$ and $I_{\max}$ are independent from the R_{int} and were computed as 4.5 mA and 30.7 mA, respectively. In Fig. 6.4*a* the internal resistance was set to 5 Ω, and the parameter I_{int}^{opt}, was calculated as 68 mA > $I_{\max}$ for the MFC ($I_{\underset{MFC}{\text{int}}}^{opt}$), while it was computed as 84.5 mA > $I_{\max}$ for the MEC ($I_{\underset{MEC}{\text{int}}}^{opt}$). Under this condition, the optimum MFC current was predicted from the simulation as 29.7 mA, while Eq. (6-37) (negative sign for the square root) was computed as 28.4 mA. Similarly, the optimum MEC current was simulated as 30 mA and Eq. (6-36) calculated as 28.8 mA. Once the internal resistance was set to 20 Ω (Fig. 6.4*b*), the I_{int}^{opt} can be computed for the MFC ($I_{\underset{MFC}{\text{int}}}^{opt}$) as 17 mA < $I_{\max}$ and for the MEC ($I_{\underset{MEC}{\text{int}}}^{opt}$) as 21 mA < $I_{\max}$. The new optimum current can be calculated from Eq. (6-36) as 17.2 mA for MFC and as 21.9 mA for MEC, while 16.8 mA for MFC and 20.8 mA for MEC were found from the simulation. Fig. 6.4*c* shows the productivity of the MxCs with R_{int} equal to 100 Ω; under this condition, the I_{int}^{opt} was equal to 1.14 mA < $\overline{I_{MxC}}^*$ for MFCs and 4.22 mA < $\overline{I_{MxC}}^*$ for MECs. The optimums from Eq. (6-29) and from the simulation were the same and were equal to 1.13 mA for MFCs, and 4.22 mA for MECs. Note that the logarithm approximation used in the analytical expressions development gives a small error between predicted and analytical optimum, particularly for MECs with low internal resistances. Finally, Fig. 6.4*d* shows all MFC productivity curves in the same plot, with the biomass concentration in the biofilm also presented in the background, varying from zero to X_{MAX} (not shown in the secondary axis). In this figure, one can see that the optimum at R_{int} = 100 Ω has a coexistence biofilm, while the other optimums (R_{int} = 20 Ω and R_{int} = 5 Ω) have a biofilm

populated only by electricigenic microorganisms. The same result is found for MECs (not shown).

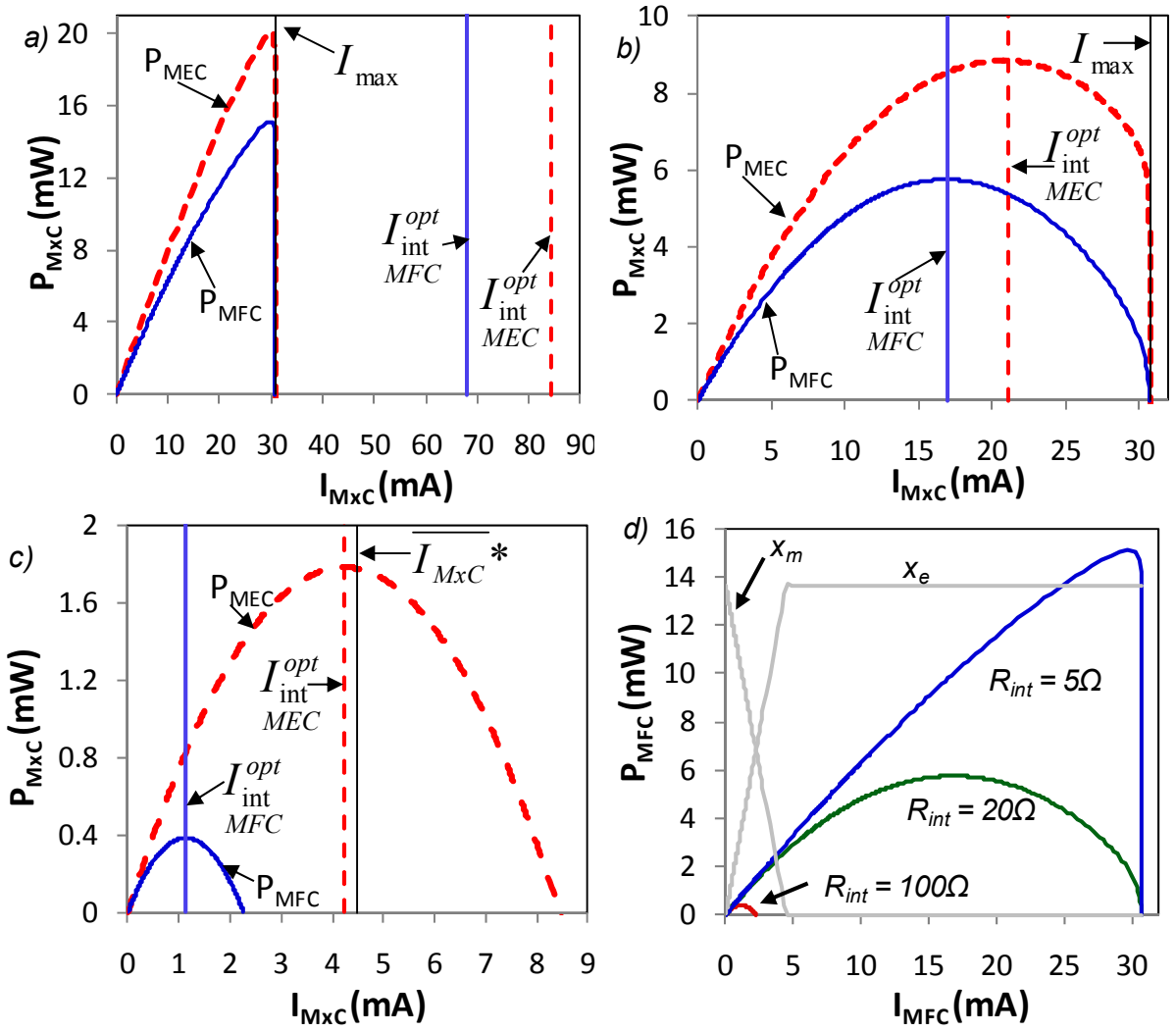

Figure 6.4. MFC and MEC steady state productivities as a function of I_{MxC} for (*a*) R_{int} = 5 Ω, (*b*) R_{int} = 20 Ω, and (*c*) R_{int} = 100 Ω. The values of $\overline{I_{MxC}}^{*}$, $I_{\max}$, and I_{int}^{opt} are also illustrated by vertical lines. MFC power curves at diverse internal resistances are compared with (*d*) the concentration of the biomass in the MFC biofilm (varying from 0% to 100% of X_{MAX}, not shown in the axis).

6.4. Alternative MEC Productivity

While the definition of productivity for MFCs is straightforward, in MECs this definition can vary. A further productivity alternative for MECs will be defined and studied in this section. This second alternative takes into account the production efficiency as the ratio of the hydrogen produced by the applied power. However, this quantity decreases monotonically with current, the

optimum being at zero current, i.e. no production. Thus, one needs to balance between the amount of hydrogen produced, and the efficiency with which it is produced. Hence, a different function for the productivity of MECs can be defined as the product of H_2 flow and the H_2 production efficiency:

$$\Phi = Q_{H2}\frac{Q_{H2}}{P_{applied}} = \frac{(Q_{H2})^2}{(I_{MEC}E_{applied})} \tag{6-40}$$

This productivity can be further simplified using the definition of H_2 flow (Eq. (5-13)):

$$\Phi = \left(\frac{Y_{H2}RT}{m_{H2}FP}\right)^2 \frac{I_{MEC}}{E_{applied}} \tag{6-41}$$

The two defined productivities functions for MECs were simulated for several currents with R_{int} = 20 Ω in Figure 6.5:

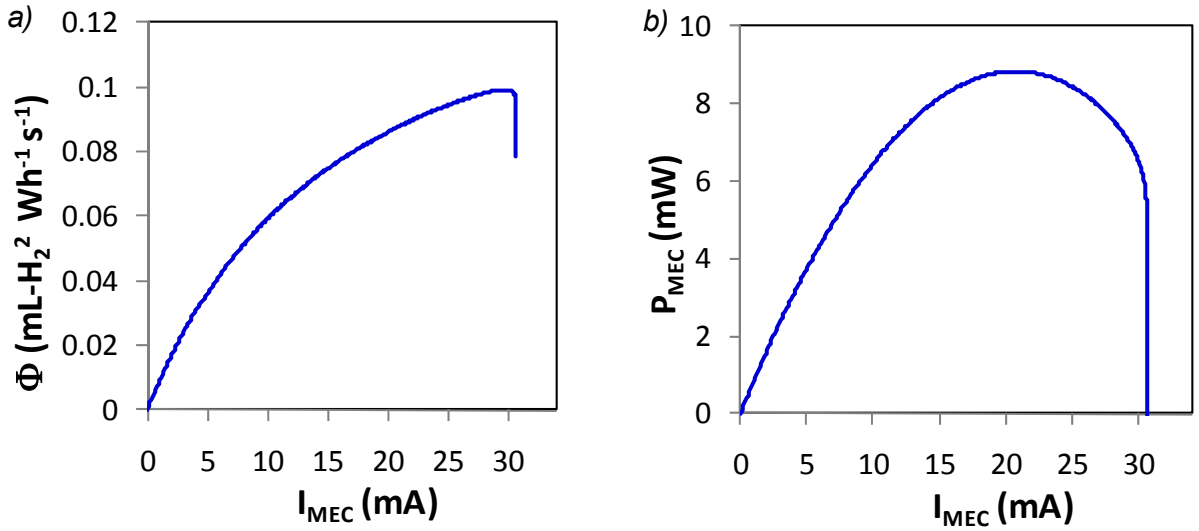

Figure 6.5. MEC steady state alternative productivity (*a*) or as defined in section 6.3.1 (*b*) as a function of I_{MxC}.

The mathematical characterization of this alternative productivity will be presented in a similar development as that found in the previous section, with a proposition used to derive an analytical expression for the optimum productivity. It will be shown that the optimum is independent from the R_{int} and corresponds to a biofilm populated only by electricigenic microorganisms.

Proposition 7. The optimum MEC productivity always presents a biofilm populated only with electricigenic microorganisms (i.e. $I_{MEC} > \overline{I}_{MxC}$) and is equal to $I_{MEC}^{opt} = \frac{I_{\max}\sqrt{-E_{CEF}}}{\sqrt{-E_{CEF}}+\sqrt{E_c}}$.

Proof. The optimum productivities can be found when $\partial\Phi/\partial I_{MEC}$ is equal to zero:

$$\frac{\partial\Phi}{\partial I_{MEC}} = \left(\frac{Y_{H2}RT}{m_{H2}FP}\right)^2\left(\frac{1}{E_{applied}} - \frac{I_{MEC}}{E_{applied}^2}\frac{\partial E_{applied}}{\partial I_{MEC}}\right) \tag{6-42}$$

So the optimal productivity of the MEC corresponds to:

$$\frac{\partial E_{applied}}{\partial I_{MEC}} = \frac{E_{applied}}{I_{MEC}} \tag{6-43}$$

The previous gradient must equal the gradient of Eq. (6-25) with respect to the current.

$$\frac{\partial\eta_{conc,A}}{\partial I_{MEC}} + R_{\text{int}} = \frac{-E_{CEF}+\eta_{conc,A}+I_{MEC}R_{\text{int}}}{I_{MEC}} \tag{6-44}$$

Therefore the optimum productivity yields:

$$\frac{\partial\eta_{conc,A}}{\partial I_{MEC}} = -E_{CEF}+\eta_{conc,A} \tag{6-45}$$

As in the preceding section, the expression of the gradient ($\partial\eta_{conc,A}/\partial I_{MEC}$) varies with the composition of the biofilm, and the analysis will be conducted independently for each biofilm region. At low $E_{applied}$ (i.e., the methanogenic region), one can see that $\Phi = 0$. However, a non-zero value of the objective function can be obtained in other regions. So, the optimum productivity is never in the methanogenic region for MECs.

In the coexistence region, $M_{ox} = \overline{M}_{ox}$, the concentration losses become constant ($\eta_{conc,A} = \overline{E}_{conc}$) and the gradient ($\partial\eta_{conc,A}/\partial I_{MEC}$) is zero. Then Eq. (6-44) leads to $E_{CEF} = \eta_{conc,A}$. However, since E_{CEF} is always negative and $\eta_{conc,A}$ is always positive, the above gradient of the objective function cannot be zero in the coexistence region. Therefore, the optimum is not in the coexistence region.

In the electricigenic region ($x_e = X_{MAX}$), the logarithmic term in Eq. (6-31) can be again approximated by $\frac{K_M}{(K_M + M_{Total})}\frac{I_{MEC}}{(I_{\max} - I_{MEC})}$. Then the gradient of $\eta_{conc,A}$ will be:

$$\frac{\partial\eta_{conc,A}}{\partial I_{MEC}} = \frac{E_c I_{\max}}{\left(I_{\max} - I_{MxC}^{opt}\right)^2} \tag{6-46}$$

By substituting Eq. (6-46) and the definition of $\eta_{conc,A}$ in Eq. (6-45) one can obtain the optimum current:

$$I_{MEC}^{opt} = \frac{I_{\max}\sqrt{-E_{CEF}}}{\sqrt{-E_{CEF}} + \sqrt{E_c}} \tag{6-47}$$

Finally by substituting Eq. (6-47) and the logarithm approximation into the MEC's electrochemical balance, one can find the optimum applied voltage:

$$E_{applied}^{opt} = \frac{I_{\max} R_{\text{int}}\sqrt{-E_{CEF}}}{\left(\sqrt{-E_{CEF}} + \sqrt{E_c}\right)} + \sqrt{E_c}\sqrt{-E_{CEF}} - E_{CEF} \tag{6-48}$$■

Proposition 7 can be confirmed by the following example. Figure 6.6*a* presents the steady state of the alternative productivity of MECs against I_{MEC}, for different values of R_{int} with all other parameters as presented in Tables A-1and A-2. As one can see from this figure, the optimum MEC productivity is independent of the R_{int}. Furthermore, optimum currents from the simulation and from Eq. (6-47) were equal to 29.8 mA and 28.5 mA, this disparity is due to the

approximation of the logarithm used for developing the analytical expression. Moreover, one can see the concentration of biomass in the biofilm (not shown in the secondary axis), with the optimum alternative productivity of the MEC presenting a biofilm fully occupied by electricigenic microorganisms. For a better comparison with the formerly defined productivity, Figure 6.6*b* presents the MEC productivity results from Fig. 6.4*a* to 6.4*c*, showing the optimum productivity for diverse internal resistances in the same plot.

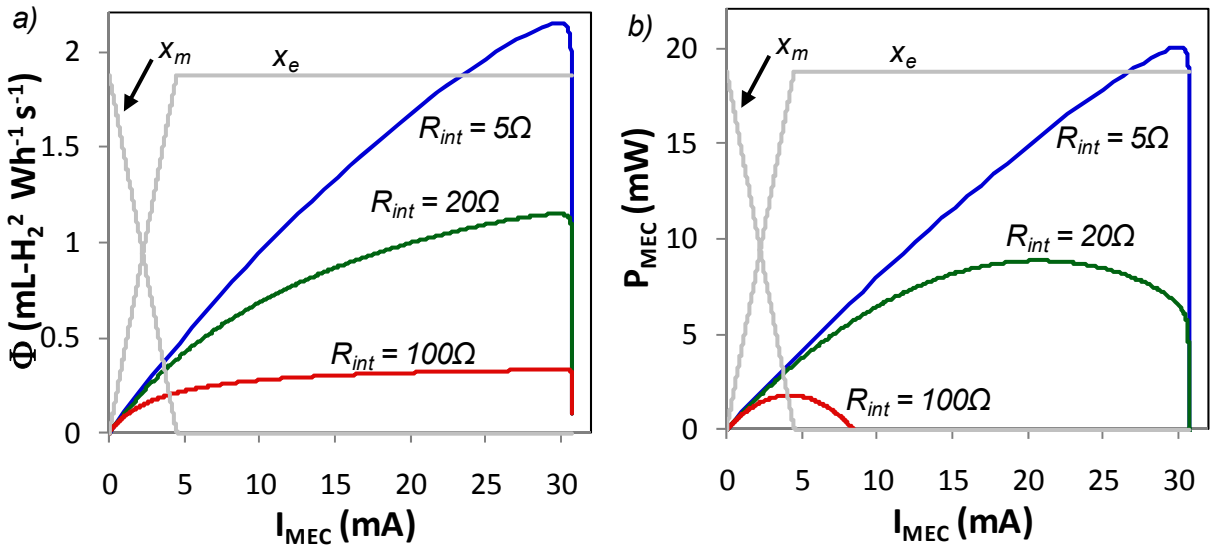

Figure 6.6. Steady state productivity of the MEC as defined in section 6.4 (*a*) and 6.3 (*b*) as a function of I_{MEC} for a R_{int} equal to either 5Ω, or 20Ω, or 100Ω. The concentration of the biomass in the MEC biofilm is also shown (varying from 0% to 100% of X_{MAX}, not shown in the axis).

6.5. Simulation of Tracking a Varying Optimum

In this section, to illustrate the variation of an optimum current with changes in R_{int} for the productivities of the MxCs, a real time optimisation algorithm is applied to track the change in the optimal operating point. The multiunit (MU) optimisation method (section 1.2.6) was used to maintain the MxCs at optimum productivities.

In Figure 6.7, the MU tracking method was used to maintain two MFCs at their optimum productivities, two MEC at the optimum productivity as defined in section 6.3, and two MECs at the alternative optimum productivity as defined in section 6.4. The initial condition for the manipulated variables were R_{ext} = 75 Ω and $E_{applied}$ = 0.55 V, the offset parameter (Δ) was set to 2

Ω (MFCs) and 0.01 V (MECs), and the biofilm was fully occupied by electricigenic microorganisms. All model parameters were kept constant except the reactors' internal resistances, which were modified from 5 Ω to 20 Ω at 145 min, and to 100 Ω at 290 min. Fig. 6.7*a* presents the currents for both MFC units, which converged to the first optimum (at R_{int} = 5 Ω) in about 25 min. The optimum for R_{int} = 20 Ω is almost immediately reached, while the optimum at R_{int} = 100 Ω takes about 120 min to converge. The variations of the manipulated variable of the MFC, R_{ext} can be observed in Fig. 6.7*b*. Fig. 6.7*c* presents the results of the productivity of the MEC, once the objective function was defined as in section 6.3. As one can see from this figure, the optimum current value is reached almost immediately for all internal resistance variations. The optimum currents calculated in Figs. 6.7*a* and 6.7*c* can be compared with the analytical expressions for the optimum current of the MxCs calculated by Eqs. (6-29), (6-36), and (6-37) (the solid horizontal black lines). Moreover, the current results for the MECs optimised using the definition of section 6.4, can be seen in Fig. 6.7*e*. In this case, the optimum current for R_{int} = 20 Ω is almost instantly reached, while for R_{int} = 100 Ω it takes about 300 min to converge. In the same figure, the analytical optimum calculated from Eq. (6-47) is presented. As one can see, variation in the internal resistance does not affect the optimum alternative productivity of the MEC. The $E_{applied}$ (manipulated variable) behaviour of the productivities defined in section 6.3 and 6.4 can be observed in Figs. 6.7*d* and 6.7*f*, respectively. Once more, the approximation of the logarithm explains the error between calculated and analytical optimums.

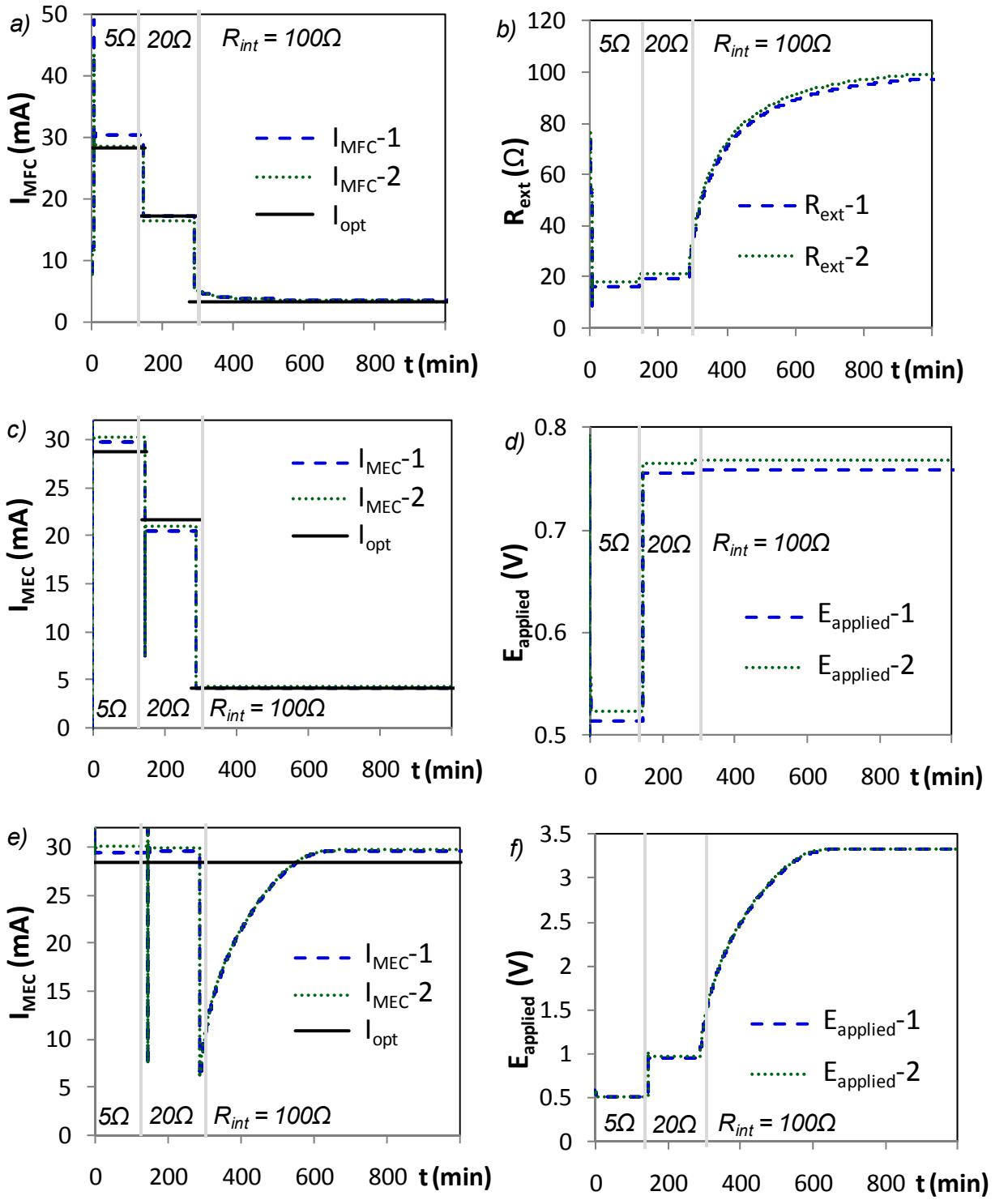

Figure 6.7. Time evolution of current for two MFCs (*a*), for two MECs optimised with the definition of section 6.3 (*c*), and for two MECs optimised with the definition of section 6.4 (*e*). Three internal resistances were used for each simulation: 5Ω to 20Ω and 100Ω (regions separated by vertical bars). The optimum currents computed by Eqs. (6-29), (6-36), (6-37), and (6-37) are represented by the solid black horizontal bars. Time progress for the manipulated variables: (*c*) R_{ext} for the MFCs units and (*d* and *f*) $E_{applied}$ for the MEC units.

6.6. Conclusion

In this section a unified model for MxCs is presented and analysed. Two species of microorganisms (electricigenic and methanogenic) competing for acetate were modelled in the anode, while the MFC and MEC mode of operation differed in the electrochemical balance. The steady state biofilm composition, a function of reactor current, was analysed. It was shown that either one of the species could dominate (competitive exclusion principle) or there could be coexistence. In this analysis, the treatment flow was adjusted to maintain a required effluent composition. Moreover, objective functions for the productivities were defined and optimised for MFCs and MECs. Two different productivity functions were defined for MECs and analytical solutions for optimum productivity were obtained for MFCs and MECs.

CONCLUSION, PERSPECTIVES AND RECOMMENDATIONS

Conclusion

The main contributions of this thesis are:

- The development and validation of MFC and MEC fast convergence multi-population dynamic models.
- Analysis of the MFC model with treatment capacity optimisation.
- Experimental proof of some results found in the MFC model analysis.
- Analysis of a unified MFC/MEC model with productivity optimisation.

The first contribution of this thesis is the development of a fast convergence model of a Microbial fuel cell, which considered the competition for acetate between electricigenic and acetoclastic methanogenic microorganisms (multi-populations). Identifiable model parameters were estimated using data from acetate fed MFCs and the start-up model accuracy was improved by making certain electrochemical parameters a function of electricigenic biofilm composition. A validation step with independent data sets confirmed the predictive capacity of the model, as it successfully correlated the external resistance and influent flow (manipulated variables) with current generation, methane production, and effluent composition for all MFC experiments. The model was also able to predict biomass growth and biofilm composition.

The influences of organic load and R_{ext} on MFC performance were studied by using the MFC model. As expected, this analysis demonstrated that the external resistance directly affected the power production (short-term MFC performance). Yet interestingly, R_{ext} also significantly influenced the biofilm microbial composition (long-term MFC performance). A steady state analysis of the model was then introduced to evaluate the biofilm microbial distribution. It was demonstrated that, independently from the initial composition of the biomass, the biofilm could be populated by electricigenic microorganisms only, or by methanogenic microorganisms only, or it could present the coexistence of both, depending on the selection of external resistance. Due to different substrate consumption rates, the three biofilm scenarios were compared in terms of treatment capacity. The coexistence scenario was shown to always present an inferior treatment

capacity, while methanogens were more effective then electricigens at high substrate compositions. In addition, a staging technique was evaluated for the MFCs, and it was proven to always be more effective than operating MFCs in parallel. The treatment capacity was maximised by optimising the design of a staging unit with two MFCs, depending on the biofilm composition of each reactor. For the most common region of operation, the best treatment capacity was found for the first MFC populated only by methanogens followed by an MFC populated only by electricigens. Finally, an additional contribution was presented: an experimental qualitative proof of the effects of external resistance on the microorganisms' concentration in the MFC biofilm.

The next contribution of this thesis was the development of a fast-convergence multi-population model of MECs. The model was capable of simulating wastewater degradation by assuming the presence of four microbial species: fermentative, electricigens, acetoclastic methanogens, and hydrogenotrophic methanogens. To avoid a complex description of carbon source and product distribution within the biofilm, three biofilm layers were assumed to contain one or more microbial species. Once more, identifiable model parameters were found with experimental results from acetate and sWW fed MECs, and the model was later validated with an independent data set. Model predictions successfully followed experimental measurements of current generation, gas production, and effluent composition for all MEC data sets.

The last contribution of this thesis lies in the analysis of a unified MFC/MEC model. This model included the competition for acetate between electricigens and methanogens. The electrochemical balance was the only difference between the MFC and MEC operation. Model analysis proved that the microbial composition of the biofilm could be determined by the reactor operation current and that the competitive exclusion principle was valid only for a specific range of operation current. An optimisation study was conducted to enhance electricity (MFC) or H_2 production (MEC) by defining productivity functions for each reactor that were maximised while maintaining the effluent composition at a required level. It was shown that depending on the definition of the objective function, MFC's and MEC's optimum productivities could have the same expressions for the optimum analytical solution, which was highly dependent on the reactor's internal resistance. In addition, an alternative productive function could be defined for MECs, leading to an optimum that was independent from the R_{int}.

Perspectives and Recommendations

Following the results presented in this thesis, a number of new research opportunities that might be further investigated and analysed in the field of MxC modelling are listed below. Recommendations will be made for model modifications and for further model analysis.

Model modifications

1. "*Influence of auxiliary operational conditions*": Certain operational conditions that were kept constant during the MxC experiments and were assumed to be constant in the model formulation may have an impact on reactor performance. Therefore, further versions of the MFC and MEC models may include, for example, the effects of pH, anode liquid conductivity, and reactor temperature. These parameters may have a direct influence on the electron transfer mechanisms, the internal resistance of the reactor, and the substrate consumption kinetics, among other effects.
2. "*Cathode reaction limitation in MxCs*": The cathode reactions and limitations could be included in the model, since this is one of the main bottlenecks of the performance of MxCs. This subject has been studied in depth for SOFCs and hydrogen fuel cells, so many cathode modelling concepts can be found in this literature and used in future MxC modelling.
3. "*Multi-population three dimension biofilm model*": Both MFC and MEC models could be expanded to include spatial variation of the biofilm thickness. This would lead to a longer time for numerical computation, but could provide interesting insights in terms of biofilm development. Note that 3D MFC modelling has been already presented (see section 1.1.3.3).
4. "*Model-based MxC reactor design enhancement*": By including precise transport phenomena to the model, such as substrate diffusion, one could study different designs for MxCs to improve the performance of the reactor. This point is interesting since several MxC designs are available and the most advantageous options for different situations are unknown.

Model analysis

1. "*Effects of operational conditions in the biofilm composition of MECs used for wastewater treatment*": As can be seen from the MEC model analysis in section 5.4, the applied voltage selection not only affects the composition of the inner biofilm layer that contains electricigens, but also affects the composition of the outer biofilm layer that contains fermentative microorganisms. This is due to the acetoclastic methanogens and electricigens in the inner biofilm layer consuming the same substrate (acetate) as the acetoclastic

methanogens in the outer biofilm layer, indirectly affecting the concentration of this biofilm layer. A steady state study analysing the space competition in the biofilm and the validity of the CEP for the different layers in the multi-population model presented in chapter 5 could be done, similarly to the analyses presented in sections 4.2 and 6.2. Following these results, analysis could be performed to optimise the treatment capacity of wastewater treatment MECs, similar to the analysis presented in chapter 4.

2. "*On-off or Periodic control strategy to maximise MFC/MEC production performance*": Throughout polarization tests in MFC experiments, an interesting behaviour was frequently observed: after reconnecting the external resistance, a large current could be drawn from the system. The MFCs were hypothesised to be acting as a capacitor, storing current during the open circuit period. The MFC model developed in chapter 3 was unable to reproduce this result and research is ongoing to study the possible advantages of an On/Off control strategy for MFCs. A further possibility would be to study the same behaviour for MECs.
3. "*Hydrogen production cogeneration unit with MFCs and MECs for wastewater treatment*": The modelling concepts presented in chapters 3 and 5 can be use to study a cogeneration unit applying MFCs and MECs to treat wastewater and produce hydrogen. The current generated by the MFCs can be used as an applied voltage for the MECs, so no external energy source would be required for the cogeneration unit. As the voltage output of a MFC is around 0.2-0.3V, several reactors in series (stacks) may be required to provide the desirable applied voltage for MECs. On the other hand, the wastewater feeding can be either distributed in series or in parallel (or even both) between all the reactors. This analysis would lead to a complex mix integer optimisation problem, with numerous possible choices for feeding and reactor placement. An example of such a cogeneration unit is shown in the following figure.

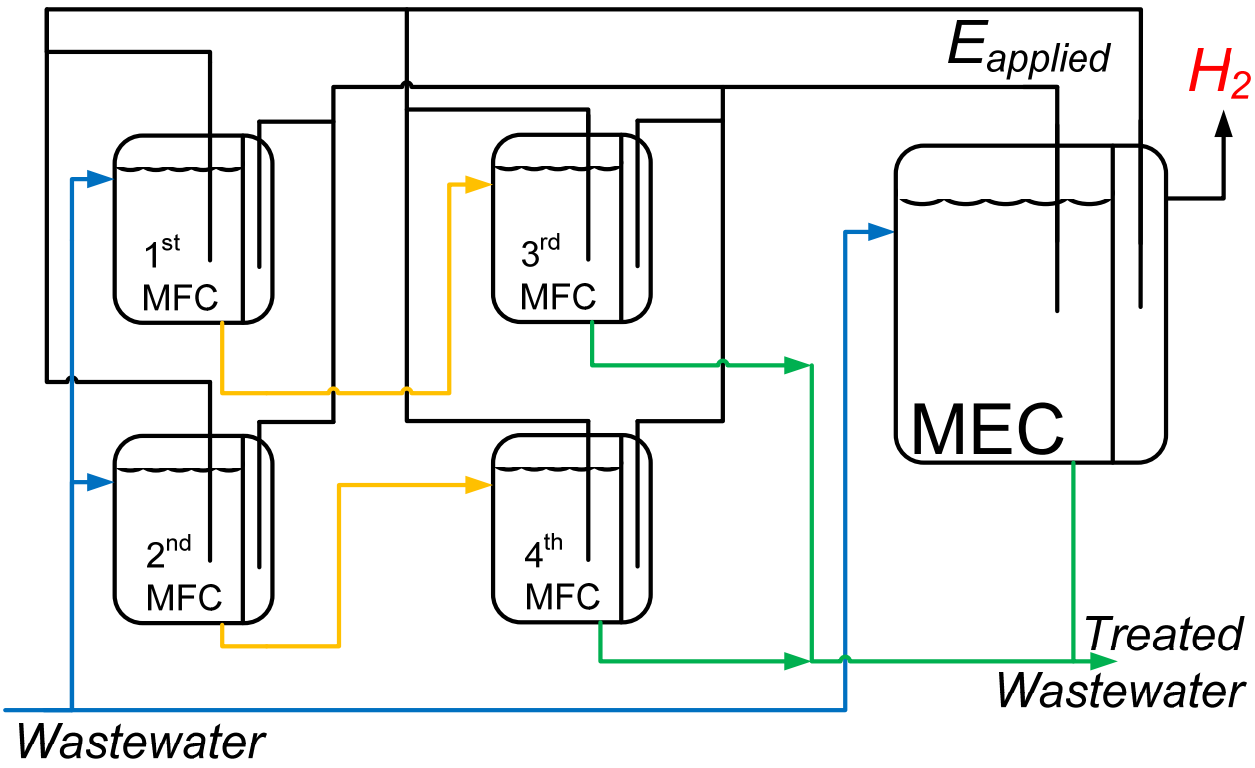

Figure C.1. Example of MFC and MEC cogeneration unit, with MFCs generating the required applied voltage for the MEC. The influent was distributed between MFCs and MECs.

The MFC and MEC technology presents an important alternative for waste treatment and renewable energy production, both key challenges facing modern society. These reactors can contribute to the development of a more sustainable use of natural resources and to the recuperation of fresh water. Intense research in the past few years has already improved the reactors' performance, leading to a four order of magnitude increase in power density, and potential future commercial applications in the years to come. This thesis presented the development of MFC and MEC multi-population, fast convergence models that were used to improve reactor performance. These models may be used in the future to continue enhancement of this technology and may contribute to the development of control strategies to better operate commercial MFC/MEC treatment units.

REFERENCE LIST

Aelterman, P., Rabaey, K., Pham, H. T., Boon, N., & Verstraete, W. (2006). Continuous electricity generation at high voltages and currents using stacked microbial fuel cells. *Environmental Science and Technology, 40*(10), 3388-3394.

Aelterman, P., Versichele, M., Marzorati, M., Boon, N., & Verstraete, W. (2008). Loading rate and external resistance control the electricity generation of microbial fuel cells with different three-dimensional anodes. *Bioresource Technology, 99*(18), 8895-8902.

Aguiar, P., Adjiman, C. S., & Brandon, N. P. (2004). Anode-supported intermediate temperature direct internal reforming solid oxide fuel cell. I: Model-based steady-state performance. *Journal of Power Sources, 138*, 120-136.

Andrews, J. F. (1968). A mathematical model for the continuous culture of microorganisms utilizing inhibitory substrates. *Biotechnology and Bioengineering, 10*(6), 707-723.

APHA. (1995). *Standard methods for the examination of water and wastewater* (19 ed.). Washington, DC: American Public Health Association.

Arcand, Y., Chavarie, C., & Guiot, S. (1994). Dynamic modelling of the population distribution in the anaerobic granular biofilm. *Water Science and Technology, 30*, 63-73.

Bae, W., & Rittmann, B. E. (1996a). Responses of intracellular cofactors to single and dual substrate limitations. *Biotechnology and Bioengineering, 49*(6), 690-699.

Bae, W., & Rittmann, B. E. (1996b). Structured model of dual-limitation kinetics. *Biotechnology and Bioengineering, 49*(6), 683-689.

Bastin, G., & Dochain, D. (1990). *On-Line Estimation and Adaptative Control of Bioreactors*. Amsterdam, The Netherlands: Elsevier Science Publishers.

Batstone, D. J., Keller, J., Angelidaki, I., Kalyuzhnyi, S. V., Pavlostathis, S. G., Rozzi, A., et al. (2002a). *Anaerobic digestion model no 1 (ADM1)*: IWA Publishing, London, UK.

Batstone, D. J., Keller, J., Angelidaki, I., Kalyuzhnyi, S. V., Pavlostathis, S. G., Rozzi, A., et al. (2002b). The IWA Anaerobic Digestion Model No 1 (ADM1) *Water Science and Technology, 45*(10), 65-73.

Batstone, D. J., Keller, J., Newell, R. B., & Newland, M. (2000). Modelling anaerobic degradation of complex wastewater. I: model development. *Bioresource Technology, 75*, 67-74.

Bernard, O., Hadj-Sadok, Z., Dochain, D., Genovesi, A., & Steyer, J. P. (2001). Dynamical model development and parameter identification for an anaerobic wastewater treatment process. *Biotechnology and Bioengineering, 75*(4), 424-438.

Biyikoglu, A. (2005). Review of proton exchange membrane fuel cell models. *International Journal of Hydrogen Energy, 30*(11), 1181-1212.

Bond, D. R., Holmes, D. E., Tender, L. M., & Lovley, D. R. (2002). Electrode-reducing microorganisms that harvest energy from marine sediments. *Science, 295*(5554), 483-485.

Bonnet, B., Dochain, D., & Steyer, J.-P. (1997). Dynamical modelling of an anaerobic digestion fluidized bed reactor. *Water Science and Technology, 36*(5), 285-292.

Buffiere, P., Steyer, J.-P., Fonade, C., & Moletta, R. (1995). Comprehensive modeling of methanogenic biofilms in fluidized bed systems: Mass transfer limitations and multisubstrate aspects. *Biotechnology and Bioengineering, 48*(6), 725-736.

Cannarozzo, M., Grosso, S., Agnew, G., Del Borghi, A., & Costamagna, P. (2007). Effects of mass transport on the performance of solid oxide fuel cells composite electrodes. *Journal of Fuel Cell Science and Technology, 4*(1), 99-106.

Chae, K.-J., Choi, M.-J., Kim, K.-Y., Ajayi, F. F., Park, W., Kim, C.-W., et al. (2010). Methanogenesis control by employing various environmental stress conditions in two-chambered microbial fuel cells. *Bioresource Technology, 101*(14), 5350-5357.

Chaparroa, A. M., Gallardo, B., Folgado, M. A., Martín, A. J., & Daza, L. (2009). PEMFC electrode preparation by electrospray: Optimization of catalyst load and ionomer content *Catalysis Today, 143*, 237–241.

Cheng, K. Y., Goen, H., & Cord-Ruwisch, R. (2008). Affinity of microbial fuel cell biofilm for the anodic potential. *Environmental Science and Technology, 42*, 3828-3834.

Degenring, D., Froemel, C., Dikta, G., & Takors, R. (2004). Sensitivity analysis for the reduction of complex metabolism models. *Journal of Process Control, 14*(7), 729-745.

Dochain, D., & Vanrolleghem, P. A. (2001). *Dynamical Modelling and Estimation in Wastewater Treatment Processes*. London: IWA Publishing.

Eddy, M. (2003). *Wastewater Engineering: Treatment and Reuse* (4 ed.). New York, NY: McGraw-Hill Science/Engineering/Math.

Esteve-Nunez, A., Rothermich, M., Sharma, M., & Lovley, D. (2005). Growth of *Geobacter sulfurreducens* under nutrient-limiting conditions in continuous culture. *Environmental Microbiology, 7*(5), 641-648.

Fan, Y., Sharbrough, E., & Liu, H. (2008). Quantification of the internal resistance distribution of microbial fuel cells. *Environmental Science and Technology, 42*, 8101-8107.

Fuel Cell Handbook. (2005) *National Energy Technology Laboratory U.S. Department of Energy*. Consulted on-line on July 29 2011, retrived from http://www.netl.doe.gov/technologies/coalpower/fuelcells/seca/pubs/FCHandbook7.pdf

Galvanauskas, V., Simutis, R., Volk, N., & Lubbert, A. (1998). Model based design of a biochemical cultivation process. *Bioprocess Engineering, 18*(3), 227-234.

Georgieva, O., Hristozov, I., Pencheva, T., Tzonkov, S., & Hitzmann, B. (2003). Mathematical modelling and variable structure control systems for fed-batch fermentation of Escherichia coli. *Chemical and Biochemical Engineering Quarterly, 17*(4), 293-299.

Geun-Cheol, G., In-Seop, C., Byung Hong, K., Mia, K., Jae-Kyung, J., Hyung Soo, P., et al. (2003). Operational parameters affecting the performance of a mediator-less microbial fuel cell. *Biosensors & Bioelectronics, 18*, 327-334.

Gray, D. M. D., Hake, J. M., & Ghosh, S. (2006). Influence of staging, mean cell residence time, and thermophilic temperature on the thermophilic anaerobic digestion process. *Water Environment Research, 78*(5), 497-509.

Hamelers, H. V. M., ter Heijne, A., Stein, N., Rozendal, R. A., & Buisman, C. J. N. (2011). Butler-Volmer-Monod model for describing bio-anode polarization curves. *Bioresource Technology, 102*, 381-387.

Hardin, G. (1960). The Competitive Exclusion Principle. *Science, 131*, 1292-1297.

Harmand, J., Rapaport, A., Dochain, D., & Lobry, C. (2008). Microbial ecology and bioprocess control: opportunities and challenges. *Journal of Process Control, 18*(9), 865-875.

He, Z., Huang, Y., Manohar, A. K., & Mansfeld, F. (2008). Effect of electrolyte pH on the rate of the anodic and cathodic reactions in an air-cathode microbial fuel cell. *Bioelectrochemistry, 74*(1), 78-82.

Hu, H., Fan, Y., & Liu, H. (2008). Hydrogen production using single-chamber membrane-free microbial electrolysis cells. *Water Research, 42*(15), 4172-4178.

Ieropoulos, I., Greenman, J., & Melhuish, C. (2008). Microbial fuel cells based on carbon veil electrodes: stack configuration and scalability. *International Journal of Energy Research, 32*, 1228-1240.

Ishii, S. i., Hotta, Y., & Watanabe, K. (2008). Methanogenesis versus electrogenesis: Morphological and phylogenetic comparisons of microbial communities. *Bioscience, Biotechnology and Biochemistry, 72*, 286-294.

Jadhav, G. S., & Ghangrekar, M. M. (2009). Performance of microbial fuel cell subjected to variation in pH, temperature, external load and substrate concentration. *Bioresource Technology, 100*(2), 717-723.

Jeyaseelan, S. (1997). A simple mathematical model for anaerobic digestion process. *Water Science and Technology, 35*, 185-191.

Kang, K. H., Jang, J. K., Pham, T. H., Moon, H., Chang, I. S., & Kim, B. H. (2003). A microbial fuel cell with improved cathode reaction as a low biochemical oxygen demand sensor. *Biotechnology Letters, 25*(16), 1357-1361.

Kim, B. H., Chang, I. S., & Gadd, G. M. (2007). Challenges in microbial fuel cell development and operation. *Applied Microbiology and Biotechnology, 76*(3), 485-494.

Kim, H.-W., Shin, H.-S., Han, S.-K., & Oh, S.-E. (2007). Response surface optimization of substrates for thermophilic anaerobic codigestion of sewage sludge and food waste. *Journal of the Air and Waste Management Association, 57*, 309-318.

Kim, H. J., Park, H. S., Hyun, M. S., Chang, I. S., Kim, M., & Kim, B. H. (2002). A mediator-less microbial fuel cell using a metal reducing bacterium, *Shewanella putrefaciens*. *Enzyme and Microbial Technology, 30*, 145-152.

Lettinga, G. (1995). Anaerobic digestion and wastewater treatment systems. *Antonie van Leeuwenhoek, 67*, 3-28.

Levisauskas, D., Galvanauskas, V., Henrich, S., Wilhelm, K., Volk, N., & Lubbert, A. (2003). Model-based optimization of viral capsid protein production in fed-batch culture of recombinant Escherichia coli. *Bioprocess and Biosystems Engineering, 25*(4), 255-262.

Levisauskas, D., Galvanauskas, V., Simutis, R., & Lubbert, A. (1999). Model based calculation of substrate/inducer feed-rate profiles in fed-batch processes for recombinant protein production. *Biotechnology Techniques, 13*(1), 37-42.

Liang, P., Huang, X., Fan, M.-Z., Cao, X.-X., & Wang, C. (2007). Composition and distribution of internal resistance in three types of microbial fuel cells. *Applied Microbiology and Biotechnology, 77*(3), 551-558.

Lin, Y.-H. (2008). Kinetics of nitrogen and carbon removal in a moving-fixed bed biofilm reactor. *Applied Mathematical Modelling, 32*(11), 2360-2377.

Liu, H., Cheng, S., & Logan, B. E. (2005). Power generation in fed-batch microbial fuel cells as a function of ionic strength, temperature, and reactor configuration. *Environmental Science and Technology, 39*, 5488-5493.

Liu, Z., Liu, J., Zhang, S., & Su, Z. (2008). A novel configuration of microbial fuel cell stack bridged internally through an extra cation exchange membrane. *Biotechnology Letters, 30*(6), 1017-1023.

Ljung, L. (1999). *System Identification: Theory for the User* (2nd ed.). New Jersey: Prentice-Hall, Inc.

Logan, B. E. (2008). *Microbial Fuel Cells* (1 ed.). Hobeken, New Jersey: John Wiley & Sons.

Logan, B. E. (2010). Scaling up microbial fuel cells and other bioelectrochemical systems. *Applied Microbiology and Biotechnology, 85*(6), 1665-1671.

Logan, B. E., Call, D., Cheng, S., Hamelers, H. V. M., Sleutels, T. H. J. A., Jeremiasse, A. W., et al. (2008). Microbial electrolysis cells for high yield hydrogen gas production from organic matter. *Environmental Science and Technology, 42*(23), 8630-8640.

Logan, B. E., Hamelers, B., Rozendal, R. A., Schroder, U., Keller, J., Freguia, S., et al. (2006). Microbial Fuel Cells: Methodology and Technology. *Environmental Science and Technology, 40*(17), 5181-5192.

Logan, B. E., & Regan, J. M. (2006a). Electricity-producing bacterial communities in microbial fuel cells. *Trends in Microbiology, 14*(12), 512-518.

Logan, B. E., & Regan, J. M. (2006b). Microbial fuel cells - Challenges and applications. *Environmental Science and Technology, 40*(17), 5172-5180.

Lopez, I., & Borzacconi, L. (2010). Modelling of slaughterhouse solid waste anaerobic digestion: Determination of parameters and continuous reactor simulation. *Waste Management, 30*, 1813-1821.

Lyon, D. Y., Buret, F., Vogel, T. M., & Monier, J.-M. (2010). Is resistance futile? Changing external resistance does not improve microbial fuel cell performance. *Bioelectrochemistry, 78*(1), 2-7.

Manuel, M.-F., Neburchilov, V., Wang, H., Guiot, S. R., & Tartakovsky, B. (2010). Hydrogen production in a microbial electrolysis cell with nickel-based gas diffusion cathodes. *Journal of Power Sources, 195*(17), 5514-5519.

Marcus, A. K., Torres, C. I., & Rittmann, B. E. (2007). Conduction-based modeling of the biofilm anode of a microbial fuel cell. *Biotechnology and Bioengineering, 98*(6), 1171-1182.

Marcus, A. K., Torres, C. I., & Rittmann, B. E. (2011). Analysis of a microbial electrochemical cell using the proton condition in biofilm (PCBIOFILM) model. *Bioresource Technology, 102*(1), 253-262.

Martin, E., Savadogo, O., Guiot, S. R., & Tartakovsky, B. (2010). The influence of operational conditions on the performance of a microbial fuel cell seeded with mesophilic anaerobic sludge. *Biochemical Engineering Journal, 51*(3), 132-139.

Moletta, R., Verrier, D., & Albagnac, G. (1986). Dynamic modelling of anaerobic digestion. *Water Research, 20*(4), 427-434.

Monod, J. (1942). *Recherches sur la Croissance des Cultures Bactériennes*. Paris: Hermann & Co.

Moon, H., In, S. C., Jae, K. J., & Kim, B. H. (2005). Residence time distribution in microbial fuel cell and its influence on COD removal with electricity generation. *Biochemical Engineering Journal, 27*, 59-65.

Mu, S. J., Zeng, Y., Wu, P., Lou, S. J., & Tartakovsky, B. (2008). Anaerobic digestion model no. 1-based distributed parameter model of an anaerobic reactor: I. Model development. *Bioresource Technology, 99*(9), 3665-3675.

Nelder, J. A., & Mead, R. (1965). A Simplex Method for Function Minimization. *The Computer Journal, 7*(4), 308-313.

Noren, D. A., & Hoffman, M. A. (2005). Clarifying the Butler-Volmer equation and related approximations for calculating activation losses in solid oxide fuel cell models. *Journal of Power Sources, 152*(1-2), 175-181.

O'Hayre, R., Cha, S.-W., Colella, W., & Prinz, F. B. (2006). *Fuel Cell Fundamentals* (1 ed.): Hoboken, N.J. : John Wiley & Sons.

Oh, S. E., & Logan, B. E. (2007). Voltage reversal during microbial fuel cell stack operation. *Journal of Power Sources, 167*(1), 11-17.

Pant, D., Van Bogaert, G., Diels, L., & Vanbroekhoven, K. (2010). A review of the substrates used in microbial fuel cells (MFCs) for sustainable energy production. *Bioresource Technology, 101*(6), 1533-1543.

Pham, T. H., Rabaey, K., Aelterman, P., Clauwaert, P., De Schamphelaire, L., Boon, N., et al. (2006). Microbial fuel cells in relation to conventional anaerobic digestion technology. *Engineering in Life Sciences, 6*(3), 285-292.

Picioreanu, C., Head, I. M., Katuri, K. P., van Loosdrecht, M. C. M., & Scott, K. (2007). A computational model for biofilm-based microbial fuel cells. *Water Research, 41*(13), 2921-2940.

Picioreanu, C., Katuri, K. P., Head, I. M., Van Loosdrecht, M. C. M., & Scott, K. (2008). Mathematical model for microbial fuel cells with anodic biofilms and anaerobic digestion. *Water Science and Technology, 57*(7), 965-971.

Picioreanu, C., Katuri, K. P., Van Loosdrecht, M. C. M., Head, I. M., & Scott, K. (2010a). Modelling microbial fuel cells with suspended cells and added electron transfer mediator. *Journal of Applied Electrochemistry, 40*, 151-162.

Picioreanu, C., Kreft, J.-U., & Van Loosdrecht, M. C. M. (2004). Particle-based multidimensional multispecies biofilm model. *Applied and Environmental Microbiology, 70*, 3024-3040.

Picioreanu, C., van Loosdrecht, M. C. M., Curtis, T. P., & Scott, K. (2010b). Model based evaluation of the effect of pH and electrode geometry on microbial fuel cell performance. *Bioelectrochemistry, 78*(1), 8-24.

Pinto, R. P., Perrier, M., Tartakovsky, B., & Srinivasan, B. (2010a). *Performance analyses of microbial fuel cells operated in series.* Paper presented at the DYCOPS - Proceedings of

9th International Symposium on Dynamics and Control of Process Systems, Leuven, Belgium.

Pinto, R. P., Srinivasan, B., Guiot, S. R., & Tartakovsky, B. (2011a). The Effect of Real-Time External Resistance Optimization on Microbial Fuel Cell Performance. *Water Research, 45*(4), 1571-1578.

Pinto, R. P., Srinivasan, B., Manuel, M.-F., & Tartakovsky, B. (2010b). A Two-Population Bio-Electrochemical Model of a Microbial Fuel Cell. *Bioresource Technology, 101*(14), 5256-5265.

Pinto, R. P., Srinivasan, B., Scapa, A., & Tartakovsky, B. (2011b). A Multi-Population Model of a Microbial Electrolysis Cell. *Environmental Science and Technology*, Published On-line.

Pinto, R. P., Srinivasan, B., & Tartakovsky, B. (2011c). *A Unified Model for Electricity and Hydrogen Production in Microbial Electrochemical Cells* Paper presented at the IFAC - Proceedings of 18th World Congress of the International Federation of Automatic Control (IFAC), Milan, Italy.

Pinto, R. P., Tartakovsky, B., Perrier, M., & Srinivasan, B. (2010c). Optimizing Treatment Performance of Microbial Fuel Cells by Reactor Staging. *Industrial and Engineering Chemistry Research, 49*(19), 9222-9229.

Pinto, R. P., Tartakovsky, B., & Srinivasan, B. (2011d). Optimizing Energy Productivity of Microbial Electrochemical Cells. *Journal of Process Control*, Submitted article.

Potter, M. C. (1915). Electrical effects accompanying the decomposition of organic compounds. II. Ionisation of gases produced during the fermentation. *Proceedings of the Royal Society of London, 91*, 465-480.

Premier, G. C., Jung Rae, K., Michie, I., Dinsdale, R. M., & Guwy, A. J. (2011). Automatic control of load increases power and efficiency in a microbial fuel cell. *Journal of Power Sources, 196*, 2013-2019.

Quarmby, J., & Forster, C. F. (1995). An examination of the structure of UASB granules. *Water Research, 29*, 2449-2454.

Rabaey, K., Clauwaert, P., Aelterman, P., & Verstraete, W. (2005). Tubular microbial fuel cells for efficient electricity generation. *Environmental Science and Technology, 39*(20), 8077-8082.

Rauch, W., Vanhooren, H., & Vanrolleghem, P. A. (1999). A simplified mixed-culture biofilm model. *Water Research, 33*(9), 2148-2162.

Reguera, G., McCarthy, K. D., Mehta, T., Nicoll, J. S., Tuominen, M. T., & Lovley, D. R. (2005). Extracellular electron transfer via microbial nanowires. *Nature Biotechnology, 435*, 1098-1101.

Rismani-Yazdi, H., Carver, S. M., Christy, A. D., & Tuovinen, I. H. (2008). Cathodic limitations in microbial fuel cells: An overview. *Journal of Power Sources, 180*, 683-694.

Rozendal, R. A. (2007). *Hydrogen production through biocatalyzed electrolysis.* Wageningen University, Wageningen, the Netherlands.

Rozendal, R. A., Hamelers, H. V. M., Euverink, G. J. W., Metz, S. J., & Buisman, C. J. N. (2006). Principle and perspectives of hydrogen production through biocatalyzed electrolysis. *International Journal of Hydrogen Energy, 31*(12), 1632-1640.

Scuras, S. E., Jobbagy, A., & Leslie Grady C.P, J. (2001). Optimization of activated sludge reactor configuration: kinetic considerations. *Water Research, 35*(18), 4277-4284.

Sheintuch, M., Tartakovsky, B., Narkis, N., & Rebhun, M. (1995). Substrate Inhibition and Multiple States in a Continuous Nitrification Process *Water Research, 29*, 953-963.

Shimoyama, T., Komukai, S., Yamazawa, A., Ueno, Y., Logan, B. E., & Watanabe, K. (2008). Electricity generation from model organic wastewater in a cassette-electrode microbial fuel cell. *Applied Microbiology and Biotechnology, 80*(2), 325-330.

Shuler, M. L., & Kargi, F. (1992). *Bioprocess Engineering*. New Jersey: Preticen-Hall.

Siddharth, S. (2006). *Green energy-anaerobic digestion.* Paper presented at the CHISA 2006 - 17th International Congress of Chemical and Process Engineering, Prague.

Srinivasan, B. (2007). Real-time optimization of dynamic systems using multiple units. *International Journal of Robust and Nonlinear Control, 17*(Copyright 2007, The Institution of Engineering and Technology), 1183-1193.

Tartakovsky, B., Manuel, M. F., Neburchilov, V., Wang, H., & Guiot, S. R. (2008a). Biocatalyzed hydrogen production in a continuous flow microbial fuel cell with a gas phase cathode. *Journal of Power Sources, 182*(1), 291-297.

Tartakovsky, B., Mehta, P., Santoyo, G., & Guiot, S. R. (2011). Maximizing Hydrogen Production in a Microbial Electrlysis Cell by Real-Time Optimization of Applied Voltage. *International Journal of Hydrogen Energy, Submitted paper*.

Tartakovsky, B., Mu, S. J., Zeng, Y., Lou, S. J., Guiot, S. R., & Wu, P. (2008b). Anaerobic digestion model No. 1-based distributed parameter model of an anaerobic reactor: II. Model validation. *Bioresource Technology, 99*(9), 3676-3684.

ter Heijne, A., Hamelers, H. V. M., Saakes, M., & Buisman, C. J. N. (2008). Performance of non-porous graphite and titanium-based anodes in microbial fuel cells. *Electrochimica Acta, 53*, 5697-5703.

Torres, C. I., Marcus, A. K., Lee, H., Parameswaran, P., Krajmalnik-Brown, R., & Rittmann, B. E. (2010). A kinetic perspective on extracellular electron transfer by anode-respiring bacteria. *FEMS Microbiology Reviews, 34*(1), 3-17.

Torres, C. I., Marcus, A. K., Parameswaran, P., & Rittmann, B. E. (2008a). Kinetic experiments for evaluating the nernst-monod model for anode-respiring bacteria (ARB) in a biofilm anode. *Environmental Science and Technology, 42*(17), 6593-6597.

Torres, C. I., Marcus, A. K., & Rittmann, B. E. (2008b). Proton transport inside the biofilm limits electrical current generation by anode-respiring bacteria. *Biotechnology and Bioengineering, 100*, 872-881.

Van Lier, J. B., Van Der Zee, F. P., Tan, N. C. G., Rebac, S., & Kleerebezem, R. (2001). Advances in high-rate anaerobic treatment: Staging of reactor systems. *Water Science and Technology, 44*, 15-25.

Wang, A., Liu, W., Cheng, S., Xing, D., Zhou, J., & Logan, B. E. (2009). Source of methane and methods to control its formation in single chamber microbial electrolysis cells. *International Journal of Hydrogen Energy, 34*(9), 3653-3658.

Wanner, O., & Gujer, W. (1985). Competition in biofilms. *Water Science and Technology, 17*(2-3 -3 pt 1), 27-44.

Wanner, O., & Gujer, W. (1986). Multispecies Biofilm Model. *Biotechnology and Bioengineering, 28*(3), 314-328.

Whang, L. M., Filipe, C. D. M., & Park, J. K. (2007). Model-based evaluation of competition between polyphosphate- and glycogen-accumulating organisms. *Water Research, 41*, 1312-1324.

Wilkinson, S. (2000). `Gastrobots' - benefits and challenges of microbial fuel cells in food powered robot applications. *Autonomous Robots, 9*(2), 99-111.

Woodward, L., Perrier, M., & Srinivasan, B. (2009a). Improved performance in the multi-unit optimization method with non-identical units. *Journal of Process Control, 19*, 205-215.

Woodward, L., Perrier, M., Srinivasan, B., Pinto, R. P., & Tartakovsky, B. (2010). Comparison of real-time methods for maximizing power output in microbial fuel cells. *AIChE Journal, 56*(10), 2742-2750.

Woodward, L., Perrier, M., Srinivasan, B., & Tartakovsky, B. (2009b). Maximizing power production in a stack of microbial fuel cells using multiunit optimization method. *Biotechnology Progress, 25*(3), 676-682.

Wu, J., Liu, Q., & Fang, H. (2006). Toward the optimization of operating conditions for hydrogen polymer electrolyte fuel cells. *Journal of Power Sources, 156*, 388-399.

Yang, Y., Tsukahara, K., Sawayama, S., & Maekawa, T. (2004). Anaerobic digestion by a fixed and fluidized hybrid reactor packed with carbon felt. *Materials Science and Engineering C, 24*(6-8 SPEC. ISS.), 893-899.

Yao, K. Z., Koran, K., McAuley, K. B., Oosthuizen, P., Peppley, B., & Xie, T. (2004). A review of mathematical models for hydrogen and direct methanol polymer electrolyte membrane fuel cells. *Fuel Cells, 4*(1-2), 3-29.

Yingru, Z., Congjie, O., & Jincan, C. (2008). A new analytical approach to model and evaluate the performance of a class of irreversible fuel cells. *International Journal of Hydrogen Energy, 33*(15), 4161-4170.

Zeng, R. J., Yuan, Z., & Keller, J. (2003). Model-based analysis of anaerobic acetate uptake by a mixed culture of polyphosphate-accumulating and glycogen-accumulating organisms. *Biotechnology and Bioengineering, 83*, 293-302.

Zeng, Y., Choo, Y. F., Kim, B.-H., & Wu, P. (2010). Modelling and simulation of two-chamber microbial fuel cell. *Journal of Power Sources, 195*(1), 79-89.

Zhang, X. C., & Halme, A. (1995). Modelling of a microbial fuel cell process. *Biotechnology Letters, 17*(8), 809-814.

Zhang, Z. (1997). Parameter estimation techniques: A tutorial with application to conic fitting. *Image and Vision Computing, 15*(1), 59-76.

APPENDIX I

Table A-1: Model parameters for MFC model. Non-identifiable model parameters were selected based on results of Marcus et al. (2007), Batstone et al. (2000), and Tartakovsky et al. (2008b).

Parameter	Description	Value	Dimension	Notes
F	Faraday constant	96485	A s mole^{-} $^{-1}$	constant
R	ideal gas constant	8.31446	J K^{-1} mol^{-1}	constant
T	MFC temperature	298.15	K	constant
Y_M	mediator yield	22.75	mg-M mg-A^{-1}	estimated
Y_{CH4}	methane yield	0.3	mL-CH_4 mg-A^{-1}	assumed
$q_{max,e}$	max. reaction rate	8.48	mg-A mg-x^{-1} d^{-1}	estimated
$q_{max,m}$	max. reaction rate	8.20	mg-A mg-x^{-1} d^{-1}	estimated
$\mu_{max,e}$	max. growth rate	1.97	d^{-1}	estimated
$\mu_{max,m}$	max. growth rate	0.1	d^{-1}	estimated
$K_{A,e}$	half-rate constant	20	mg-A L^{-1}	assumed
$K_{A,m}$	half-rate constant	80	mg-A L^{-1}	assumed
m	e^{-} transferred per mol of mediator	2	mole^{-} mol-M^{-1}	assumed
γ	mediator molar mass	663400	mg-M mol-M^{-1}	assumed
M_{Total}	mediator fraction	0.05	mg-M mg- x^{-1}	assumed
K_M	half-rate constant	0.2.M_{Total}	mg-M L^{-1}	assumed
β	red-ox coefficient	0.5		assumed
i_0	exchange current density	1	A m^{2} $^{-1}$	assumed
$K_{d,e}$	decay rate	0.02.$\mu_{max,e}$	d^{-1}	assumed
$K_{d,m}$	decay rate	0.02.$\mu_{max,m}$	d^{-1}	assumed
$X_{MAX,e}$	max biofilm density	512.5	mg-x L^{-1}	assumed
$X_{MAX,m}$	max biofilm density	525	mg-x L^{-1}	assumed
K_x	parameter in Eq. (3-7)	0.04	L mg-x^{-1}	estimated
R_{MIN}	minimum R_{int}	25	Ω	measured
R_{MAX}	maximum R_{int}	2000	Ω	measured
E_{MIN}	minimum E_{OCP}	0.01	V	measured
E_{MAX}	maximum E_{OCP}	0.61-0.66*	V	measured
K_R	parameter in Eqs. (3-20) and (3-21)	0.024**	L mg-x^{-1}	estimated

* average OCP values after first 20 days of MFC operation were 0.66, 0.66, 0.61, and 0.61V for MFC-1 to MFC-4, respectively.

** note that the value of this parameter was incorrectly published in Pinto, Srinivasan, Manuel, and Tartakovsky (2010b). the correct value is presented in this thesis.

Table A-2: Additional parameters for MEC model. Non-identifiable model parameters were assumed based on modelling results of Batstone et al. (D. J. Batstone et al., 2002a). MEC model parameters identical to the MFC model parameters were presented in Tabel A.1.

Parameter	Description	Value	Dimension	Notes
P	cathode pressure	1	atm	constant
Y_{CH4}	methane yield	0.28	mL-CH_4 mg-S^{-1}	assumed
T	MEC temperature	303.15	K	constant
$q_{max,e}$	max. reaction rate	14.0	mg-A mg-x^{-1} d^{-1}	estimated
$q_{max,m}$	max. reaction rate	14.12	mg-A mg-x^{-1} d^{-1}	estimated
$q_{max,f}$	max. reaction rate	16.28	mg-S mg-x^{-1} d^{-1}	estimated
$\mu_{max,f}$	max. growth rate	0.2	d^{-1}	assumed
$\mu_{max,h}$	max. growth rate	0.45	d^{-1}	assumed
$K_{S,f}$	half-rate constant	250	mg-S L^{-1}	assumed
m_{H2}	e^- transferred per mol of H_2	2	mole^- mol-H_2^{-1}	assumed
$K_{d,f}$	decay rate	0.004	d^{-1}	assumed
$K_{d,h}$	decay rate	0.01	d^{-1}	assumed
$X_{MAX,1}$	max. biofilm density	900**	mg-x L^{-1}	assumed
$X_{MAX,2}$	max. biofilm density	512.5**	mg-x L^{-1}	assumed
R_{MIN}	minimum internal resistance	20 / 35*	Ω	measured
Y_M	yield in Eq. (20)	36.6	mg-M mg-S^{-1}	estimated
Y_{COD}	yield	0.75	mg-A mg-S^{-1}	estimated
Y_h·$X_{MAX,3}$	yield and max. biofilm density	750 / 1680*	mg-x L^{-1}	estimated
E_{CEF}	counter-electromotive force	-0.34 / -0.36*	V	estimated
$Y_{H2/CH4}$	yield between H_2 and CH_4	0.25	L-CH_4 L-H_2^{-1}	assumed
Y_{H2}	cathode efficiency	0.8		assumed

* Range for parameters that vary between MEC data sets
** Based on protein measurements (unpublished)

Table A-3: Weight constants from Eq. (2-2) used in the parameter estimation procedure.

Weight – State Variable	MFC-1	MFC-2	MEC-1	MEC-2
w_S- sCOD	0	0	0	34.5
w_A- Volatile Fatty Acids (VFA)	20	20	1	2.25
w_{Qa}- Anode methane production	0	0.1	0	9.25
w_{Imec}- MEC current	0	0	125	67.8
$w_{Eoutput}$- MFC voltage	80	80	0	0
w_{Qc}- Cathode methane production	0	0	40	0
w_{H2}- Hydrogen production	0	0	100	40